

Frequency-Domain Controller Design by Linear Programming

THÈSE N° 4370 (2009)

PRÉSENTÉE LE 15 MAI 2009

À LA FACULTÉ SCIENCES ET TECHNIQUES DE L'INGÉNIEUR

LABORATOIRE D'AUTOMATIQUE

PROGRAMME DOCTORAL EN INFORMATIQUE, COMMUNICATIONS ET INFORMATION

ÉCOLE POLYTECHNIQUE FÉDÉRALE DE LAUSANNE

POUR L'OBTENTION DU GRADE DE DOCTEUR ÈS SCIENCES

PAR

Marc KUNZE

acceptée sur proposition du jury:

Prof. D. Bonvin, président du jury
Prof. R. Longchamp, Dr A. Karimi, directeurs de thèse
Prof. H. Bleuler, rapporteur
Prof. L. Guzzella, rapporteur
Prof. M. Steinbuch, rapporteur



ÉCOLE POLYTECHNIQUE
FÉDÉRALE DE LAUSANNE

Suisse
2009

A mes parents, à Annick

Remerciements

La thèse relatée dans cet ouvrage est le fruit de cinq années passées au sein du Laboratoire d'Automatique de l'Ecole Polytechnique Fédérale de Lausanne. Cette période très riche professionnellement m'a permis d'acquérir de solides bases dans le domaine de l'automatique. C'est pourquoi, j'aimerais saisir l'occasion de remercier les personnes qui ont contribué à cette réussite.

Tout d'abord, je tiens à remercier les professeurs Roland Longchamp et Dominique Bonvin ainsi que le Dr. Denis Gillet de m'avoir accueilli au sein du laboratoire. Cette thèse a également pu être réalisée grâce aux nombreux conseils de mes directeurs de thèse Roland Longchamp et Alireza Karimi. Je tiens tout particulièrement à remercier Ali qui m'a toujours accueilli dans son bureau pour de nombreuses discussions et qui a su me motiver lors de certains moments difficiles.

Je tiens également à remercier vivement le président du jury Dominique Bonvin ainsi que les professeurs Hannes Bleuler, Lino Guzzella et Maarten Steinbuch pour avoir accepté d'examiner mon travail.

Ce travail est également le résultat d'une étroite collaboration que j'ai eue avec ETEL S.A. Je remercie donc tous les collaborateurs

de cette entreprise avec qui j'ai pu avoir de très nombreux échanges : Ralph Coleman, Michel Mathia, Vincent Very et Max Bögli.

J'espère enfin que cette thèse ne comporte pas trop d'erreurs d'anglais. En tous les cas, de nombreuses erreurs ont pu être évitées grâce à la relecture attentive d'Ale. Un grand merci pour tout ce temps investi !

Si ce travail a pu se réaliser sans aucune tracasserie administrative, c'est grâce au soutien du secrétariat. Merci donc à Marie-Claire, Ruth, Francine, Homeira et Sol.

Ces années ont passé à une vitesse folle, ceci grâce à l'excellente atmosphère qui a toujours régné au labo. Merci donc à tous mes collègues pour ces très bons moments. Un merci tout particulier à Basile, Damien, Daniel, Klaske, Philippe, Pierre, Sylvain et Yvan. Si le temps a paru si court c'est aussi grâce à mes amis de l'EPFL avec qui j'ai partagé mes pauses de midi, mais surtout les apéros du vendredi soir. Merci donc à Ben, Nico, André, Fabien, Steve, Pierrick et Pascal.

Merci enfin à Christophe, mon collègue et ami pour les nombreuses discussions sur les mille et une façons de rénover une maison. Merci à Sébastien avec qui j'ai partagé le bureau quelque temps dans une très bonne atmosphère mais surtout avec qui j'ai partagé la folle aventure de la patrouille.

Un grand merci également à Mark mon collègue de bureau, ami et compagnon de rando avec qui j'ai partagé de très bons moments. J'espère que l'on aura encore l'occasion d'en partager beaucoup d'autres ensemble.

Durant ces années, je me suis également découvert une nouvelle passion : le ski de randonnée et ceci grâce à Gorka. Merci beaucoup au petit Basque pour l'initiation et pour toutes les sorties organisées. L'aventure de la patrouille restera gravée à jamais dans ma mémoire ! J'espère que l'on pourra encore vivre dans l'avenir d'autres aventures fortes !

Finalement je tiens à remercier de tout coeur Annick pour le soutien qu'elle m'a apporté durant toute la thèse et plus particulièrement pour la patience qu'elle a eue ce dernier hiver lorsque mon

temps était principalement consacré à la rédaction de thèse, aux joies du ski et à la rénovation de la maison.

Abstract

In this thesis, a new framework to design controllers in the frequency domain is proposed. The method is based on the shaping of the open-loop transfer function in the Nyquist diagram. A line representing a lower approximation for the crossover frequency and a line representing a new linear robustness margin guaranteeing lower bounds for the classical robustness margins are defined and used as constraints. A linear programming approach is proposed to tune fixed-order linearly parameterized controllers for stable single-input single-output linear time-invariant plants. Two optimization problems are proposed and solved by linear programming. In the first one, the new robustness margin is maximized given a lower approximation of the crossover frequency, whereas in the second one, the closed-loop performance in terms of load disturbance rejection, output disturbance rejection and tracking is maximized subject to constraints on the new robustness margin. The method can directly consider multi-model systems. Moreover, this new framework can be used directly with frequency-domain data. Thus, it can also consider systems with frequency-domain uncertainties.

Using the same framework, an extension of the method is proposed to tune fixed-order linearly parameterized gain-scheduled con-

trollers for stable single-input single-output linear parameter varying plants. This method directly computes a linear parameter varying controller from a linear parameter varying model or from a set of frequency-domain data in different operating points and no interpolation is needed. In terms of closed-loop performance, this approach leads to extremely good results. However, the global stability cannot be guaranteed for fast parameter variations and should be analyzed a posteriori.

Nevertheless, for certain classes of switched systems and linear parameter varying systems, it is also possible to guarantee the stability within the design framework. This can be accomplished by adding constraints based on the phase difference of the characteristic polynomials of the closed-loop systems.

This frequency-domain methodology has been tested on numerous simulation examples and implemented experimentally on a high-precision double-axis positioning system. The results show the effectiveness and simplicity of the proposed methodologies.

Keywords: robust controller; gain-scheduled controller; linear programming; Nyquist diagram; frequency-domain data; quadratic stability.

Résumé

Dans cette thèse, une nouvelle méthodologie est proposée afin de synthétiser des régulateurs dans le domaine fréquentiel. La méthode est basée sur le façonnage de la fonction de transfert en boucle ouverte dans le diagramme de Nyquist. Une droite représentant une approximation inférieure de la fréquence de croisement et une droite représentant une nouvelle marge linéaire de robustesse garantissant des bornes inférieures pour les marges de robustesse classiques sont définies et utilisées comme contraintes. Une approche par programmation linéaire est proposée afin de synthétiser des régulateurs linéairement paramétrisés d'ordre fixe pour des systèmes linéaires, stables, monovariés et stationnaires. Deux problèmes d'optimisation sont proposés et résolus par programmation linéaire. Dans le premier, la nouvelle marge de robustesse est maximisée pour une approximation inférieure de la fréquence de croisement donnée, alors que dans le deuxième, la performance en boucle fermée en termes de rejet de perturbations et d'asservissement est maximisée avec des contraintes sur la nouvelle marge de robustesse. La méthode peut directement considérer des systèmes multi-modèles. De plus, cette nouvelle méthodologie peut être directement utilisée avec des données fréquentielles.

Ainsi, elle peut aussi considérer des systèmes avec des incertitudes fréquentielles.

En utilisant la même méthodologie, une extension est proposée afin de synthétiser des régulateurs linéairement paramétrisés à gains programmés d'ordre fixe pour des systèmes linéaires, stables, mono-variables et à paramètres variants. Cette méthode synthétise directement un régulateur linéaire à paramètres variants à partir d'un système linéaire à paramètres variants ou à partir d'un ensemble de données fréquentielles dans différents points de fonctionnement et ceci sans qu'aucune interpolation ne soit nécessaire. Cette approche donne d'excellents résultats en terme de performance en boucle fermée. Cependant, la stabilité globale n'est pas garantie pour des variations rapides des paramètres et devrait être analysée a posteriori.

En revanche, pour certaines classes de systèmes à structure variable et de systèmes linéaires à paramètres variants, il est aussi possible de garantir la stabilité en utilisant la même méthodologie. Cela peut être accompli en ajoutant des contraintes basées sur la différence de phase des polynômes caractéristiques des systèmes en boucle fermée.

Cette méthodologie basée dans le domaine fréquentiel a été testée sur de nombreux exemples par simulation et implémentée expérimentalement sur un système de positionnement à deux axes de haute précision. Les résultats montrent l'efficacité et la simplicité des méthodologies proposées.

Mots-clés : régulateur robuste ; régulateur à gains programmés ; programmation linéaire ; diagramme de Nyquist ; données fréquentielles ; stabilité quadratique.

Contents

1	Introduction	1
1.1	Motivation	1
1.2	State of the Art	3
1.2.1	Frequency-domain data-based methods	3
1.2.2	Gain-scheduling methods	5
1.2.3	Quadratic stability conditions	7
1.3	Organization and Contributions of the Thesis	7
2	Frequency-Domain Robust Controller Design by Linear Programming	11
2.1	Introduction	11
2.2	Preliminaries	12
2.2.1	Plant model	12
2.2.2	Controller parameterization	12
2.2.3	Design specifications	13
2.3	Controller Design by Linear Programming	15
2.3.1	Linear robustness margin	15
2.3.2	Lower approximation of the crossover frequency	17
2.3.3	Optimization for robustness	19
2.3.4	Optimization for performance	20
2.4	Simulation Results	23

2.4.1	System with delay	23
2.4.2	Non-minimum phase system	25
2.5	Conclusions	31
3	Frequency-Domain Gain-Scheduled Controller	
	Design by Linear Programming	33
3.1	Introduction	33
3.2	Preliminaries	34
3.2.1	Plant model	34
3.2.2	Controller parameterization	34
3.3	Extension to Design Gain-Scheduled Controllers	36
3.3.1	Optimization for robustness	36
3.3.2	Optimization for performance	37
3.3.3	LPV parametric model	39
3.4	Simulation Results	40
3.5	Conclusions	43
4	Guaranteeing Quadratic Stability	47
4.1	Introduction	47
4.2	Quadratic Stability of Two Systems	48
4.2.1	Quadratic stability and positive realness	48
4.2.2	Linear constraints to assure quadratic stability of two systems	51
4.2.3	Linear constraints to assure quadratic stability of certain classes of LPV systems	58
4.3	Quadratic Stability of Three Systems	60
4.3.1	Basic idea	60
4.3.2	Linear constraints to assure quadratic stability of three systems	62
4.4	Simulation Results	64
4.4.1	Switched system with two subsystems	64
4.4.2	Switched system with three subsystems	68
4.4.3	LPV system	75
4.5	Conclusions	82

5	Application to an Industrial Double-Axis Positioning System	85
5.1	Introduction	85
5.2	Description of the System	87
5.3	Non-Parametric Identification	88
5.4	Controller Design and Experimental Results	90
5.4.1	Robust controller design and experimental results	90
5.4.2	Gain-scheduled controller design	97
5.5	Stability Analysis	98
5.5.1	LPV Parametric identification	99
5.5.2	Stability analysis using Lyapunov theory	102
5.6	Conclusions	104
6	Conclusions and Perspectives	107
6.1	Contributions	107
6.2	Perspectives	108
A	Quadratic Stability and Positive Realness in Discrete Time	111
A.1	Quadratic Stability of Two Systems in Discrete Time	111
A.2	Quadratic Stability of Three Systems in Discrete Time	115
	Curriculum Vitæ	123

List of Acronyms

CQLF	common quadratic Lyapunov function
FRF	frequency response function
IAE	integrated absolute error
IE	integrated error
KYP	Kalman-Yakubovich-Popov
LFT	linear fractional transformation
LMI	linear matrix inequality
LPMSM	linear permanent magnet synchronous motor
LPV	linear parameter varying
LTi	linear time-invariant
PID	proportional-integral-derivative
QFT	quantitative feedback theory
RHP	right half-plane
SISO	single-input single-output
SPR	strictly positive real

Introduction

1.1 Motivation

The first application of feedback control dates back to about 300 B.C. with the water clocks. Since this time, more and more systems use feedback control. Nowadays, automatic control systems are present everywhere: in cars, in houses, in computers, basically in any modern device. For this reason, automatic control has been the subject of many researches since the middle of the 19th century. Numerous different methods have been proposed and are still proposed to design the feedback loop of a system automatically.

Despite the large amount of methods and controller structures available, hand-tuned Proportional-Integral-Derivative (PID) controllers are still used in a lot of applications, because of their extreme simplicity and the intuitive effect of each term of the controller. In many cases, using an automatic design method or another controller structure could bring improvements in the performances. However, these more complex methods and controller structures are not widespread, because they are too complicated and not intuitive enough to be used by an operator. For example, in the development stage of a high-precision positioning system, the controllers can be

computed by engineers using complex control theories. Once the system is used in the production line, some adjustments of the parameters of the controller always need to be done because, for example, of changes in dynamics due to ageing of components or because of changes of the task. If the method used is too complicated, the operator cannot do it himself. Consequently, the presence of an engineer is required giving rise to a cost increase.

In order to have a method easily implementable on a real system and applicable by an operator, there are a few points that should be considered. First of all, measurement-based methods are easier to use than model-based methods. It means that, if possible, the controllers should be computed using directly data in the time domain or frequency domain. Building physical models of systems based on first principles is complex and time consuming, in addition to being source of many errors. Furthermore, identifying and validating control-oriented parametric models based on the measurements is a non-trivial effort requiring iterative procedures. Moreover, the mismatch between the plants and the parametric models can sometimes lead to poor performance.

Secondly, the method should compute controllers such that the closed-loop systems are robust with respect to uncertainties, disturbances and noise that are always present. Thus, it should be possible to design controllers to get closed-loop systems with a certain level of robustness. Moreover, closed-loop systems should fulfil some performance requirements in terms of bandwidth, disturbance rejection time, steady state errors, etc. The frequency domain offers several ways to measure these robustness and performance requirements. For example, robustness can be measured by gain, phase and modulus margins. Therefore, the method should preferably be frequency-domain based.

Thirdly, it would be interesting to have a method capable of designing controllers for systems having multi-model uncertainties. Often, systems have dynamics slightly changing for different operating points. This kind of changes can be expressed by multi-model un-

certainties. Only a few methods are available that consider this type of uncertainties.

Finally, it should be possible to design fixed-order controllers. As the controllers have to be implemented on computers with limited amount of memory and limited amount of computing power, the order of the controllers cannot be too large. Often, methods compute controllers having at least the same order as the plant models. Although techniques exist to reduce the order of the controllers once the design is finished, by fixing the order of the controllers beforehand, the number of steps needed for the design is reduced.

To sum up, in order to be appropriate for the industry, a method to design controllers should preferably be measurement-based, work in the frequency domain, be able to deal with multi-model uncertainties and design fixed-order controllers.

1.2 State of the Art

The work reported in this thesis gives contributions in the three following domains: controller design based on frequency-domain data, gain-scheduled controller design and quadratic stability conditions. The following sections present separately the state of the art of each one of these subjects.

1.2.1 Frequency-domain data-based methods

The first controller design method based on frequency-domain data can be found at the beginning of the years 1940 with the Ziegler-Nichols method [45]. This method proposes to measure the critical gain and critical oscillation period of systems in closed-loop, which are then used to calculate the parameters of PID controllers by means of some empirical formulas. This method, while being appreciated by its simplicity, often leads to poor results in terms of robustness and performance. Therefore, some methods propose to reformulate the Ziegler-Nichols tuning rules [17].

In order to measure the critical gain and critical oscillation period, the system must be brought to the limit of stability, which is a difficult task. In [22] a method is proposed to measure the critical gain and critical oscillation period automatically using a relay. This method is commonly called the standard relay method. Thus, automatic tuning of controllers can be realized. The standard relay method measures only one frequency point, which is sometimes not enough to fulfil the requirements for complex systems. Different enhancements of the standard relay method are proposed to measure more than one frequency point [4, 41]. For example, in [16], it is proposed to measure the gain and phase margins, but also the infinity-norm of the sensitivity function and complementary sensitivity function using a relay. A frequency criterion is defined based on these measured values. Then, a controller minimizing this frequency criterion is computed iteratively using the Gauss-Newton algorithm. The problem is that an initial controller is needed. Moreover, this optimization problem is not convex. Therefore, there is no guarantee about the convergence of the criterion to the global optimum.

Given that all the above mentioned methods are based on a few number of frequency points, they often lead to poor results in case of complex systems having resonances. Non-parametric models of systems based on frequency-domain data contain many points on a wide range of frequencies and are easily obtained. A method that exploits either non-parametric or parametric models is the one proposed by Bode [5]. This well-known method, contained in all classical textbooks, proposes a graphical powerful tool based on the Bode plots to analyze and design control systems.

Another method, called the Quantitative Feedback Theory (QFT) [19] also offers the possibility to compute controllers with robust performance using frequency-domain data or transfer functions with parametric or non-parametric uncertainty models. QFT is based on the translation of robust performance specifications and uncertainty models into so-called QFT bounds. These bounds, displayed on a Nichols chart, serve as a guide for shaping the nominal loop transfer function. Nevertheless, the success of the design depends on the

experience of the user. In order to avoid these problems, some automatic loop-shaping methods have been proposed [9, 43, 46]. In [9] for example, it is proposed to convert the open-loop QFT bounds into closed-loop QFT bounds and to transform them such that they can be written using linear inequalities. A controller is then automatically tuned by linear programming. The drawback of this method is that the closed-loop poles have to be fixed a priori. It is therefore impossible to use it to address multi-model problems.

Other methods have been proposed for tuning controllers based on frequency-domain data. An example of the last is [25], where a method for digital PID and first order controller synthesis is developed. In this method all stabilizing controllers are determined using only frequency-domain data. In [11], a method using a sampled version of the \mathcal{H}_∞ and \mathcal{H}_2 problems is proposed in order to perform optimal controller synthesis using non-parametric models. The Youla parameter is introduced to convexify the problem and map the set of stabilizing controllers onto the set of stable transfer functions. The main innovation presented in this paper is to propose relations on the frequency response coefficients of the Youla parameter in order to guarantee both stability and causality using Cauchy's residue theorem. This method can unfortunately not treat multi-model cases.

To the best of our knowledge, no other significant method using directly frequency-domain data exists. In contrast, there exist a lot of frequency-domain methods using parametric models including, for example, the \mathcal{H}_2 and \mathcal{H}_∞ methods [44].

1.2.2 Gain-scheduling methods

In the case of some mechatronic systems, such as the double-axis positioning system studied in this thesis, the dynamics changes as a function of some scheduling parameters. Often, these changes are neglected and robust model-based or data-based controllers are designed. Nowadays, systems are required to be more and more accurate, it is therefore no longer possible to neglect changes in dynamics.

Instead, it is interesting to take those directly into account by making the controllers dependent on the scheduling parameters in order to improve the performances. The corresponding synthesis procedure is commonly referred as gain-scheduling (see the survey papers [29,36]). Basically two classes of methods can be distinguished: the classical gain-scheduling methods and the direct Linear Parameter Varying (LPV) controller design methods.

The classical gain-scheduling methods proceed in two steps. First, a finite grid of operating points is chosen within the whole range of operating points and a controller is designed for each of these selected operating points based on the local model. An interpolation between the controllers is subsequently made in order to get a gain-scheduled or LPV controller. Usually, the gain-scheduled controller is obtained by interpolation between the parameters of the local controllers. However, different methods exist. For example in [34] an affine interpolation between the poles, zeros and gains of the local controllers is made, resulting in an affine state-space representation of the LPV controller. Classical gain-scheduling methods give good closed-loop performance and are simple to use; no LPV model is needed; controllers can be designed easily using for example a classical loop-shaping method; the implementation of the controller is straightforward. The major drawback lies in the fact that the global stability of the closed-loop system is not always assured, in particular for fast variations of the scheduling parameters.

Direct LPV controller design methods are based on LPV models. These approaches are different from the classical gain-scheduling methods since they involve the direct synthesis of a controller rather than its construction from a family of local linear controllers designed by Linear Time-Invariant (LTI) methods. The direct methods can be divided into two main categories: methods using a small-gain Linear Fractional Transformation (LFT) approach [2] and methods using a Lyapunov-based approach [3]. The major advantage of these methods is that they assure the global stability of the closed-loop system. Unfortunately, they are more conservative than the classical gain-scheduling methods, leading to poorer closed-loop performance.

Moreover, as mentioned in [42], they are often affected by numerical conditioning and by practical implementation problems.

1.2.3 Quadratic stability conditions

As explained above, Lyapunov-based approaches are often used to guarantee global stability of LPV systems when designing the controllers or to analyze it after the design. These approaches use either quadratic Lyapunov functions or parameter-dependent quadratic Lyapunov functions to take into account the maximum rate of variation of the scheduling parameters and thus reduce conservatism. The quadratic stability of switched systems is guaranteed or analyzed similarly (see the survey papers [31,32]). Several methods propose conditions to guarantee the existence of a Common Quadratic Lyapunov Function (CQLF). For example, in [30], a condition based on the Lie algebra is proposed. Namely, the switched systems are stable if the associated matrix Lie algebra is solvable. In [37], algebraic conditions are derived for the existence of a CQLF for a finite number of stable second-order LTI systems. Unfortunately, none of these methods are frequency-domain based.

1.3 Organization and Contributions of the Thesis

A new framework to design controllers in the frequency domain is presented in Chapter 2. This new framework is based on the shaping of the open-loop transfer function in the Nyquist diagram by linear programming. First of all, it is shown that, by using a linearly parameterized controller, every point of the open-loop transfer function can be written as a linear function of the controller parameters in the Nyquist diagram. Then, it is observed that optimization methods with constraints on the classical robustness margins (the gain, phase and modulus margins) lead to nonconvex optimization problems [21]. In order to avoid this disadvantage, a new linear robustness margin represented by a line is defined to replace the classical robustness

margins. For the same reason, the crossover frequency is replaced by a line corresponding to its lower approximation. Using the new robustness margin and the lower approximation of the crossover frequency as constraints, optimization problems using linear programming are defined to design fixed-order linearly parameterized controllers. The first optimization problem proposes to maximize the new robustness margin while the second proposes to maximize the closed-loop performance in terms of load disturbance rejection, output disturbance rejection and tracking. The method is able to directly consider multi-model systems. Moreover, this new framework can be used directly with frequency-domain data, which is a clear advantage. Consequently, it also allows to consider systems with frequency-domain uncertainties.

A large class of nonlinear systems has dynamics varying as a function of some scheduling parameters and thus belongs to the class of LPV systems. For this reason, an extension of the framework to design gain-scheduled controllers for LPV systems is very useful and is proposed in Chapter 3. Once again, the key idea is to design a linearly parameterized gain-scheduled controller. With this parameterization, every point of the open-loop transfer function can be written as a linear function of the controller parameters in the Nyquist diagram. Therefore, all the concepts defined in Chapter 2 can be used to design gain-scheduled controllers. The method either needs frequency-domain data in different operating points or LPV models.

So far, quadratic stability when designing controllers for multi-model systems or global stability when designing gain-scheduled controllers for LPV systems are not considered. These two subjects are addressed in Chapter 4. First of all, a theorem making the link between quadratic stability and Strictly Positive Realness (SPRness) properties is established. Subsequently, SPRness properties are transformed into linear constraints in the Nyquist diagram. These new constraints allow quadratic stability of switched systems composed of up to three subsystems and certain classes of LPV systems to be guaranteed. It should be noted that, in order to guarantee

quadratic stability, parametric models of the systems are absolutely necessary.

In Chapter 5, the new framework is used to design controllers for a real industrial system that is a high-precision double-axis positioning system. First of all, a robust controller is designed. A gain-scheduled controller is then designed to improve the robustness margin. The results obtained prove that this new method is easily applicable on a real system.

Finally, Chapter 6 concludes the manuscript and gives a number of perspectives associated to the design framework developed in this thesis.

It should be noted that, in Chapters 2, 3 and 4, the theory is developed for continuous-time models. However, the proposed approach can also be applied to discrete-time models straightforwardly.

Frequency-Domain Robust Controller Design by Linear Programming

2.1 Introduction

In this chapter, a new framework for designing controllers is presented, based on the shaping of the open-loop transfer function in the Nyquist diagram. The idea is to use the advantages provided by the Nyquist diagram to propose a new method that is easy to use and easy to implement. The above mentioned advantages are the simplicity of interpreting the classical robustness margins and the crossover frequency. Unfortunately, if these robustness and performance specifications are used as constraints to design controllers, they lead to nonconvex optimization problems. Consequently, they are replaced by lines, corresponding to lower bounds on these specifications, in order to use them as constraints in optimization problems solved by linear programming.

This chapter is organized as follows: in Section 2.2 the class of models, controllers and the control objectives are defined. Section 2.3 introduces a new linear stability margin, a lower approximation for the crossover frequency and presents the linear optimization problems. Simulation results are given in Section 2.4. Finally, Section 2.5 gives some concluding remarks.

2.2 Preliminaries

2.2.1 Plant model

The class of LTI Single-Input Single-Output (SISO) systems with no pole in the Right Half-Plane (RHP) is considered. It is assumed that a set of non-parametric models in the frequency domain is available. This set can be obtained either by spectral analysis from several identification experiments at different operating points or from parametric models in the form of rational transfer functions with pure time delay. It is supposed that the dynamics of the system is captured by a finite number of frequency points N . The number of models in the set is m and so the model set can be represented by:

$$\mathcal{M} = \{G_i(j\omega_k) \mid k = 1, \dots, N; i = 1, \dots, m\} \quad (2.1)$$

2.2.2 Controller parameterization

The class of linearly parameterized controllers is considered:

$$K(s) = \rho^T \phi(s) \quad (2.2)$$

where:

$$\rho^T = [\rho_1 \ \rho_2 \ \dots \ \rho_{n_p}] \quad (2.3)$$

$$\phi^T(s) = [\phi_1(s) \ \phi_2(s) \ \dots \ \phi_{n_p}(s)] \quad (2.4)$$

n_p is the number of controller parameters and $\phi_i(s), i = 1, \dots, n_p$ are rational basis functions with no RHP pole. With this parameterization, every point on the Nyquist diagram of $K(j\omega)G_i(j\omega)$ can be written as a linear function of the controller parameters ρ :

$$K(j\omega_k)G_i(j\omega_k) = \rho^T \phi(j\omega_k)G_i(j\omega_k) = \rho^T \mathcal{R}_i(\omega_k) + j\rho^T \mathcal{I}_i(\omega_k) \quad (2.5)$$

where $\mathcal{R}_i(\omega_k)$ and $\mathcal{I}_i(\omega_k)$ are respectively the real and the imaginary part of $\phi(j\omega_k)G_i(j\omega_k)$.

It should be mentioned that PID controllers are a special case of this parameterization with for example:

$$\rho^T = [K_p \ K_i \ K_d] \quad (2.6)$$

$$\phi^T(s) = \left[1 \ \frac{1}{s} \ \frac{s}{1+T_f s} \right] \quad (2.7)$$

where T_f (supposed to be known) is the time constant of the filter applied to the derivative term.

2.2.3 Design specifications

Optimizing load disturbance rejection is considered as the desired performance for the closed-loop system. In general, in order to reject low frequency disturbances, the controller permanent gain at low frequencies must be maximized. For a rational continuous-time controller of order n_c with fixed denominator $R(s)$,

$$K(s) = \frac{k_{n_c}s^{n_c} + \dots + k_1s + k_0}{R(s)} \quad (2.8)$$

this corresponds to maximizing k_0 . According to (2.2), k_0 is a linear combination of the parameters of the linearly parameterized controller:

$$k_0 = \sum_{i=1}^{n_p} \gamma_i \rho_i \quad (2.9)$$

where γ_i are the coefficients of the linear combination which depend on the basis functions $\phi_i(s)$. For the particular case of the denominator containing only one integrator, maximizing k_0 corresponds to minimizing the Integrated Error (IE) defined by:

$$\text{IE} = \int_0^\infty e(t) dt \quad (2.10)$$

where e is the error between the reference and the output of the plant. This can be proved by assuming that in (2.8) $R(s) = sR'(s)$ where:

$$R'(s) = 1 + r_1 s + \dots + r_{n_c-1} s^{n_c-1}. \quad (2.11)$$

Then, the control law becomes:

$$u(t) + r_1 \frac{du(t)}{dt} + \dots + r_{n_c-1} \frac{d^{(n_c-1)}u(t)}{dt^{(n_c-1)}} = k_0 \int_0^\infty e(t)dt + k_1 e(t) + \dots + k_{n_c} \frac{d^{(n_c-1)}e(t)}{dt^{(n_c-1)}} \quad (2.12)$$

where u is the control signal. Furthermore, it is assumed that the error is initially zero ($e(0) = 0$) and that a unit step disturbance is applied at the process input. Since the closed-loop system is stable and has integral action, the control error will go to zero at infinity ($e(\infty) = 0$). Thus:

$$u(\infty) - u(0) = k_0 \int_0^\infty e(t)dt \quad (2.13)$$

Since the disturbance is applied at the process input, the change in control signal is equal to the change of the disturbance:

$$u(\infty) - u(0) = 1 \quad (2.14)$$

Using (2.13) and (2.14), IE becomes:

$$\text{IE} = \frac{1}{k_0} \quad (2.15)$$

Thus, if k_0 is maximized, the integrated error IE is minimized. For the special case of a PID controller, k_0 corresponds to K_i . As a result maximizing K_i corresponds to minimizing IE. It should be mentioned that IE is a good approximation of the Integrated Absolute Error (IAE) for well-damped systems.

It should be noted that by maximizing k_0 not only the IE of the load disturbance rejection is minimized but also the IE of the output disturbance rejection and the IE of the tracking. The IE of the output disturbance rejection and the IE of the tracking can be good

approximations of, respectively, the IAE of the output disturbance rejection and the IAE of the tracking since, in these cases, the oscillations can be decreased by increasing the modulus margin. Thus, by maximizing the low frequency gain of the controller, the load disturbance rejection, the output disturbance rejection and the tracking are improved.

The crossover frequency ω_c and the robustness margins (gain, phase and modulus margins) are also design specifications.

2.3 Controller Design by Linear Programming

The classical robustness indicators such as the gain, phase and modulus margins as well as the performance indicator, the crossover frequency ω_c , are nonlinear functions of the controller parameters. Moreover, the optimization methods with constraints on these values lead to nonconvex optimization problems [21] and cannot be solved efficiently. In this section, a new stability margin together with a lower approximation for the crossover frequency will be defined. This lead to linear constraints for the optimization problems in which robustness and/or performance are maximized. These optimization problems can be solved efficiently by a linear programming approach.

For sake of simplicity, the optimization problems will be defined for one model. In the multi-model case, only the number of constraints must be increased by a factor m and the problems can still be solved by linear programming.

2.3.1 Linear robustness margin

Let us consider a straight line d_1 in the complex plane crossing the negative real axis between 0 and -1 with an angle $\alpha \in (0^\circ, 90^\circ]$ (see Fig. 4.2). The new linear stability margin $\ell \in (0, 1)$ is the distance between the critical point -1 and d_1 where it crosses the negative real axis. If the Nyquist curve of the open-loop transfer function lies on

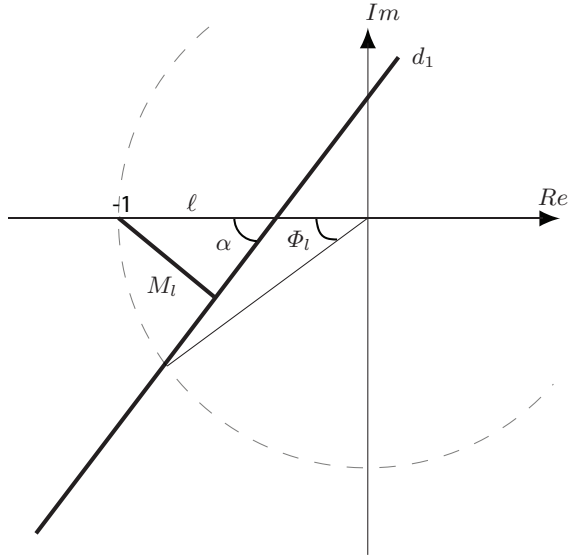


Fig. 2.1. New linear margin ℓ with respect to the classical robustness margins. The lower bounds for the phase and modulus margins are Φ_l and M_l respectively.

the right side of d_1 , the following lower bounds on the conventional robustness margins are ensured (see Fig. 4.2):

$$G_m \geq \frac{1}{1 - \ell} \quad (2.16)$$

$$\Phi_m \geq \Phi_l = \arccos \left((1 - \ell) \sin^2 \alpha + \cos \alpha \sqrt{1 - (1 - \ell)^2 \sin^2 \alpha} \right) \quad (2.17)$$

$$M_m \geq M_l = \ell \sin \alpha \quad (2.18)$$

where G_m, Φ_m and M_m are respectively the gain, phase and modulus margins [27] and Φ_l and M_l respectively the lower bounds for the phase and modulus margins. For a fixed value of α , all lower bounds

are increasing functions of the new margin ℓ . Therefore, ℓ can be used as a measure of robustness and can be maximized to optimize the robustness of the system. On the other hand, for a fixed value of ℓ , the phase and modulus margins increase with increasing α . As the modulus margin increases, the maximum of the sensitivity function decreases and consequently the system becomes better damped, but the bandwidth may decrease. This is due to the Bode sensitivity integral relation also called the area formula [12]. Thus, α can possibly be used as a design variable for tradeoff between the damping and the bandwidth of the closed-loop system. If two of the three conventional margins are given, it is easy to find the corresponding values for the linear margin. For example, if the gain margin must be equal to 3 and the modulus margin equal to 0.6, (2.16) imposes $\ell = 0.66$ and (2.18) imposes $\alpha = 64.16^\circ$. Generally, the typical values for the gain, phase and modulus margins are respectively between 2 and 5, 30° and 60° and 0.5 and 0.77 [39]. Using (2.16), the above mentioned values lead to a typical value of ℓ between 0.5 and 0.8. If the same values are used in (2.17) and (2.18), a typical value of α between 37° and 90° is obtained.

2.3.2 Lower approximation of the crossover frequency

Let us consider another straight line d_2 in the complex plane tangent to the unit circle centered at the origin which crosses the negative real axis with an angle β . The part of d_2 between d_1 and the imaginary axis is a linear approximation of the unit circle in this region. Now, assuming that the open-loop Nyquist curve intersects d_2 at a frequency called ω_x ; it is clear from Fig. 2.2 that the crossover frequency ω_c is always greater than or equal to ω_x . Hence, ω_x which is a lower approximation of the crossover frequency can be used as a measure of the time-domain performance (i. e. greater ω_x means faster disturbance rejection and smaller rise time for tracking response). In order to prevent the Nyquist curve approaching the critical point from the left side at frequencies lower than ω_x , β should be chosen such that:

$$\beta \leq \arcsin\left(\frac{1}{\ell + 1}\right) \quad (2.19)$$

in order to prevent deterioration of the gain margin assured by d_1 and:

$$\beta \leq \arcsin(1 - \ell \sin \alpha) \quad (2.20)$$

in order to prevent deterioration of the modulus margin assured by d_1 . For example if ℓ is equal to 0.6 and α to 60° , β should be smaller than 28.71° .

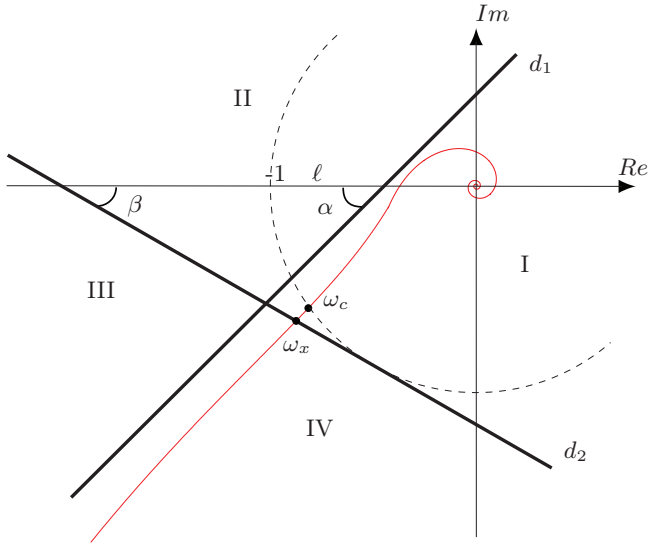


Fig. 2.2. Linear constraints for robustness and performance, with four regions: I, II, III and IV. The crossover frequency and the lower approximation of the crossover frequency are respectively ω_c and ω_x .

2.3.3 Optimization for robustness

Before explaining the optimization problem, it should be noted that the number of integral terms in the open-loop transfer function $L(s)$ determines where the low frequency points of $L(s)$ are located. For instance, if $L(s)$ contains two integral terms, the low frequency part of the Nyquist diagram will be located in region III (see Fig. 2.2). The number of integral terms will determine the constraints of the optimization problem.

In this subsection, it is supposed that a desired crossover frequency ω_c is given and the objective is to find the best controller in terms of the robustness margins. The design variables for the optimization problem are ω_x , α and β . In order to guarantee an achieved crossover frequency greater than the desired one, ω_x is chosen equal to ω_c . As explained in Subsection 2.3.1, α is generally chosen between 37° and 90° depending on the control objective. In order to have a good linear approximation of the unit circle $\beta = 30^\circ$ can be chosen (care should be taken to respect the inequalities (2.19) and (2.20)).

The design method is the same whether the open-loop transfer function $L(s)$ contains one or two integrators. The Nyquist diagram of $L(j\omega)$ at very low frequencies is located in region III or IV (depending on the number of integrators in $L(s)$) whereas at very high frequencies it is located in region I (see Fig. 2.2). In order to ensure a certain distance from the critical point, the Nyquist curve should not enter region II. On the other hand, the Nyquist curve necessarily intersects d_2 at ω_x . As a result, the open-loop Nyquist curve $L(j\omega)$ should lie in either region III or IV for frequencies less than ω_x and in region I for frequencies larger than ω_x . Thus, the following linear optimization problem is considered:

$$\max_{\rho} \ell$$

Subject to:

$$\begin{aligned} \rho^T (\cot \alpha \mathcal{I}(\omega_k) - \mathcal{R}(\omega_k)) + \ell &\leq 1 && \text{for } \omega_k > \omega_x \\ \rho^T (\cos \beta \mathcal{I}(\omega_k) + \sin \beta \mathcal{R}(\omega_k)) &> -1 && \text{for } \omega_k > \omega_x \\ \rho^T (\cos \beta \mathcal{I}(\omega_k) + \sin \beta \mathcal{R}(\omega_k)) &\leq -1 && \text{for } \omega_k \leq \omega_x \end{aligned} \quad (2.21)$$

The first line corresponds to the constraint that the Nyquist curve has to be below d_1 for $\omega_k > \omega_x$, the second line corresponds to the constraint that the Nyquist curve has to be above d_2 for $\omega_k > \omega_x$ and the third line corresponds to the constraint that the Nyquist curve has to be below d_2 for $\omega_k \leq \omega_x$.

This optimization problem leads to the controller parameters that cancel the integral term if there is any in the controller (reducing the integral action increases the robustness of the closed-loop system). Therefore, in order to preserve the integral effect of the controller, for example in a PID controller, an additional constraint $K_i > K_{\min}$ can be added.

2.3.4 Optimization for performance

Another control objective is to consider some constraints for the robustness margins and optimize the closed-loop performance in terms of the load disturbance rejection, the output disturbance rejection and the tracking. The last can be achieved by maximizing k_0 (K_i for PID controllers) which also leads to minimizing the integrated error IE for the controller containing one integrator. The design variables are limited to the linear robustness margin ℓ and α . When $L(s)$ contains only one integrator, the open-loop Nyquist curve should lie in region I or IV, thus a simple optimization problem can be defined as follows:

$$\begin{aligned} & \max_{\rho} k_0 \\ \text{Subject to:} & \quad \rho^T (\cot \alpha \mathcal{I}(\omega_k) - \mathcal{R}(\omega_k)) + \ell \leq 1 \quad \forall \omega_k \end{aligned} \quad (2.22)$$

For the case of two integrators in $L(s)$, the constraints should be modified such that $L(j\omega)$ at low frequencies can be located in region III. This can be obtained using a straight line on the complex plane. The line d_2 can be used again to divide the complex plane in four regions. Once again β should be chosen in order to respect the inequalities (2.19) and (2.20). The optimization problem can then be formulated as:

$$\begin{aligned} & \max_{\rho} k_0 \\ \text{Subject to:} & \quad \rho^T (\cot \alpha \mathcal{I}(\omega_k) - \mathcal{R}(\omega_k)) + \ell \leq 1 \quad \text{for } \omega_k > \omega_x \\ & \quad \rho^T (\cos \beta \mathcal{I}(\omega_k) + \sin \beta \mathcal{R}(\omega_k)) \leq -1 \quad \text{for } \omega_k \leq \omega_x \end{aligned} \quad (2.23)$$

where ω_x is this time a lower bound for the crossover frequency rather than a lower approximation, as it can be located anywhere in region IV, and not necessarily at the intersection with d_2 . A good choice for ω_x , in this case, is the open-loop bandwidth.

Remarks:

- The robustness and performance can be optimized simultaneously with a mixed criterion in the form of:

$$\max_{\rho} k_0 + \lambda \ell \quad (2.24)$$

where λ is a weighting factor to be chosen.

- The case of three integrators in $L(s)$ will be studied when the application is considered (see Chapter 5).
- The approach proposed to design controllers does not take into consideration the input sensitivity function $U(s)$:

$$U(s) = \frac{K(s)}{1 + K(s)G(s)} \quad (2.25)$$

It is therefore possible that the control input becomes too large when the closed-loop bandwidth is chosen much greater than the open-loop bandwidth. Two possibilities exist to solve this problem:

- Filter the reference signal with a first order filter of the form $1/(1 + Ts)$ in order to take out the high frequency part of the signal.
- Introduce additional constraints to prevent the input sensitivity function from being too large at high frequencies. Let us first suppose that $K(s)G(s)$ is much smaller than 1 at high frequencies. Then, in order to limit $U(s)$ at high frequencies, additional constraints can be introduced to limit the magnitude of $K(s)$. To keep the method linear, the constraints are added on the real and imaginary parts of $K(s)$ instead of on its magnitude:

$$\begin{aligned} -K_u &< \rho^T \mathcal{R}_\phi(\omega_k) < K_u \text{ for } \omega_k > \omega_u \\ -K_u &< \rho^T \mathcal{I}_\phi(\omega_k) < K_u \text{ for } \omega_k > \omega_u \end{aligned} \quad (2.26)$$

where $\mathcal{R}_\phi(\omega_k)$ and $\mathcal{I}_\phi(\omega_k)$ are respectively the real and the imaginary part of $\phi(j\omega_k)$. K_u is the limit of the absolute value of the real and imaginary part of $K(s)$ and ω_u is the frequencies above which the constraints are applied.

- A lower bound for the modulus margin M_l is guaranteed as a function of the linear robustness margin ℓ that is used as a constraint. It follows from the circle criterion [26] that the closed-loop system will remain stable with a static nonlinearity in the loop, provided that the nonlinearity is bounded by two straight lines with slopes $1/(1 + M_l)$ and $1/(1 - M_l)$. In the special case of a vertical new linear stability margin ($\alpha = 90^\circ$), the nonlinearity has to be bounded by two straight lines with slopes 0 and $1/(1 - \ell)$.

2.4 Simulation Results

The design method is tested on two different examples taken from [35] to illustrate its properties.

2.4.1 System with delay

Let us consider the following parametric plant model:

$$G_1(s) = \frac{1}{(s+1)^3} e^{-5s} \quad (2.27)$$

This model captures typical dynamics with long dead time encountered in the process industry. Different PID controllers are designed and compared with those obtained with the method proposed by [35]. Panagopoulos' method is chosen to make the comparison, since it also designs PID controllers by optimizing the load disturbance rejection with constraints on the modulus margin. The particularity of Panagopoulos' method is that it uses a set point weight and also filters the reference signal with a first-order filter. To do a fair comparison between these two methods, the first-order filter used in Panagopoulos' method is also used in the proposed method.

It should be noted that the Ziegler-Nichols' method gives very poor results for this example [39] (pages 145-146). For this reason this method is not considered in the current comparison.

First of all, the frequency response of G_1 is evaluated at $N = 8000$ equally spaced frequency points between 0 and 80 rad/s. Then PID controllers are designed for this plant using the optimization problem (2.22) to optimize the load disturbance rejection. The controller designed using Panagopoulos' method has a modulus margin equal to 0.5. A first controller is designed with ℓ fixed to 0.707 and α to 45° to obtain the same specification for the modulus margin. Then a second controller is designed with ℓ fixed to 0.5 and α to 90° to see the effect of α on the closed-loop responses. The time constant of the derivative part of the PID controllers T_f is set to 0.1 s.

The Nyquist plots of the open-loop transfer functions obtained with the proposed method and with Panagopoulos' method are shown in Fig. 2.3. It can be observed that the Nyquist plots obtained by the proposed method (solid and dashed) respect the constraint represented by the linear margin. The responses of the closed-loop systems to a set point change and load disturbance are compared in Fig. 2.4. It can be seen that for the proposed method with $\ell = 0.707$ and $\alpha = 45^\circ$, the overshoot of the load disturbance rejection is about the same as the one obtained with Panagopoulos' method, but the response is slower. The tracking response is significantly improved by the proposed method with $\ell = 0.5$ and $\alpha = 90^\circ$.

Now, let the control objective be to maximize the robustness of the closed-loop system at the cost of reducing the crossover frequency from 0.17 to 0.1 rad/s. The constraints of (2.21) together with the mixed criterion (2.24) are used. In this approach, four parameters must be chosen. In order to have a crossover frequency of at least 0.1 rad/s, the lower approximation of the crossover frequency ω_x is set to 0.1 rad/s. To have a well-damped system, $\alpha = 60^\circ$ is chosen. To proceed one can start with $\beta = 20^\circ$ then according to the results this value can be slightly adapted to respect the inequalities (2.19) and (2.20). Finally λ is tuned for the tradeoff between robustness and performance of the load disturbance rejection (for this example $\lambda = 50$ is chosen). The Nyquist plots of the open-loop transfer functions obtained with the proposed method using the mixed criterion and with Panagopoulos' method are shown in Fig. 2.5. It can be noticed that the Nyquist plot obtained by the proposed method satisfies the constraints imposed by d_1 and d_2 and leads to a linear margin ℓ of 0.750 and a crossover frequency of 0.1 rad/s. The responses of the closed-loop systems to a set point change and load disturbance are compared in Fig. 2.6. Although the robustness is improved, the load disturbance rejection capability is still acceptable.

For the sake of simplicity of the comparison between these controllers, the details of the designs, the related performances and robustness achieved are shown in Table 2.1, where ω_c stands for the crossover frequency (in [rad/s]), o_s for the overshoot (in [%]), t_s for

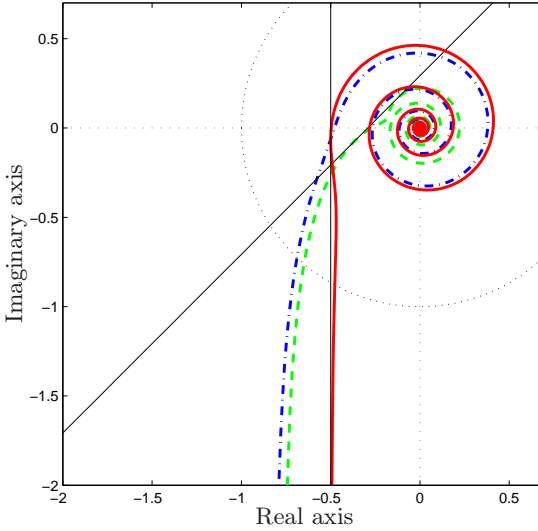


Fig. 2.3. Nyquist plots of the open-loop transfer functions for G_1 (solid: proposed method with $\ell = 0.5$ and $\alpha = 90^\circ$, dashed: proposed method with $\ell = 0.707$ and $\alpha = 45^\circ$, dashed-dotted: Panagopoulos' method).

the settling time to 1% (in [s]), IAE_s for the integrated absolute error of the set point change, o_d for the overshoot (in [%]), t_d for the settling time to 1% (in [s]) and IAE_d for the integrated absolute error of the load disturbance.

2.4.2 Non-minimum phase system

Let us consider the following non-minimum phase system:

$$G_2(s) = \frac{1 - 2s}{(s + 1)^3} \quad (2.28)$$

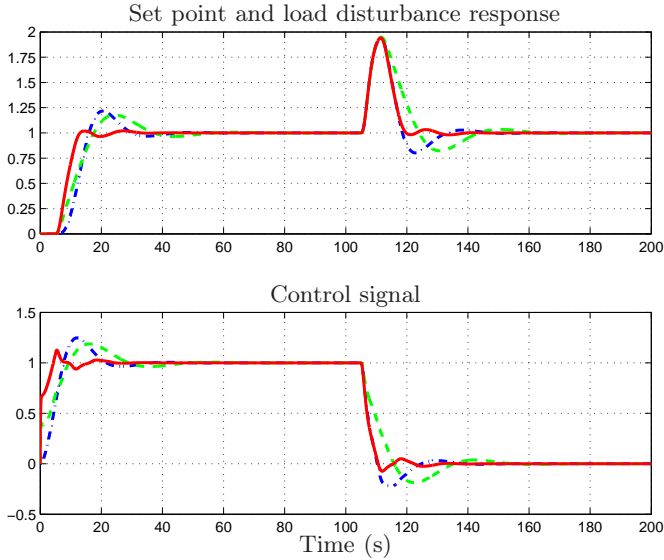


Fig. 2.4. Set point and load disturbance responses for G_1 (solid: proposed method with $\ell = 0.5$ and $\alpha = 90^\circ$, dashed: proposed method with $\ell = 0.707$ and $\alpha = 45^\circ$, dashed-dotted: Panagopoulos' method).

Although a zero in the RHP is uncommon in process control, this model is considered with the aim of demonstrating the wide applicability of the method.

The first step is to evaluate G_2 in $N = 8000$ equally spaced frequency points between 0 and 80 rad/s. Next two PID controllers for optimization of the load disturbance rejection are designed using the same specifications considered for G_1 . The Nyquist plots of the open-loop transfer functions obtained with the proposed method and with Panagopoulos' method are shown in Fig. 2.7. It can be observed that the Nyquist plots obtained by the proposed method

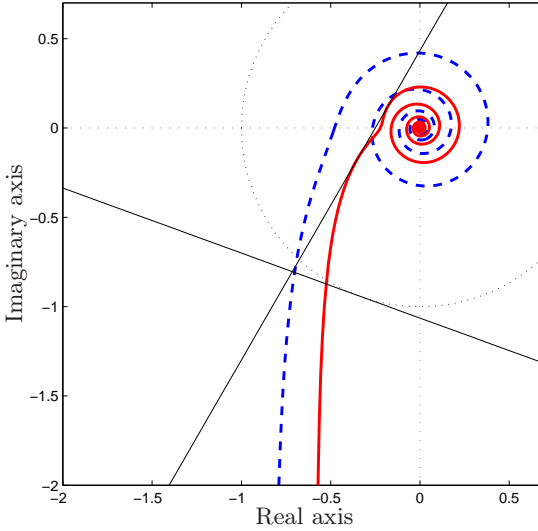


Fig. 2.5. Nyquist plots of the open-loop transfer functions for G_1 (solid: proposed method with the mixed criterion ($\alpha = 60^\circ$, $\beta = 20^\circ$, $\omega_x = 0.1$ rad/s, $\lambda = 50$), dashed: Panagopoulos' method).

(solid and dashed) respect the constraint represented by the linear margin. The responses of the closed-loop systems to a set point change and load disturbance are compared in Fig. 2.8. It can be seen that for the proposed method with $\ell = 0.707$ and $\alpha = 45^\circ$, the overshoot of the load disturbance rejection is once again about the same as the one obtained with Panagopoulos' method, but the response is slower. The tracking response is significantly improved by the proposed method with $\ell = 0.5$ and $\alpha = 90^\circ$. To facilitate the comparison between the different controllers, the details of the designs are shown in Table 2.2.

Table 2.1. Properties of the controllers obtained for the system G_1 .

Method	Panagopoulo's method	Max K_i	Max K_i	Max $K_i + 50\ell$
		$\ell = 0.707$ $\alpha = 45^\circ$	$\ell = 0.5$ $\alpha = 90^\circ$	$\alpha = 60^\circ$
K_p	0.555	0.241	0.608	0.263
K_i	0.173	0.127	0.139	0.106
K_d	0.966	0.678	1.039	0.640
M_m	0.50	0.57	0.50	0.66
ω_c	0.17	0.12	0.14	0.10
o_s	21.68	17.83	2.04	7.75
t_s	41.70	53.37	30.57	40.52
IAE _s	14.21	13.83	9.16	13.00
o_d	94.50	94.88	94.27	94.92
t_d	44.31	59.79	37.02	46.95
IAE _d	9.10	12.20	7.54	11.38

Table 2.2. Properties of the controllers obtained for the system G_2 .

Method	Panagopoulo's method	Max K_i	Max K_i
		$\ell = 0.707$ $\alpha = 45^\circ$	$\ell = 0.5$ $\alpha = 90^\circ$
K_p	0.542	0.247	0.541
K_i	0.262	0.196	0.208
K_d	0.428	0.278	0.428
M_m	0.50	0.56	0.51
ω_c	0.28	0.19	0.23
o_s	10.19	14.08	0.15
t_s	17.71	30.45	12.69
IAE _s	7.92	8.09	5.85
o_d	107.34	97.74	103.02
t_d	18.94	34.18	16.67
IAE _d	6.11	8.23	6.10

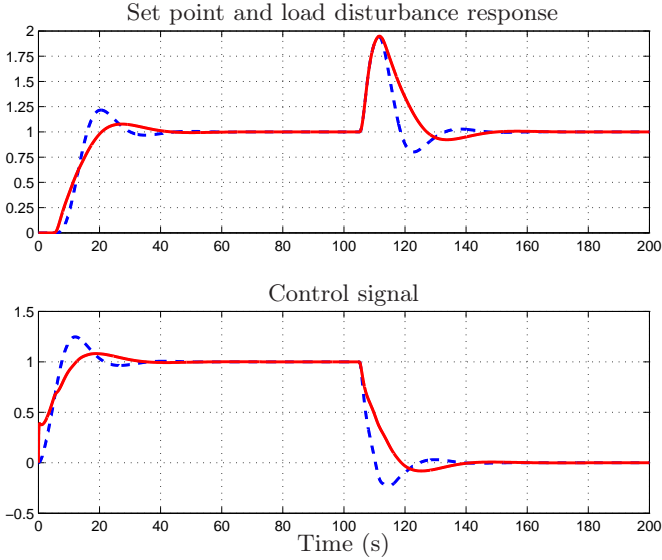


Fig. 2.6. Set point and load disturbance responses for G_1 (solid: proposed method with the mixed criterion ($\alpha = 60^\circ$, $\beta = 20^\circ$, $\omega_x = 0.1$ rad/s, $\lambda = 50$), dashed: Panagopoulos' method).

In a general way, the proposed method gives about the same results as Panagopoulos' method in terms of load disturbance rejection. On the other hand, it gives better results in terms of set point tracking when the design parameters α is increased. Furthermore, this method is easier to implement, since it uses a linear programming approach compared to the nonconvex optimisation used by Panagopoulos' method.

In these two examples, 8000 frequency points are used. This shows that the linear programming approach can work with a high number of constraints. However, it should be noted that the number

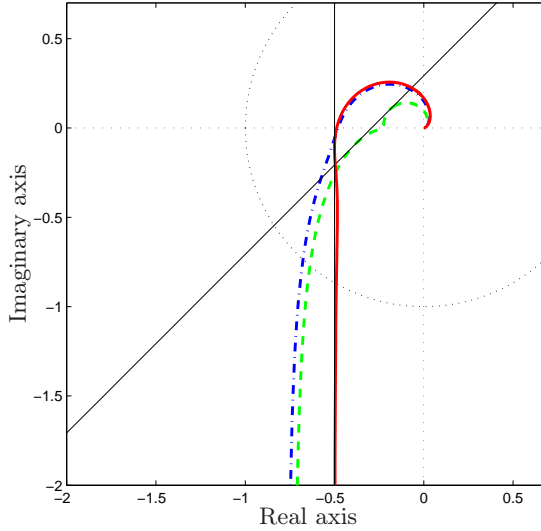


Fig. 2.7. Nyquist plots of the open-loop transfer functions for G_2 (solid: proposed method with $\ell = 0.5$ and $\alpha = 90^\circ$, dashed: proposed method with $\ell = 0.707$ and $\alpha = 45^\circ$, dashed-dotted: Panagopoulos' method).

of frequency points could be drastically reduced without changing the results.

The proposed method has been tested on two simple examples to show clearly how it works. However, it should be noted that, in Chapter 5, the method will be applied to a real application where its capability to deal with multi-model systems will be highlighted.

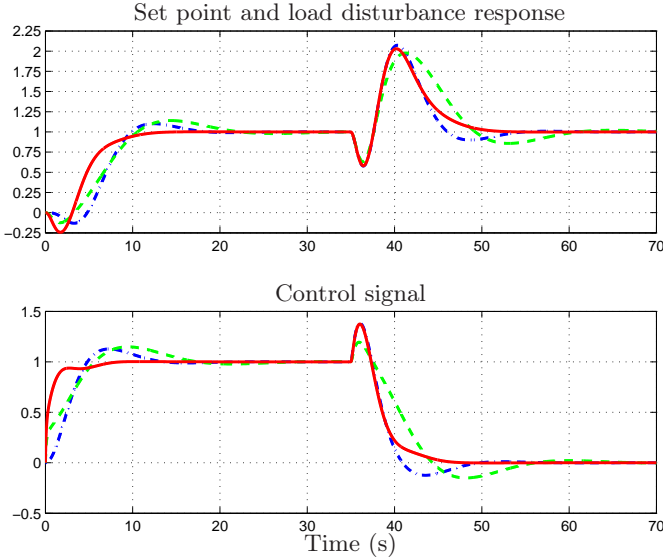


Fig. 2.8. Set point and load disturbance responses for G_2 (solid: proposed method with $\ell = 0.5$ and $\alpha = 90^\circ$, dashed: proposed method with $\ell = 0.707$ and $\alpha = 45^\circ$, dashed-dotted: Panagopoulos' method).

2.5 Conclusions

In this chapter, robust fixed-order controller design is formulated as a linear optimization problem. The proposed method is based on frequency loop-shaping in the Nyquist diagram. The classical robustness and performance specifications are represented as linear constraints in the Nyquist diagram. Therefore, there are only a few design variables which are directly related to the robustness (linear margin ℓ and α) and performance (lower approximation of the crossover frequency ω_x) of the closed-loop systems. The control objective is to maximize the robustness margin or optimize the

closed-loop performance in terms of load disturbance rejection, output disturbance rejection and tracking. The method is very simple and requires only the frequency response of the plants. This frequency response can be obtained either from a parametric model or directly from frequency-domain data. Multi-model systems or systems with frequency-domain uncertainties can be taken into account straightforwardly. The method is very appropriate to design PID controllers, yet it can also be applied to design higher-order linearly parameterized controllers in discrete or continuous time with fixed denominators. Simulation results show that the method can be applied to systems with large time-delay as well as non-minimum phase systems.

Frequency-Domain Gain-Scheduled Controller Design by Linear Programming

3.1 Introduction

A large class of nonlinear systems can be represented by a set of linear models that approximate the dynamics of the systems in different operating points. The dynamic behavior of such systems varies as a function of some scheduling parameters. Many electromechanical systems, such as for example components mounters, H-drives and electromagnetic levitation systems belong to this class of systems. For such examples, the scheduling parameter is the position, as their dynamics change as a function of the position. In order to improve the performances of these systems, gain-scheduled or LPV controllers are designed. In these controllers, controller parameters are functions of the scheduling parameters.

In this chapter, it is proposed to extend the design framework presented in the last chapter to design gain-scheduled controllers for this large class of systems. The design is also based on loop-shaping in the Nyquist diagram, since it is shown that the constraints on the robustness and performance are linear even with gain-scheduled controllers. This method has two advantages: one is to design directly gain-scheduled controllers without an interpolation step, the other is that parametric models are not necessary.

This chapter is organized as follows: in Section 3.2 the class of models and controllers are defined. Section 3.3 shows the extensions of the optimization problems to design gain-scheduled controllers. Simulation results are given in Section 3.4. Finally, Section 3.5 gives some concluding remarks.

3.2 Preliminaries

3.2.1 Plant model

The class of SISO LPV systems, varying according to a n_θ -dimensional vector θ of scheduling parameters, is considered. The linear systems for frozen scheduling parameters are supposed to have no RHP pole. It is assumed that a set of frequency-domain data is available. This set is obtained either from an LPV parametric model or by doing several non-parametric identification experiments for different values of θ . It is supposed that the dynamics of the system is captured by a finite number of frequency points N and that a sufficiently large number m of models is available to have a fine grid with respect to θ . Then, the set can be presented by:

$$\mathcal{M} = \{G(j\omega_k, \theta_l) \mid k = 1, \dots, N; l = 1, \dots, m\}, \quad (3.1)$$

where ω_k and θ_l are, respectively, particular values of the frequency ω and of the scheduling parameters θ .

3.2.2 Controller parameterization

The class of linearly parameterized controllers is considered:

$$K(s, \theta) = \rho^T(\theta)\phi(s), \quad (3.2)$$

where

$$\rho^T(\theta) = [\rho_1(\theta) \ \rho_2(\theta) \ \dots \ \rho_{n_p}(\theta)] . \quad (3.3)$$

Given that the aim is to design an LPV controller, the controller parameters depend on θ . Let us assume that $\rho_i(\theta)$ is a polynomial in θ of order p_c , i.e.:

$$\rho_i(\theta) = (\rho_{i,p_c})^T \theta^{p_c} + \dots + (\rho_{i,1})^T \theta + (\rho_{i,0})^T \mathbf{1}, \quad (3.4)$$

where $\mathbf{1}$ is an n_θ -dimensional vector of ones and θ^k denotes element-by-element power of k of vector θ . The controller is therefore completely characterized by the real vectors $\rho_{i,p_c}, \dots, \rho_{i,1}, \rho_{i,0}$.

As an example, the parameterization of a PID controller depending on a scalar θ can be expressed as:

$$\rho^T(\theta) = [K_p(\theta) \ K_i(\theta) \ K_d(\theta)], \quad (3.5)$$

$$\phi^T(s) = \left[1 \ \frac{1}{s} \ \frac{s}{1+T_f s} \right], \quad (3.6)$$

where T_f (which is supposed to be known) is the time constant of the filter applied to the derivative term. The parameters could be polynomials in θ of order 2:

$$K_p(\theta) = K_{p,2}\theta^2 + K_{p,1}\theta + K_{p,0}, \quad (3.7)$$

$$K_i(\theta) = K_{i,2}\theta^2 + K_{i,1}\theta + K_{i,0}, \quad (3.8)$$

$$K_d(\theta) = K_{d,2}\theta^2 + K_{d,1}\theta + K_{d,0}. \quad (3.9)$$

The parameterization of the controller (see (3.2)) allows us to write every point on the Nyquist diagram of the open-loop $L(j\omega, \theta_l) = K(j\omega, \theta_l)G(j\omega, \theta_l)$ as a linear function of the parameters of the vectors $\rho_{i,p_c}, \dots, \rho_{i,1}, \rho_{i,0}$:

$$\begin{aligned} K(j\omega_k, \theta_l)G(j\omega_k, \theta_l) &= \rho^T(\theta_l)\phi(j\omega_k)G(j\omega_k, \theta_l) \\ &= \rho^T(\theta_l)\mathcal{R}(\omega_k, \theta_l) + j\rho^T(\theta_l)\mathcal{I}(\omega_k, \theta_l) \\ &= (M\bar{\theta}_l)^T \mathcal{R}(\omega_k, \theta_l) + j(M\bar{\theta}_l)^T \mathcal{I}(\omega_k, \theta_l), \end{aligned} \quad (3.10)$$

where

$$M = \begin{bmatrix} (\rho_{1,p_c})^T & \dots & (\rho_{1,1})^T & (\rho_{1,0})^T \\ \vdots & \ddots & \vdots & \vdots \\ (\rho_{n_p,p_c})^T & \dots & (\rho_{n_p,1})^T & (\rho_{n_p,0})^T \end{bmatrix}, \quad (3.11)$$

$$\bar{\theta}_l = [\theta_l^{p_c} \dots \theta_l \mathbf{1}]^T, \quad (3.12)$$

$\mathcal{R}(\omega_k, \theta_l)$ and $\mathcal{I}(\omega_k, \theta_l)$ are, respectively, the real and the imaginary parts of $\phi(j\omega_k)G(j\omega_k, \theta_l)$.

3.3 Extension to Design Gain-Scheduled Controllers

Every point of the open-loop $L(j\omega, \theta_l)$ can be written on the Nyquist diagram as a linear function of the parameters of the controllers. Therefore, the same tools as used in Chapter 2 can be used in order to design gain-scheduled controllers. The LPV plants considered must have a fixed number of integral terms for all θ , since the number of integral terms in the open-loop transfer function $L(s, \theta_l)$ determine the constraints of the optimization problems.

3.3.1 Optimization for robustness

In this subsection, it is supposed that a desired crossover frequency ω_c is given and the objective is to find the best controller in terms of the robustness margins. The design variables for the optimization problem are ω_x , α and β (see Fig. 2.2). In order to guarantee an achieved crossover frequency larger than the desired one, ω_x is chosen equal to ω_c . The design method is the same whether the open-loop transfer function $L(s, \theta_l)$ contains one or two integrators. The Nyquist diagram of $L(j\omega, \theta_l)$ at very low frequencies is located in region III or IV and at very high frequencies in region I (see Fig. 2.2). In order to ensure a certain distance from the critical point, the Nyquist curve should not enter region II. On the other hand, the Nyquist curve necessarily intersects d_2 at ω_x . As a result,

the open-loop Nyquist curve $L(j\omega, \theta_l)$ should lie in region III or IV for frequencies less than ω_x and in region I for frequencies greater than ω_x . Consequently, the following linear optimization problem is considered:

$$\begin{aligned}
 & \max_M \quad \ell \\
 & \text{subject to:} \\
 & (M\bar{\theta}_l)^T (\cot \alpha \mathcal{I}(\omega_k, \theta_l) - \mathcal{R}(\omega_k, \theta_l)) + \ell \leq 1 \\
 & \quad \text{for } \omega_k > \omega_x, \quad l = 1, \dots, m, \\
 & (M\bar{\theta}_l)^T (\cos \beta \mathcal{I}(\omega_k, \theta_l) + \sin \beta \mathcal{R}(\omega_k, \theta_l)) > -1 \\
 & \quad \text{for } \omega_k > \omega_x, \quad l = 1, \dots, m, \\
 & (M\bar{\theta}_l)^T (\cos \beta \mathcal{I}(\omega_k, \theta_l) + \sin \beta \mathcal{R}(\omega_k, \theta_l)) \leq -1 \\
 & \quad \text{for } \omega_k \leq \omega_x, \quad l = 1, \dots, m.
 \end{aligned} \tag{3.13}$$

3.3.2 Optimization for performance

Another control objective is to consider some constraints for the robustness margins and maximize the closed-loop performance in terms of the load disturbance rejection, the output disturbance rejection and the tracking. This can be done by maximizing

$$K_{\min} = \min_{l=1, \dots, m} k_0(\theta_l) = \min_{l=1, \dots, m} \sum_{i=1}^{n_p} \gamma_i \rho_i(\theta_l), \tag{3.14}$$

which is the minimum of the controller permanent gain at low-frequency between all the operating points. The design variables are limited to the linear robustness margin ℓ and α . When $L(s, \theta_l)$ contains only one integrator, the open-loop Nyquist curve should lie in region I or IV. Thus a simple optimization problem can be defined as follows:

$$\begin{aligned}
& \max_M K_{\min} \\
& \text{subject to:} \\
& (M\bar{\theta}_l)^T (\cot \alpha \mathcal{I}(\omega_k, \theta_l) - \mathcal{R}(\omega_k, \theta_l)) + \ell \leq 1 \\
& \quad \forall \omega_k, \quad l = 1, \dots, m, \\
& \sum_{i=1}^{n_p} \gamma_i \rho_i(\theta_l) - K_{\min} \geq 0 \quad \text{for } l = 1, \dots, m,
\end{aligned} \tag{3.15}$$

For the case of two integrators in $L(s, \theta_l)$, the constraints should be modified such that $L(j\omega, \theta_l)$ at low frequencies can be located in region III. This can be obtained using a straight line in the complex plane. The line d_2 can be used again to divide the complex plane in four regions. The Nyquist diagram of $L(j\omega, \theta_l)$ should lie in region I or IV for the frequencies larger than ω_x and in region III or IV for the frequencies less than ω_x . The optimization problem can therefore be formulated as

$$\begin{aligned}
& \max_M K_{\min} \\
& \text{subject to:} \\
& (M\bar{\theta}_l)^T (\cot \alpha \mathcal{I}(\omega_k, \theta_l) - \mathcal{R}(\omega_k, \theta_l)) + \ell \leq 1 \\
& \quad \text{for } \omega_k > \omega_x, \quad l = 1, \dots, m, \\
& (M\bar{\theta}_l)^T (\cos \beta \mathcal{I}(\omega_k, \theta_l) + \sin \beta \mathcal{R}(\omega_k, \theta_l)) \leq -1 \\
& \quad \text{for } \omega_k \leq \omega_x, \quad l = 1, \dots, m, \\
& \sum_{i=1}^{n_p} \gamma_i \rho_i(\theta_l) - K_{\min} \geq 0 \quad \text{for } l = 1, \dots, m,
\end{aligned} \tag{3.16}$$

where ω_x is this time a lower bound for the crossover frequency rather than a lower approximation as it can be located anywhere in region IV, and not necessarily at the intersection with d_2 .

3.3.3 LPV parametric model

When a set of non-parametric models is available, the optimization methods presented above can be directly applied to compute an LPV controller as the number of models and the number of frequency points are finite. On the other hand, if an LPV parametric model is available, the number of models corresponding to different values of the scheduling parameters and the number of frequency points are infinite, leading to an infinite number of linear constraints if using the proposed method. In order to solve this problem, the first step is to go from an infinite number of frequency points to a finite number of frequency points by gridding the frequency domain. If the gridding of the frequency domain is not desired, it is still possible to use the generalized Kalman-Yakubovich-Popov (KYP) method proposed in [18] at the cost of more complexity. At this point the number of constraints is still infinite, since the number of models corresponding to different values of the scheduling parameters θ is still infinite. This problem can be solved using two different ways:

- Gridding θ . If the number of parameters in θ is not large, this approach is feasible since the linear programming method handles efficiently a very large number of constraints.
- Discretizing θ using a randomized approach [8, 13]. This method allows getting a finite number of constraints. It means that the solution found satisfies the original set of constraints (infinite number of constraints) with a certain probabilistic level.

There are two advantages for the use of LPV parametric models:

- One can use a finer grid on the operating points to be sure that between the identified models the constraints are satisfied.
- The global stability can be analyzed a posteriori as it will be shown in Chapter 5 or guaranteed within the design framework as it is explained in the next chapter.

3.4 Simulation Results

The design method is applied to a system having a resonance whose frequency changes as a function of a scheduling parameter θ . Consider the following LPV plant model:

$$G(s, \theta) = \frac{\omega_0^2(\theta)}{s^2 + 2\zeta\omega_0(\theta)s + \omega_0^2(\theta)}, \quad (3.17)$$

where

$$\omega_0(\theta) = 2 + 0.2\theta, \quad (3.18)$$

$$\zeta = 0.1, \quad (3.19)$$

$$\theta \in [-1, 1]. \quad (3.20)$$

This model could represent the dynamics of a mechatronic system, where the frequency of the resonance is a function of the moving mass. The objective is to design a PID controller with the following structure

$$K(s) = \frac{K_d s^2 + K_p s + K_i}{s(1 + Ts)} \quad (3.21)$$

that maximizes the robustness of the closed-loop system with a crossover frequency of about 3.3 rad/s. This crossover frequency is chosen because it is about 20% larger than the crossover frequency of the nominal model ($\theta = 0$) in open-loop.

First, a PID controller is designed for the nominal model using the optimization problem (2.21). The design variable ω_x is specified at 3.3 rad/s, α at 90° and β at 20° . In order to soften the constraints to a certain extent, a tolerance on ω_x is used, meaning that the frequencies near ω_x (up to 2.5 %) can be anywhere and not necessarily in region I, III or IV. The time constant T of the filter of the PID controller is set to 0.1 s. $G(s, 0)$ is evaluated at $N = 3000$ equally spaced points between 0 and 30 rad/s. The Nyquist plot of the open-loop transfer function obtained by the design is shown in Fig. 3.1. It can be observed that the Nyquist plot respects the constraints represented by the two lines and leads to a linear margin ℓ of

0.743. The response of the closed-loop system to a set point change is shown in Fig. 3.2. It can be seen that the response is satisfactory (small overshoot). The PID controller obtained by the design for

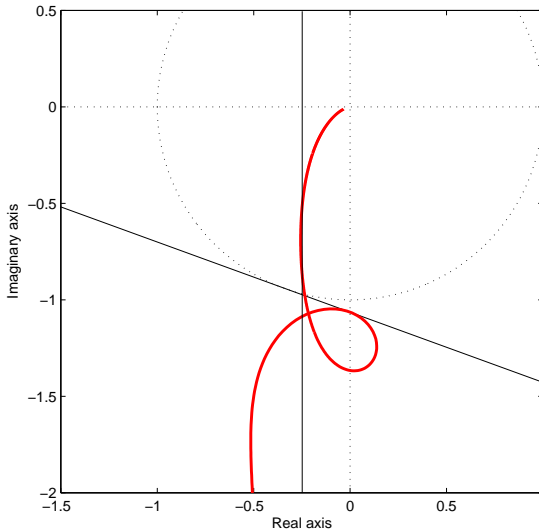


Fig. 3.1. Nyquist plot of the open-loop transfer function of the PID controller and the nominal model of G .

the nominal model is the following:

$$K(s) = \frac{0.8447s^2 + 0.2132s + 3.2891}{s(1 + 0.1s)} \quad (3.22)$$

Now, a robust PID controller is designed for the LPV model using the same design variables. 21 equally spaced discrete values of θ are taken between -1 and 1. Once again, for each discretized value θ_i ,

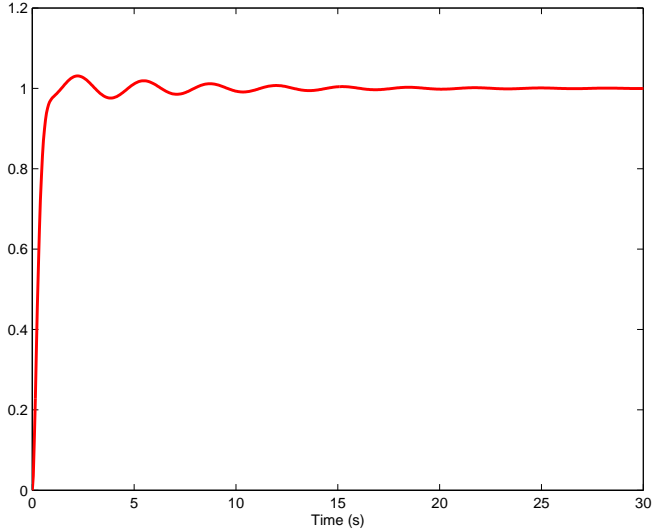


Fig. 3.2. Set point response of the PID controller and the nominal model of G .

$G(s, \theta_l)$ is evaluated at $N = 3000$ equally spaced points between 0 and 30 rad/s. No solution is obtained from the optimization problem for the whole range of θ . A solution is obtained only if $\theta \in [-0.18, 0.18]$. This shows the relevance to design a gain-scheduled controller.

Thus, a gain-scheduled PID controller with the following form

$$K(s, \theta) = \frac{1}{s(1 + Ts)} \left[(K_{d,1}\theta + K_{d,0})s^2 + (K_{p,1}\theta + K_{p,0})s + (K_{i,1}\theta + K_{i,0}) \right] \quad (3.23)$$

is designed using the optimization problem (3.13) with the same design variables. As it can be seen in (3.23), the order p_c of the poly-

nomial in θ describing the parameters of the controller is set to 1. As before, 21 equally spaced discrete values of θ are taken between -1 and 1 and $G(s, \theta_l)$ is evaluated at $N = 3000$ equally spaced points between 0 and 30 rad/s. The gain-scheduled PID controller parameters are shown in Table 3.1. The Nyquist plots of the open-loop transfer functions obtained by the design are shown in Fig. 3.3 for three particular values of θ (-1, 0 and 1). It can be observed that the Nyquist plots respect the constraints represented by the two lines and lead to a linear margin ℓ of 0.733. The responses of the closed-loop system to a set point change using the gain-scheduled PID controller are shown in Fig. 3.4 for three particular values of θ (-1, 0 and 1). It can be seen that the responses to a set point change are very good (small overshoots). The response of the closed-loop system to a set point change using the PID controller designed for the nominal model is also shown in Fig. 3.4 for $\theta = -1$. The response is more oscillatory, which justifies the use of the gain-scheduled controller. Thanks to the gain-scheduled PID controller, it is possible to have about the same performances and robustness for different values of θ , which is not possible using a robust PID controller.

Table 3.1. Parameters of the gain-scheduled PID controller.

$K_{d,1}$	$K_{d,0}$	$K_{p,1}$	$K_{p,0}$	$K_{i,1}$	$K_{i,0}$
-0.1832	0.8825	0.0049	0.2156	-0.1017	3.4154

3.5 Conclusions

In this chapter, gain-scheduled fixed-order linearly parameterized controller design is formulated as a linear optimization problem. The proposed method uses the design framework developed in Chapter 2. Thus, it is also based on frequency loop-shaping in the Nyquist

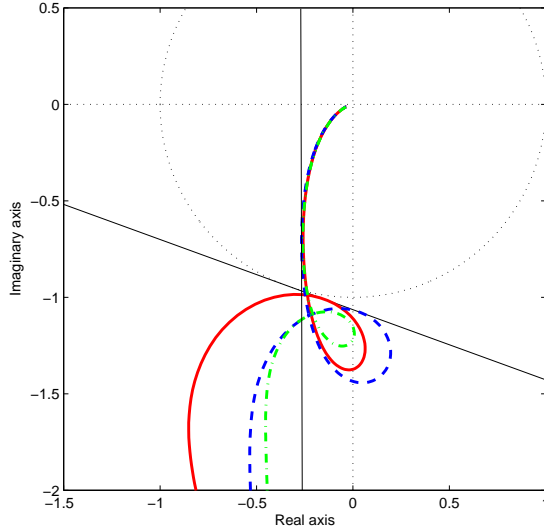


Fig. 3.3. Nyquist plots of the open-loop transfer functions of the gain-scheduled PID controller and G for $\theta = -1$ (solid), $\theta = 0$ (dashed) and $\theta = 1$ (dashed-dotted).

diagram. The control objective is either to maximize the robustness margin with constraint on the lower approximation of the crossover frequency or to maximize the closed-loop performance with constraint on the linear robustness margin. This method requires either the frequency response of LPV plants in different operating points or discrete or continuous-time LPV models and needs no interpolation to get the LPV controllers, which constitutes a real advantage, since the procedure of designing local controllers and interpolating between them can be very difficult.

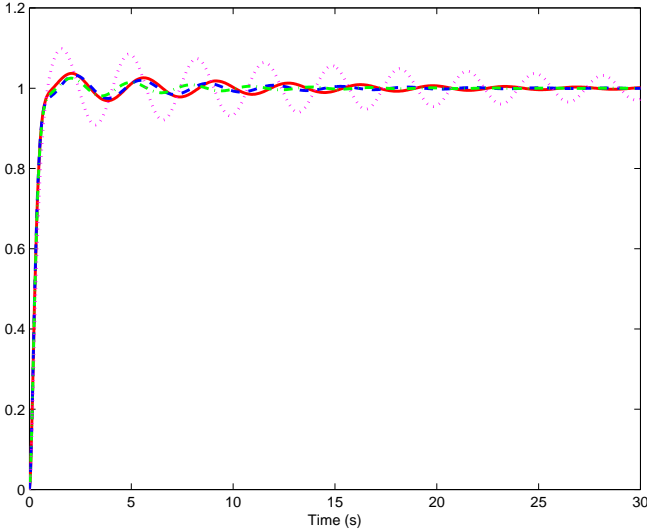


Fig. 3.4. Set point responses of the gain-scheduled PID controller and G for $\theta = -1$ (solid), $\theta = 0$ (dashed) and $\theta = 1$ (dashed-dotted) compared to the set point response of the PID controller designed for the nominal model and G for $\theta = -1$ (dotted).

Simulation results show that the method can compute gain-scheduled controllers with robustness margins that are unachievable with classical robust controllers.

This method is better than the classical gain-scheduling methods since it reduces the number of step needed to design the controllers, but is similar in the sense that the global stability of the closed-loop systems is not guaranteed.

Guaranteeing Quadratic Stability

4.1 Introduction

The method proposed in Chapter 2 can directly compute controllers for multi-model systems assuring robust stability. Nevertheless, this frequency-domain method can not be applied to switched systems because it does not ensure quadratic stability. It means that the closed-loop systems are stable for anyone of the model belonging to the systems set as long as this model is fixed during operation. If the model varies during operation (which is the case for switched systems), the stability is no longer guaranteed.

The method proposed in Chapter 3 to design gain-scheduled controllers also does not guarantee global stability of the closed-loop systems. For slow variations of the scheduling parameters, the systems may be globally stable but, for fast variations of the scheduling parameters, the systems are certainly not globally stable.

In order to guarantee the quadratic stability of switched systems or LPV systems, some frequency-domain constraints have to be added in the Nyquist diagram. To do it, a theorem making the link between quadratic stability using Lyapunov theory and SPRness properties is used. Indeed, this theorem shows the link between

time-domain conditions and frequency-domain conditions to obtain quadratic stability. This type of analysis needs a parametric model. So, in this chapter, it is supposed that the parametric models of the systems are available.

This chapter is organized as follows. In Section 4.2, the quadratic stability of two systems is studied. First of all, the theorem used to make the link between time-domain and frequency-domain conditions for quadratic stability is presented. Then, the linear constraints to guarantee the quadratic stability of two systems, rising from this theorem, are presented. Finally, it is proposed to use these constraints to guarantee the quadratic stability of certain classes of LPV systems. In Section 4.3, the method is extended to guarantee the quadratic stability of three systems. Simulation results to show the effectiveness of the method are given in Section 4.4. Finally, Section 4.5 gives some concluding remarks.

4.2 Quadratic Stability of Two Systems

4.2.1 Quadratic stability and positive realness

Let a stable monic polynomial of order n be defined as:

$$c(s) = s^n + c_1 s^{n-1} + \dots + c_n. \quad (4.1)$$

We can assign to this polynomial a vector C :

$$C = [c_1 \ c_2 \ \dots \ c_n] \quad (4.2)$$

and a matrix A :

$$A = \begin{bmatrix} -c_1 & -c_2 & \dots & -c_{n-1} & -c_n \\ 1 & 0 & & 0 & 0 \\ 0 & 1 & \dots & 0 & 0 \\ \vdots & \vdots & & \vdots & \vdots \\ 0 & 0 & \dots & 1 & 0 \end{bmatrix}. \quad (4.3)$$

Then the relation between SPRness and the quadratic stability can be stated in the following theorem, which is directly related to the equivalence between bounded real lemma and positive real lemma [1]. This result may be known by the experts in the domain. However, to the best of the author's knowledge, the way that it is formulated is new.

Theorem 4.1 *Consider $c_1(s)$ and $c_2(s)$, two stable polynomials of order n , then the following statements are equivalent:*

1. $\frac{c_1(s)}{c_2(s)}$ and $\frac{c_2(s)}{c_1(s)}$ are SPR.
2. $|\arg(c_1(j\omega)) - \arg(c_2(j\omega))| < \frac{\pi}{2} \quad \forall \omega$.
3. A_1 and A_2 are quadratically stable meaning that:
 $\exists P = P^T > 0 \in \mathbb{R}^{n \times n}$ such that
 $A_1^T P + P A_1 < 0,$
 $A_2^T P + P A_2 < 0.$

Proof: (1) \Leftrightarrow (2): This equivalence is immediate. It comes from the definition of SPR transfer function: $\frac{c_1(j\omega)}{c_2(j\omega)}$ is in the RHP, so $-\frac{\pi}{2} < \arg(c_1(j\omega)) - \arg(c_2(j\omega)) < \frac{\pi}{2} \quad \forall \omega$. For more details see [20].

(1) \Rightarrow (3): Consider the transfer function $\frac{c_1(s)}{c_2(s)}$:

$$\frac{c_1(s)}{c_2(s)} = 1 + \frac{c_1(s) - c_2(s)}{c_2(s)}. \quad (4.4)$$

Using a controllable canonical form, (4.4) leads to the following state space realization:

$$\left[\begin{array}{c|c} A_2 & B \\ \hline C_1 - C_2 & 1 \end{array} \right] \quad (4.5)$$

with $B = [1 \ 0 \ \dots \ 0]^T$.

Using the KYP lemma, (4.5) is SPR iff [40]:

$$\exists P = P^T > 0 \text{ s.t.}$$

$$\begin{bmatrix} A_2^T P + P A_2 & P B - (C_1 - C_2)^T \\ B^T P - (C_1 - C_2) & -2 \end{bmatrix} < 0. \quad (4.6)$$

Using the Schur lemma, we have:

$$A_2^T P + P A_2 + \frac{1}{2}[PB - (C_1 - C_2)^T][B^T P - (C_1 - C_2)] < 0. \quad (4.7)$$

Adding and subtracting $\frac{1}{2}PB(C_1 - C_2) + \frac{1}{2}(C_1 - C_2)^T B^T P$ to (4.7), we get:

$$(A_2 - B(C_1 - C_2))^T P + P(A_2 - B(C_1 - C_2)) + \frac{1}{2}(PB + (C_1 - C_2)^T)(B^T P + (C_1 - C_2)) < 0. \quad (4.8)$$

Knowing that $A_1 = A_2 - B(C_1 - C_2)$ gives:

$$A_1^T P + P A_1 + \frac{1}{2}[PB - (C_2 - C_1)^T][B^T P - (C_2 - C_1)] < 0. \quad (4.9)$$

Since the third terms in (4.7) and (4.9) are positive semi-definite, we obtain $A_1^T P + P A_1 < 0$ and $A_2^T P + P A_2 < 0$. This proves that A_1 and A_2 are quadratically stable.

(3) \Rightarrow (1): This equivalence is proved using the bounded real lemma. If A_1 and A_2 are quadratically stable, it means that the following matrix is stable:

$$\frac{A_1 + A_2}{2} + \gamma B \frac{C_2 - C_1}{2} \quad (4.10)$$

for all values of γ between -1 and 1. According to the bounded real lemma we have [44]:

$$\left(\frac{A_1 + A_2}{2}\right)^T P + P \left(\frac{A_1 + A_2}{2}\right) + P B B^T P + \left(\frac{C_2 - C_1}{2}\right)^T \left(\frac{C_2 - C_1}{2}\right) < 0. \quad (4.11)$$

It is well known that the bounded real lemma is equivalent to the positive real lemma with [1]:

$$\bar{A} = A - BC = \frac{A_1 + A_2}{2} - B \frac{C_2 - C_1}{2} = A_2, \quad (4.12)$$

$$\bar{B} = B, \quad (4.13)$$

$$\bar{C} = -2C = C_1 - C_2, \quad (4.14)$$

$$\bar{D} = 1 \quad (4.15)$$

and

$$\bar{P} = 2P. \quad (4.16)$$

Thus, we get:

$$\begin{aligned} \exists \bar{P} = \bar{P}^T > 0 \text{ s.t. } & \begin{bmatrix} \bar{A}^T \bar{P} + \bar{P} \bar{A} & \bar{P} \bar{B} - \bar{C}^T \\ \bar{B}^T \bar{P} - \bar{C} & -\bar{D} - \bar{D}^T \end{bmatrix} = \\ & \begin{bmatrix} A_2^T \bar{P} + \bar{P} A_2 & \bar{P} B - (C_1 - C_2)^T \\ B^T \bar{P} - (C_1 - C_2) & -2 \end{bmatrix} < 0. \end{aligned} \quad (4.17)$$

This inequality is the same as (4.6). Thus, we can conclude that $\frac{c_1(s)}{c_2(s)}$ is SPR. Using the properties of SPR systems, the inverse, $\frac{c_2(s)}{c_1(s)}$, is also SPR. ■

This theorem is useful to create new linear constraints in the Nyquist diagram in order to ensure the quadratic stability of switched systems composed of two subsystems.

It should be noted that this theorem is valid for continuous-time systems. However, a similar theorem can be stated for discrete-time systems. This theorem is developed in Appendix A.

4.2.2 Linear constraints to assure quadratic stability of two systems

The idea is to transform the second property of Theorem 4.1, which is a frequency-domain condition, into linear constraints on the open-loop transfer function in the Nyquist diagram. Then, quadratic stability is obtained by adding these new constraints in the linear programming method presented in Chapter 2.

Main idea

Let us consider the following ratio:

$$\frac{1 + K(s)G_1(s)}{1 + K(s)G_2(s)} = \frac{(K_d(s)G_{d,1}(s) + K_n(s)G_{n,1}(s)) G_{d,2}(s)}{(K_d(s)G_{d,2}(s) + K_n(s)G_{n,2}(s)) G_{d,1}(s)} \quad (4.18)$$

where $K_n(s)$ and $K_d(s)$ are respectively the numerator and denominator of the controller, $G_{n,1}(s)$ and $G_{d,1}(s)$ the numerator and denominator of $G_1(s)$ and $G_{n,2}(s)$ and $G_{d,2}(s)$ the numerator and denominator of $G_2(s)$. It should be noted that $K_d(s)G_{d,1}(s) + K_n(s)G_{n,1}(s)$ is the characteristic polynomial of one of the stable closed-loop system thus, it can be replaced by $c_1(s)$ and $K_d(s)G_{d,2}(s) + K_n(s)G_{n,2}(s)$ is the characteristic polynomial of the other stable closed-loop system and can be replaced by $c_2(s)$. Therefore, (4.18) can be written as:

$$\frac{1 + K(s)G_1(s)}{1 + K(s)G_2(s)} = \frac{c_1(s) G_{d,2}(s)}{c_2(s) G_{d,1}(s)}, \quad (4.19)$$

leading to:

$$\frac{c_1(s)}{c_2(s)} = \frac{1 + K(s)G_1(s) G_{d,1}(s)}{1 + K(s)G_2(s) G_{d,2}(s)}. \quad (4.20)$$

Using the second property of Theorem 4.1, the closed-loop system is quadratically stable iff:

$$|\arg(1 + K(j\omega)G_1(j\omega)) - \arg(1 + K(j\omega)G_2(j\omega)) + \arg(G_{d,1}(j\omega)) - \arg(G_{d,2}(j\omega))| < \frac{\pi}{2} \quad \forall \omega. \quad (4.21)$$

Replacing $\arg(G_{d,1}(j\omega)) - \arg(G_{d,2}(j\omega))$ by $\Delta(\omega)$, we have:

$$-\frac{\pi}{2} - \Delta(\omega) < \arg(1 + K(j\omega)G_1(j\omega)) - \arg(1 + K(j\omega)G_2(j\omega)) < \frac{\pi}{2} - \Delta(\omega) \quad \forall \omega. \quad (4.22)$$

It should be noted that $\Delta(\omega)$ is known since the parametric models of the systems are known. These inequalities can be simply transformed into linear constraints in the Nyquist diagram.

Let us consider the simple case when $\Delta(\omega)$ is zero for all frequencies (the denominators of the two systems are identical), thus (4.22) becomes:

$$|\arg(1 + K(j\omega)G_1(j\omega)) - \arg(1 + K(j\omega)G_2(j\omega))| < \frac{\pi}{2} \forall \omega. \quad (4.23)$$

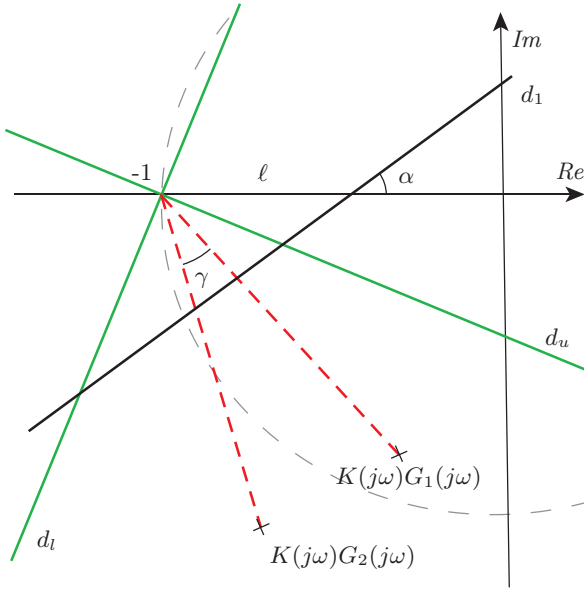


Fig. 4.1. Linear constraints for quadratic stability when $\Delta(\omega) = 0$ (d_u , d_i) and for robust stability (d_1).

In this case, the idea is to add, to the line d_1 assuring the robust stability, two perpendicular lines d_u and d_l passing through the -1 point to assure the quadratic stability (see Fig. 4.1). If $K(j\omega)G_1(j\omega)$ and $K(j\omega)G_2(j\omega)$ are between these two lines, γ , the difference between the arguments of $1 + K(j\omega)G_1(j\omega)$ and $1 + K(j\omega)G_2(j\omega)$, is always less than $\pi/2$, thus respecting Inequality (4.23). It should be noted as well that Fig. 4.1 is a good illustration of the restrictions added by the quadratic stability. Indeed, the region where $K(j\omega)G_1(j\omega)$ and $K(j\omega)G_2(j\omega)$ can be placed to assure robust and quadratic stability is smaller than the region assuring only robust stability.

Since the open-loop transfer functions are strictly proper, it is impossible to respect the constraints defined by d_u and d_l at high frequencies as depicted in Fig. 4.1. At high frequencies, the region defined by d_u and d_l should include the origin of the Nyquist diagram. This problem is solved by defining the lines d_u and d_l as a function of the frequency. To do it, a desired open-loop transfer function $L_d(s)$ is introduced. For each frequency, d_u and d_l are defined such that the vector $1 + L_d(j\omega)$ is the angle bisector of the two lines. In other words, d_l and d_u have a phase difference of, respectively, $-\pi/4$ and $\pi/4$ with respect to $1 + L_d(j\omega)$.

The choice of $L_d(s)$ plays a crucial role since the constraints depend on it. There are some simple choices that usually lead to good results for simple models. For example $L_d = w_c/s$ is an appropriate choice for low-order stable systems having one integrator in their open-loop transfer function.

This idea works for the simple case when $\Delta(\omega)$ equals zero. However, for the more general case when $\Delta(\omega)$ is different from zero, $K(j\omega)G_1(j\omega)$ and $K(j\omega)G_2(j\omega)$ have to be located in different regions. Examining Inequality (4.22), these regions should have an offset of $\Delta(\omega)$ between them. This is why $K(j\omega)G_1(j\omega)$ should be between the lines $d_{l,1}$ and $d_{u,1}$ ($d_{l,1}$ and $d_{u,1}$ have a phase difference of, respectively, $-\pi/4 - \Delta(\omega)/2$ and $\pi/4 - \Delta(\omega)/2$ with respect to $1 + L_d(j\omega)$) and $K(j\omega)G_2(j\omega)$ between the lines $d_{l,2}$ and $d_{u,2}$ ($d_{l,2}$

and $d_{u,2}$ have a phase difference of, respectively, $-\pi/4 + \Delta(\omega)/2$ and $\pi/4 + \Delta(\omega)/2$ with respect to $1 + L_d(j\omega)$ (see Fig. 4.2).

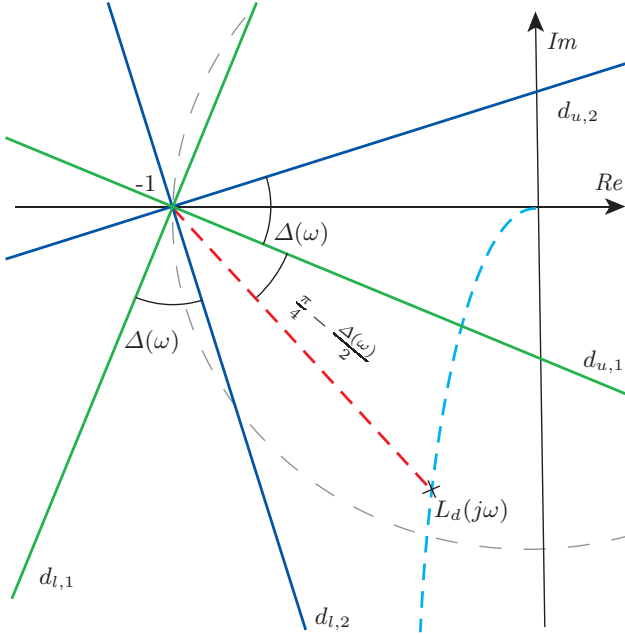


Fig. 4.2. Linear constraints to ensure quadratic stability in the Nyquist diagram.

Representing by linear constraints

The line $d_{u,1}$ can be described by:

$$y - m_{u,1}(\omega)x - m_{u,1}(\omega) = 0 \quad (4.24)$$

where x and y are, respectively, the coordinates of the real and imaginary axes and $m_{u,1}(\omega)$ the slope of $d_{u,1}$ at the frequency ω . Depending on the value of $\Delta(\omega)$ the constraints for $K(j\omega)G_1(j\omega)$ will be changed. Two cases should be considered. In the first case, when $-3\pi/4 < \Delta(\omega)/2 < \pi/4$, $K(j\omega)G_1(j\omega)$ and $L_d(j\omega)$ must be on the same side of $d_{u,1}$. This can be expressed by the following linear constraint:

$$\begin{aligned} & (\mathcal{I}_{L_d}(\omega) - m_{u,1}(\omega)\mathcal{R}_{L_d}(\omega) - m_{u,1}(\omega)) \\ & (\rho^T(\mathcal{I}_1(\omega) - m_{u,1}(\omega)\mathcal{R}_1(\omega)) - m_{u,1}(\omega)) \geq 0 \end{aligned} \quad (4.25)$$

where $\mathcal{I}_{L_d}(\omega)$ and $\mathcal{R}_{L_d}(\omega)$ are, respectively, the imaginary and real parts of $L_d(j\omega)$. This case is shown in Fig. 4.2. In the second case, when $\pi/4 < \Delta(\omega)/2 < 5\pi/4$, $K(j\omega)G_1(j\omega)$ and $L_d(j\omega)$ must not be on the same side of $d_{u,1}$, consequently \geq in Inequality (4.25) should be replaced by \leq . For the sake of simplicity, the following function is defined:

$$f_1(\Delta(\omega)) = \text{sgn} \left(\cos \left(\frac{\Delta(\omega)}{2} + \frac{\pi}{4} \right) \right) \quad (4.26)$$

which is negative when $\pi/4 < \Delta(\omega)/2 < 5\pi/4$. Thus, the following linear constraint is defined regardless of the value of $\Delta(\omega)/2$:

$$\begin{aligned} & f_1(\Delta(\omega))[\mathcal{I}_{L_d}(\omega) - m_{u,1}(\omega)\mathcal{R}_{L_d}(\omega) - m_{u,1}(\omega)] \\ & [\rho^T(\mathcal{I}_1(\omega) - m_{u,1}(\omega)\mathcal{R}_1(\omega)) - m_{u,1}(\omega)] \geq 0 \end{aligned} \quad (4.27)$$

For similar reason we define:

$$f_2(\Delta(\omega)) = \text{sgn} \left(\cos \left(\frac{\Delta(\omega)}{2} - \frac{\pi}{4} \right) \right) \quad (4.28)$$

Thus, linear constraints can be written for lines $d_{l,1}$, $d_{u,2}$ and $d_{l,2}$:

$$\begin{aligned} & f_2(\Delta(\omega))[\mathcal{I}_{L_d}(\omega) - m_{l,1}(\omega)\mathcal{R}_{L_d}(\omega) - m_{l,1}(\omega)] \\ & [\rho^T(\mathcal{I}_1(\omega) - m_{l,1}(\omega)\mathcal{R}_1(\omega)) - m_{l,1}(\omega)] \geq 0 \end{aligned} \quad (4.29)$$

$$f_2(\Delta(\omega))[\mathcal{I}_{L_d}(\omega) - m_{u,2}(\omega)\mathcal{R}_{L_d}(\omega) - m_{u,2}(\omega)] \\ [\rho^T(\mathcal{I}_2(\omega) - m_{u,2}(\omega)\mathcal{R}_2(\omega)) - m_{u,2}(\omega)] \geq 0 \quad (4.30)$$

$$f_1(\Delta(\omega))[\mathcal{I}_{L_d}(\omega) - m_{l,2}(\omega)\mathcal{R}_{L_d}(\omega) - m_{l,2}(\omega)] \\ [\rho^T(\mathcal{I}_2(\omega) - m_{l,2}(\omega)\mathcal{R}_2(\omega)) - m_{l,2}(\omega)] \geq 0 \quad (4.31)$$

where $m_{l,1}(\omega)$, $m_{u,2}(\omega)$ and $m_{l,2}(\omega)$ are, respectively, the slopes of $d_{l,1}$, $d_{u,2}$ and $d_{l,2}$ at the frequency ω . It should be noted that when one of these lines is vertical at a particular frequency, the slope becomes infinity. Thus, the inequalities given above should not be used. For example, (4.27) should be replaced by:

$$f_1(\Delta(\omega))[\mathcal{R}_{L_d}(\omega) + 1][\rho^T\mathcal{R}_1(\omega) + 1] \geq 0. \quad (4.32)$$

These new constraints assure the quadratic stability between two systems. Thus, they should simply be added to the optimization problems defined in Chapter 2 in order to guarantee the quadratic stability of systems with two subsystems in the set. For this purpose, a sufficient number of frequencies should be chosen between 0 and infinity. For example, when the quadratic stability is needed, the optimization problem (2.22) becomes:

$$\max_{\rho} k_0$$

subject to:

$$\begin{aligned} & \rho^T(\cot \alpha \mathcal{I}_i(\omega_k) - \mathcal{R}_i(\omega_k)) + \ell \leq 1 \quad \forall \omega_k, i = 1, 2 \\ & f_1(\Delta(\omega_k))[\mathcal{I}_{L_d}(\omega_k) - m_{u,1}(\omega_k)\mathcal{R}_{L_d}(\omega_k) - m_{u,1}(\omega_k)] \\ & [\rho^T(\mathcal{I}_1(\omega_k) - m_{u,1}(\omega_k)\mathcal{R}_1(\omega_k)) - m_{u,1}(\omega_k)] \geq 0 \quad \forall \omega_k \\ & f_2(\Delta(\omega_k))[\mathcal{I}_{L_d}(\omega_k) - m_{l,1}(\omega_k)\mathcal{R}_{L_d}(\omega_k) - m_{l,1}(\omega_k)] \\ & [\rho^T(\mathcal{I}_1(\omega_k) - m_{l,1}(\omega_k)\mathcal{R}_1(\omega_k)) - m_{l,1}(\omega_k)] \geq 0 \quad \forall \omega_k \\ & f_2(\Delta(\omega_k))[\mathcal{I}_{L_d}(\omega_k) - m_{u,2}(\omega_k)\mathcal{R}_{L_d}(\omega_k) - m_{u,2}(\omega_k)] \\ & [\rho^T(\mathcal{I}_2(\omega_k) - m_{u,2}(\omega_k)\mathcal{R}_2(\omega_k)) - m_{u,2}(\omega_k)] \geq 0 \quad \forall \omega_k \\ & f_1(\Delta(\omega_k))[\mathcal{I}_{L_d}(\omega_k) - m_{l,2}(\omega_k)\mathcal{R}_{L_d}(\omega_k) - m_{l,2}(\omega_k)] \\ & [\rho^T(\mathcal{I}_2(\omega_k) - m_{l,2}(\omega_k)\mathcal{R}_2(\omega_k)) - m_{l,2}(\omega_k)] \geq 0 \quad \forall \omega_k \end{aligned} \quad (4.33)$$

In the theory developed above, the same controller is used for the two systems, but it should be noted that each system can have its own controller only with minor changes in the optimization problem, as long as the controllers have the same denominator. If it is not the case, the definition of $\Delta(\omega)$ must be replaced by:

$$\begin{aligned} \Delta(\omega) = \arg(G_{d,1}(j\omega)) + \arg(K_{d,1}(j\omega)) \\ - \arg(G_{d,2}(j\omega)) - \arg(K_{d,2}(j\omega)) \end{aligned} \quad (4.34)$$

4.2.3 Linear constraints to assure quadratic stability of certain classes of LPV systems

The new linear constraints presented in the last subsection can also be used to guarantee the quadratic stability of LPV systems whose closed-loop characteristic polynomials have an affine dependency on one scheduling parameter. In this case, in order to ensure the quadratic stability of these systems, it is sufficient to impose the quadratic stability constraints on the two open-loop systems corresponding to the extremities of the range of the scheduling parameter. In particular, this class of systems is composed by:

- LPV systems with affine dependency on one scheduling parameter with fixed controllers.
- LPV systems with affine dependency on one scheduling parameter only in the denominator with LPV controllers with affine dependency on one scheduling parameter. For example, to guarantee the global stability of this class of system, the optimization problem (3.15) becomes:

$$\max_M K_{\min}$$

subject to:

$$\begin{aligned}
& (M\bar{\theta}_l)^T (\cot \alpha \mathcal{I}(\omega_k, \theta_l) - \mathcal{R}(\omega_k, \theta_l)) + \ell \leq 1 \\
& \quad \forall \omega_k, \quad l = 1, \dots, m \\
& \sum_{i=1}^{n_p} \gamma_i \rho_i(\theta_1) - K_{\min} \geq 0 \\
& \sum_{i=1}^{n_p} \gamma_i \rho_i(\theta_m) - K_{\min} \geq 0 \\
& f_1(\Delta(\omega_k)) [\mathcal{I}_{L_d}(\omega_k) - m_{u,1}(\omega_k) \mathcal{R}_{L_d}(\omega_k) - m_{u,1}(\omega_k)] \\
& [\rho^T (\mathcal{I}(\omega_k, \theta_1) - m_{u,1}(\omega_k) \mathcal{R}(\omega_k, \theta_1)) - m_{u,1}(\omega_k)] \quad (4.35) \\
& \geq 0 \quad \forall \omega_k \\
& f_2(\Delta(\omega_k)) [\mathcal{I}_{L_d}(\omega_k) - m_{l,1}(\omega_k) \mathcal{R}_{L_d}(\omega_k) - m_{l,1}(\omega_k)] \\
& [\rho^T (\mathcal{I}(\omega_k, \theta_1) - m_{l,1}(\omega_k) \mathcal{R}(\omega_k, \theta_1)) - m_{l,1}(\omega_k)] \\
& \geq 0 \quad \forall \omega_k \\
& f_2(\Delta(\omega_k)) [\mathcal{I}_{L_d}(\omega_k) - m_{u,2}(\omega_k) \mathcal{R}_{L_d}(\omega_k) - m_{u,2}(\omega_k)] \\
& [\rho^T (\mathcal{I}(\omega_k, \theta_m) - m_{u,2}(\omega_k) \mathcal{R}(\omega_k, \theta_m)) - m_{u,2}(\omega_k)] \\
& \geq 0 \quad \forall \omega_k \\
& f_1(\Delta(\omega_k)) [\mathcal{I}_{L_d}(\omega_k) - m_{l,2}(\omega_k) \mathcal{R}_{L_d}(\omega_k) - m_{l,2}(\omega_k)] \\
& [\rho^T (\mathcal{I}(\omega_k, \theta_m) - m_{l,2}(\omega_k) \mathcal{R}(\omega_k, \theta_m)) - m_{l,2}(\omega_k)] \\
& \geq 0 \quad \forall \omega_k
\end{aligned}$$

An example is given in Section 4.4 to illustrate the method.

It should be noted that for other classes of LPV systems, these additional constraints do not guarantee the quadratic stability. Nevertheless, they guarantee that the systems corresponding to the extremities of the range of the scheduling parameter are quadratically stable, which is a necessary but not sufficient condition for quadratic stability of LPV systems.

4.3 Quadratic Stability of Three Systems

4.3.1 Basic idea

As it is explained in Subsection 4.2.2, the new linear constraints guarantee the quadratic stability of switched systems composed of two subsystems. A question directly arises: is it possible to extend this result to more than two subsystems? In other words, is the equivalence between SPRness and quadratic stability presented in Subsection 4.2.1 for two stable polynomials extensible to three polynomials? The answer to this question is given in [37] where it is proved that the SPRness of the ratio of each pair of polynomials is not sufficient to guarantee the quadratic stability of the three systems associated with these polynomials. In other words, pairwise quadratic stability of three systems is not sufficient to guarantee their quadratic stability.

The question that arises from this fact is: what is the region in the space of the coefficients of the polynomials that is quadratically stable if the three systems are pairwise quadratically stable? The theorem presented below answers to this question.

Theorem 4.2 *Consider $c_1(s)$, $c_2(s)$ and $c_3(s)$, three stable polynomials of order n and A_1 , A_2 and A_3 , their associated matrix. If the ratio of each pair of polynomials, $\frac{c_1(s)}{c_2(s)}$, $\frac{c_1(s)}{c_3(s)}$ and $\frac{c_2(s)}{c_3(s)}$, is SPR, then the three matrices A_4 , A_5 and A_6 associated with the stable polynomials $c_4(s)$, $c_5(s)$ and $c_6(s)$ are quadratically stable, where $c_4(s) = \frac{c_1(s)+c_2(s)}{2}$, $c_5(s) = \frac{c_2(s)+c_3(s)}{2}$ and $c_6(s) = \frac{c_3(s)+c_1(s)}{2}$.*

Proof: Define P_1 as the common Lyapunov matrix for A_1 and A_2 , P_2 as the common Lyapunov matrix for A_2 and A_3 and P_3 as the common Lyapunov matrix for A_3 and A_1 . Consider the transfer function $\frac{c_2(s)}{c_1(s)}$. Using the KYP lemma, $\frac{c_2(s)}{c_1(s)}$ is SPR iff [40]:

$$\exists P_1 = P_1^T > 0 \text{ s.t. } \begin{bmatrix} A_1^T P_1 + P_1 A_1 & P_1 B - (C_2 - C_1)^T \\ B^T P_1 - (C_2 - C_1) & -2 \end{bmatrix} < 0. \quad (4.36)$$

For the same reason, $\frac{c_3(s)}{c_1(s)}$ is SPR iff;

$$\begin{aligned} \exists P_3 = P_3^T > 0 \text{ s.t.} \\ \begin{bmatrix} A_1^T P_3 + P_3 A_1 & P_3 B - (C_3 - C_1)^T \\ B^T P_3 - (C_3 - C_1) & -2 \end{bmatrix} < 0. \end{aligned} \quad (4.37)$$

By adding (4.36) and (4.37), we get:

$$\begin{aligned} \begin{bmatrix} A_1^T (P_1 + P_3) + (P_1 + P_3) A_1 \\ B^T (P_1 + P_3) - (C_2 + C_3 - 2C_1) \\ (P_1 + P_3) B - (C_2 + C_3 - 2C_1)^T \\ -4 \end{bmatrix} < 0. \end{aligned} \quad (4.38)$$

Dividing (4.38) by 2, we get the condition for $\frac{(c_2(s)+c_3(s))/2}{c_1(s)}$ to be SPR. According to the results of Theorem 4.1, it means that $P_1 + P_3$ is a Lyapunov matrix for $(A_2 + A_3)/2$. Additionally, P_2 is also a Lyapunov matrix for $(A_2 + A_3)/2$, thus $P_1 + P_2 + P_3$ is a Lyapunov matrix for $(A_2 + A_3)/2$. Similarly, we can show that $P_1 + P_2 + P_3$ is a Lyapunov matrix for $(A_1 + A_2)/2$ and $(A_1 + A_3)/2$. Since $(A_2 + A_3)/2$ is A_5 , $(A_1 + A_2)/2$ is A_4 and $(A_1 + A_3)/2$ is A_6 , the three matrices A_4 , A_5 and A_6 are quadratically stable. ■

Remarks:

- This theorem is graphically represented in Fig. 4.3. The dashed triangle has polynomials at each corner whose associated systems are pairwise quadratically stable, while the associated systems of all polynomials in the filled triangle are quadratically stable.
- This theorem can be extended to more than three systems using the same idea. The problem is that, with more systems, the region of quadratic stability becomes very small, leading to a very conservative result.
- As Theorem 4.1, this theorem is developed for continuous-time systems. Once again, a similar theorem can be stated for discrete-time systems. This theorem is developed in Appendix A.

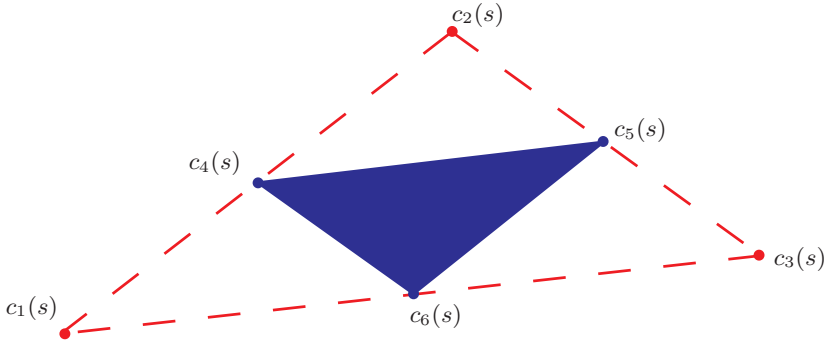


Fig. 4.3. Region of quadratic stability (filled) in the space of the coefficients of the polynomials.

4.3.2 Linear constraints to assure quadratic stability of three systems

As it is explained in the previous subsection, in order to guarantee the quadratic stability of three systems having A_4 , A_5 and A_6 as state matrices, it is sufficient to constrain the systems having A_1 , A_2 and A_3 as state matrices to be pairwise quadratically stable. This can be done using the linear constraints presented in Subsection 4.2.2. In order to use these constraints, the transfer functions $G_1(s)$, $G_2(s)$ and $G_3(s)$ representing the open-loop systems have to be built given $G_4(s)$, $G_5(s)$ and $G_6(s)$. To do it, consider the relation between $c_4(s)$, $c_5(s)$ and $c_6(s)$ and $c_1(s)$, $c_2(s)$ and $c_3(s)$:

$$\begin{bmatrix} c_4(s) \\ c_5(s) \\ c_6(s) \end{bmatrix} = \begin{bmatrix} 1/2 & 1/2 & 0 \\ 0 & 1/2 & 1/2 \\ 1/2 & 0 & 1/2 \end{bmatrix} \begin{bmatrix} c_1(s) \\ c_2(s) \\ c_3(s) \end{bmatrix} \quad (4.39)$$

The inversion of the matrix (4.39) yields:

$$\begin{bmatrix} c_1(s) \\ c_2(s) \\ c_3(s) \end{bmatrix} = \begin{bmatrix} 1 & -1 & 1 \\ 1 & 1 & -1 \\ -1 & 1 & 1 \end{bmatrix} \begin{bmatrix} c_4(s) \\ c_5(s) \\ c_6(s) \end{bmatrix} \quad (4.40)$$

Using the property that $c_i(s)$ is the characteristic polynomial of the closed-loop system having A_i as state matrix, we can write:

$$\begin{aligned} c_1(s) &= c_4(s) - c_5(s) + c_6(s) \\ &= K_d(s)G_{d,4}(s) + K_n(s)G_{n,4}(s) \\ &\quad - K_d(s)G_{d,5}(s) - K_n(s)G_{n,5}(s) \\ &\quad + K_d(s)G_{d,6}(s) + K_n(s)G_{n,6}(s) \\ &= K_d(s)(G_{d,4}(s) - G_{d,5}(s) + G_{d,6}(s)) \\ &\quad + K_n(s)(G_{n,4}(s) - G_{n,5}(s) + G_{n,6}(s)) \\ &= K_d(s)G_{d,1}(s) + K_n(s)G_{n,1}(s) \end{aligned} \quad (4.41)$$

Thus, the transfer function $G_1(s)$ is:

$$G_1(s) = \frac{G_{n,4}(s) - G_{n,5}(s) + G_{n,6}(s)}{G_{d,4}(s) - G_{d,5}(s) + G_{d,6}(s)} \quad (4.42)$$

Similarly:

$$G_2(s) = \frac{G_{n,4}(s) + G_{n,5}(s) - G_{n,6}(s)}{G_{d,4}(s) + G_{d,5}(s) - G_{d,6}(s)} \quad (4.43)$$

$$G_3(s) = \frac{-G_{n,4}(s) + G_{n,5}(s) + G_{n,6}(s)}{-G_{d,4}(s) + G_{d,5}(s) + G_{d,6}(s)} \quad (4.44)$$

It should be noted that $G_1(s)$, $G_2(s)$ and $G_3(s)$ are not necessarily stable, even if $G_4(s)$, $G_5(s)$ and $G_6(s)$ are stable. Considering that this frequency-domain method only applies to stable systems, the stability of $G_1(s)$, $G_2(s)$ and $G_3(s)$ should be tested a priori. If $G_1(s)$, $G_2(s)$ or $G_3(s)$ are not stable, the method can not be applied.

In order to guarantee the quadratic stability of switched systems composed of three subsystems $G_4(s)$, $G_5(s)$ and $G_6(s)$, it is now sufficient to use the constraints presented in Subsection 4.2.2 on the pairs

$\{K(s)G_1(s), K(s)G_2(s)\}$, $\{K(s)G_1(s), K(s)G_3(s)\}$ and $\{K(s)G_2(s), K(s)G_3(s)\}$.

As for the previous case, each subsystem ($G_4(s)$, $G_5(s)$ and $G_6(s)$) can have its own controller ($K_4(s)$, $K_5(s)$ and $K_6(s)$). In this case, the linear constraints should be applied to the pairs $\{K_1(s)G_1(s), K_2(s)G_2(s)\}$, $\{K_1(s)G_1(s), K_3(s)G_3(s)\}$ and $\{K_2(s)G_2(s), K_3(s)G_3(s)\}$ where:

$$K_1(s)G_1(s) = \frac{K_{n,4}(s)G_{n,4}(s) - K_{n,5}(s)G_{n,5}(s) + K_{n,6}(s)G_{n,6}(s)}{K_d(s)(G_{d,4}(s) - G_{d,5}(s) + G_{d,6}(s))} \quad (4.45)$$

$$K_2(s)G_2(s) = \frac{K_{n,4}(s)G_{n,4}(s) + K_{n,5}(s)G_{n,5}(s) - K_{n,6}(s)G_{n,6}(s)}{K_d(s)(G_{d,4}(s) + G_{d,5}(s) - G_{d,6}(s))} \quad (4.46)$$

$$K_3(s)G_3(s) = \frac{-K_{n,4}(s)G_{n,4}(s) + K_{n,5}(s)G_{n,5}(s) + K_{n,6}(s)G_{n,6}(s)}{K_d(s)(-G_{d,4}(s) + G_{d,5}(s) + G_{d,6}(s))} \quad (4.47)$$

Once again, if the denominators of the controllers are different, (4.34) must be used.

An interesting result in [37] should be noted: N_m stable second order LTI systems are quadratically stable if every three-tuple of systems is quadratically stable. As we can constrain three systems to be quadratically stable, we can constrain N_m second-order systems to be quadratically stable.

The design of controllers for a switched system composed of three subsystems is illustrated in the next section.

4.4 Simulation Results

4.4.1 Switched system with two subsystems

To show the effectiveness of the method, it is applied to the following switched system composed of two subsystems:

$$G_1(s) = \frac{0.5}{s^2 + 0.2s + 0.5} \quad , \quad G_2(s) = \frac{1.5}{s^2 + 0.2s + 1.5}.$$

The objective is to design a PID controller with the following structure:

$$K(s) = \frac{K_d s^2 + K_p s + K_i}{s(1 + Ts)} \quad (4.48)$$

for each subsystem maximizing the performance in terms of tracking. Two cases are addressed: first, two controllers will be designed without taking care of quadratic stability, then two controllers will be designed with the additional linear constraints, thus assuring quadratic stability.

For the first case, the linear programming approach that maximizes the performance in terms of tracking is used to design the two controllers. The design variables ℓ is set to 0.8 and α to 75° to get a good modulus margin and a well-damped closed loop-system. The time constant T of the filter in the PID controller is set to 0.1. To be able to use the proposed method, the subsystems $G_1(s)$ and $G_2(s)$ are evaluated at 50 logarithmically spaced points between 0.1 and 100 rad/s. Table 4.1 shows the parameters of the PID controllers $K_1(s)$ and $K_2(s)$ obtained for, respectively, the systems $G_1(s)$ and $G_2(s)$. The Nyquist plots of the open-loop transfer functions of the two subsystems with the two controllers are shown in Fig. 4.4. It can be observed that the Nyquist plots respect the linear robustness constraint (red line). The responses of the closed-loop subsystems to a set point change are shown in Fig. 4.5.

Table 4.1. Parameters of the PID controllers $K_1(s)$ and $K_2(s)$ designed for $G_1(s)$ and $G_2(s)$.

	K_d	K_p	K_i
$K_1(s)$	9.815	1.589	5.2
$K_2(s)$	3.281	0.5179	5.135

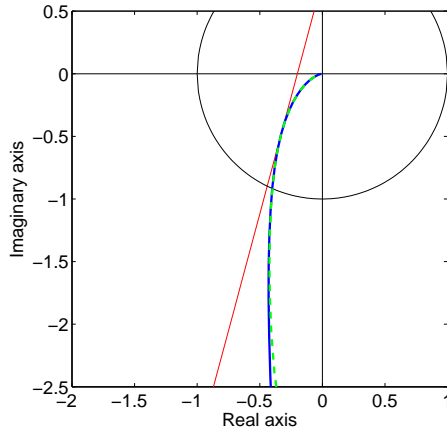


Fig. 4.4. Nyquist plots of the open-loop transfer functions $K_1(j\omega)G_1(j\omega)$ (solid) and $K_2(j\omega)G_2(j\omega)$ (dashed).

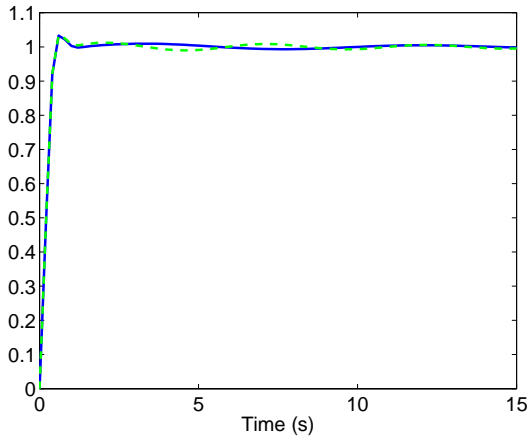


Fig. 4.5. Set point response for G_1 (solid) and G_2 (dashed).

Finally, the phase difference between the two characteristic polynomials of the two closed-loop subsystems is shown in Fig. 4.6. It can be observed that for certain frequencies, the phase difference is greater than $\pi/2$. This means that the switched system composed of these two subsystems is not quadratically stable. This is confirmed by the fact that no common Lyapunov function could be found for the two subsystems.

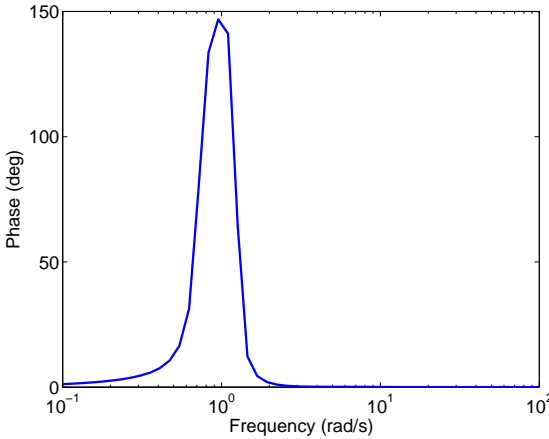


Fig. 4.6. Phase difference between the two characteristic polynomials of the closed-loop subsystems.

For the second case, the same optimization problem is used with the difference that the constraints to ensure the quadratic stability are added. In order to add these constraints, a desired open-loop transfer function $L_d(s)$ has to be chosen. $L_d(s)$ is chosen equal to $\omega_c/(s(1 + Ts))$ where ω_c is equal to 2.5 rad/s. This value is the largest for which the optimization problem is feasible.

Table 4.2 shows the parameters of the PID controllers $K_{qs,1}(s)$ and $K_{qs,2}(s)$ obtained for, respectively, the systems $G_1(s)$ and $G_2(s)$

assuring quadratic stability. The Nyquist plots of the open-loop transfer functions of the two subsystems with the two controllers are shown in Fig. 4.7. It can be observed that the Nyquist plots respect the linear robustness constraint (red line). The responses of the closed-loop subsystems to a set point change are shown in Fig. 4.8. It can be seen that the responses are a little more oscillatory than the responses of the first case (see Fig. 4.5).

Table 4.2. Parameters of the PID controllers $K_{qs,1}(s)$ and $K_{qs,2}(s)$ designed for $G_1(s)$ and $G_2(s)$ assuring quadratic stability.

	K_d	K_p	K_i
$K_{qs,1}(s)$	8.94	3.262	3.903
$K_{qs,2}(s)$	2.867	1.2	3.356

Finally, the phase difference between the two characteristic polynomials of the two closed-loop subsystems is shown in Fig. 4.9. It can be observed that for all the frequencies, the phase is smaller than $\pi/2$ in absolute value. This means that the switched system is quadratically stable. This is confirmed by the fact that a matrix P could be found satisfying the quadratic stability conditions:

$$P = \begin{bmatrix} 0.0177 & 0.0176 & 0.0588 & 0.0137 \\ 0.0176 & 0.8221 & 0.4975 & 0.6571 \\ 0.0588 & 0.4975 & 2.1600 & 0.7830 \\ 0.0137 & 0.6571 & 0.7830 & 1.8765 \end{bmatrix} \quad (4.49)$$

4.4.2 Switched system with three subsystems

To illustrate the theory developed for switched systems composed of three subsystems, consider a system with a pair of complex poles whose frequency takes three different values depending on the conditions of use ($\omega_{0,4} = \sqrt{0.8}$, $\omega_{0,5} = \sqrt{1}$ and $\omega_{0,6} = \sqrt{1.2}$). The damping

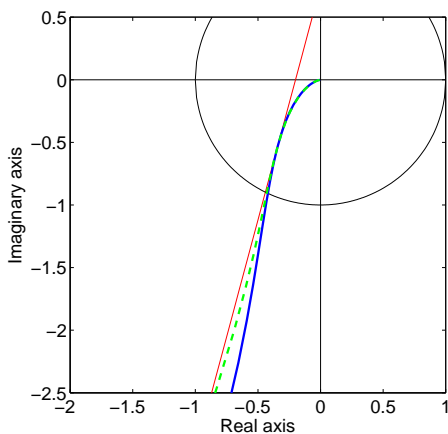


Fig. 4.7. Nyquist plots of the open-loop transfer functions $K_1(j\omega)G_1(j\omega)$ (solid) and $K_2(j\omega)G_2(j\omega)$ (dashed) guaranteeing quadratic stability.

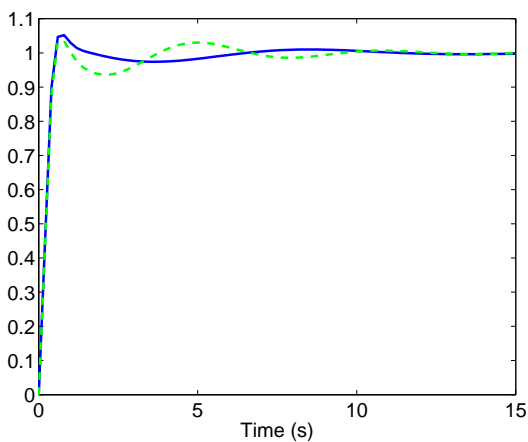


Fig. 4.8. Set point response for G_1 (solid) and G_2 (dashed) guaranteeing quadratic stability.

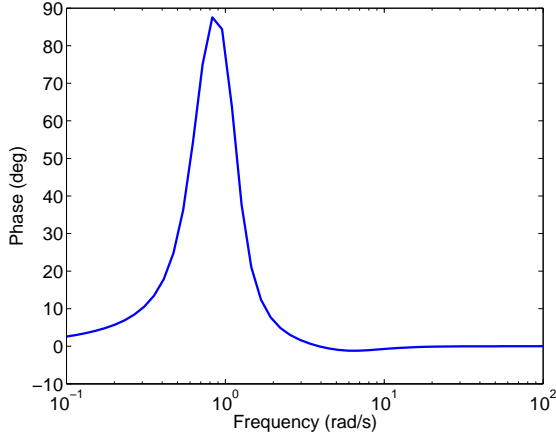


Fig. 4.9. Phase difference between the two characteristic polynomials of the closed-loop subsystems guaranteeing quadratic stability.

coefficient ζ is fixed to 0.1. Thus, the three different subsystems composing the switched system are:

$$G_{ss,4}(s) = \frac{\omega_{0,4}^2}{s^2 + 2\zeta\omega_{0,4}s + \omega_{0,4}^2} = \frac{0.8}{s^2 + 0.18s + 0.8} \quad (4.50)$$

$$G_{ss,5}(s) = \frac{\omega_{0,5}^2}{s^2 + 2\zeta\omega_{0,5}s + \omega_{0,5}^2} = \frac{1}{s^2 + 0.2s + 1} \quad (4.51)$$

$$G_{ss,6}(s) = \frac{\omega_{0,6}^2}{s^2 + 2\zeta\omega_{0,6}s + \omega_{0,6}^2} = \frac{1}{s^2 + 0.22s + 1.2} \quad (4.52)$$

The objective is to design a PID controller with the following structure:

$$K(s) = \frac{K_d s^2 + K_p s + K_i}{s(1 + Ts)} \quad (4.53)$$

for each subsystem that maximizes the performance in terms of tracking. Two cases are addressed: first, three controllers ($K_4(s)$, $K_5(s)$

and $K_6(s)$) are designed without considering quadratic stability, then three controllers ($K_{qs,4}(s)$, $K_{qs,5}(s)$ and $K_{qs,6}(s)$) are designed with the additional linear constraints assuring quadratic stability.

For the first case, the linear programming approach that maximizes the performance in terms of tracking is used to design each controller. This corresponds to the optimization problem (2.22). The design variable ℓ is set to 0.8 and α to 75° to get a good modulus margin and a well-damped closed-loop system. The time constant T of the filter in the PID controller is set to 0.1. To be able to use the proposed method, the subsystems $G_{ss,4}(s)$, $G_{ss,5}(s)$ and $G_{ss,6}(s)$ are evaluated at 100 logarithmically spaced points between 0.1 and 100 rad/s. Table 4.3 shows the parameters of the PID controllers $K_4(s)$, $K_5(s)$ and $K_6(s)$ obtained by the design method. The Nyquist plots of the open-loop transfer functions are shown in Fig. 4.10. It can be seen that the Nyquist plots respect the linear robustness margin. The responses of the closed-loop subsystems to a set point change are shown in Fig. 4.11.

Table 4.3. Parameters of the PID controllers $K_4(s)$, $K_5(s)$ and $K_6(s)$ designed for $G_{ss,4}(s)$, $G_{ss,5}(s)$ and $G_{ss,6}(s)$.

	K_d	K_p	K_i
$K_4(s)$	6.039	1.087	5.06
$K_5(s)$	4.114	0.6825	5.055
$K_6(s)$	4.897	0.8191	5.07

As explained in Subsections 4.3.1 and 4.3.2, quadratic stability is achieved if the absolute value of the phase difference between all possible pairs of characteristic polynomials of the closed-loop systems $K_1(s)G_{ss,1}$, $K_2(s)G_{ss,2}$ and $K_3(s)G_{ss,3}$ is less than 90° . $K_1(s)G_{ss,1}$, $K_2(s)G_{ss,2}$ and $K_3(s)G_{ss,3}$ are computed using (4.45), (4.46) and (4.47). These phase differences are plotted in Fig. 4.12. It is imme-

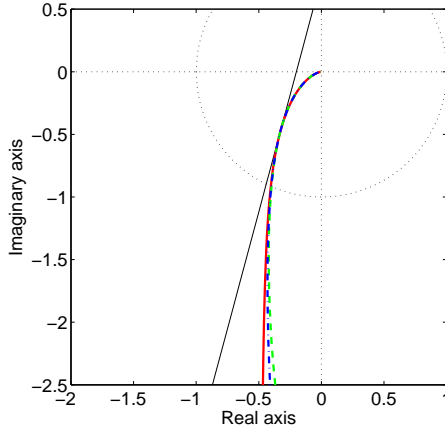


Fig. 4.10. Nyquist plots of the open-loop transfer functions $K_4(j\omega)G_{ss,4}(j\omega)$ (solid), $K_5(j\omega)G_{ss,5}(j\omega)$ (dashed) and $K_6(j\omega)G_{ss,6}(j\omega)$ (dashed-dotted).

diately seen that, for certain frequencies, the phase difference is larger than 90° . Thus, the switched system is not quadratically stable.

It is then meaningful to design three controllers $K_{qs,4}(s)$, $K_{qs,5}(s)$ and $K_{qs,6}(s)$ guaranteeing quadratic stability. In order to fulfil this requirement, the same optimization problem is used with the additional constraints on the pairs $\{K_{qs,1}(s)G_{ss,1}(s), K_{qs,2}(s)G_{ss,2}(s)\}$, $\{K_{qs,1}(s)G_{ss,1}(s), K_{qs,3}(s)G_{ss,3}(s)\}$ and $\{K_{qs,2}(s)G_{ss,2}(s), K_{qs,3}(s)G_{ss,3}(s)\}$. It should be noted that $G_{ss,1}$, $G_{ss,2}$ and $G_{ss,3}$ are stable consequently, the proposed method can be applied. To use the additional constraints, a desired open-loop transfer function $L_d(s)$ has to be chosen. $L_d(s)$ is chosen equal to $\omega_c/(s(1+Ts))$ where ω_c is equal to 4.3 rad/s, the crossover frequency obtained with the first design.

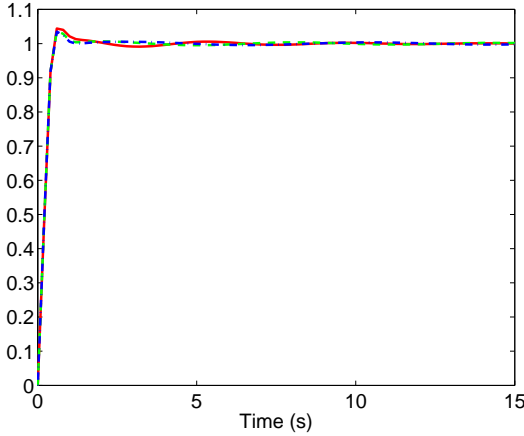


Fig. 4.11. Set point response of the closed-loop systems $K_4(s)G_{ss,4}(s)$ (solid), $K_5(s)G_{ss,5}(s)$ (dashed) and $K_6(s)G_{ss,6}(s)$ (dashed-dotted).

Table 4.4 shows the parameters of the PID controllers $K_{qs,4}(s)$, $K_{qs,5}(s)$ and $K_{qs,6}(s)$ obtained by the design. The Nyquist plots of the open-loop transfer functions are shown in Fig. 4.13. The Nyquist plots respect the linear robustness margin. Moreover they are similar with the Nyquist plots of the first design (see Fig. 4.10). The responses of the closed-loop subsystems to a set point change are shown in Fig. 4.14. They are more oscillatory than the responses obtained by the first design. This is due to the constraints added to guarantee quadratic stability.

Finally, the phase difference between all possible pairs of characteristic polynomials of the closed-loop systems $K_{qs,1}(s)G_{ss,1}(s)$, $K_{qs,2}(s)G_{ss,2}(s)$ and $K_{qs,3}(s)G_{ss,3}(s)$ are shown in Fig. 4.15. As expected, the absolute values are smaller than 90° , proving the quadratic stability. This is confirmed by the fact that a matrix P could be found satisfying the quadratic stability conditions:

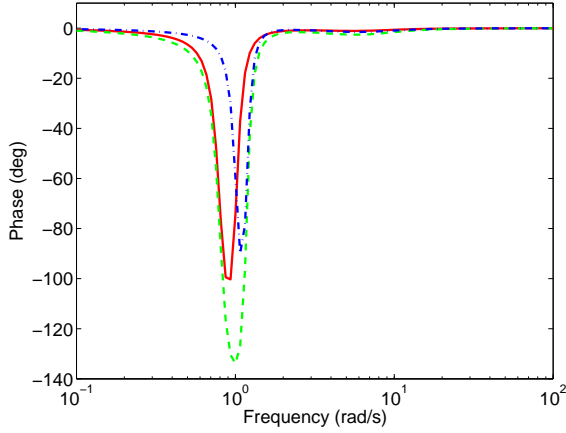


Fig. 4.12. Phase difference between the characteristic polynomials of the closed-loop systems $K_1(s)G_{ss,1}(s)$, $K_2(s)G_{ss,2}(s)$ (solid), $K_1(s)G_{ss,1}(s)$, $K_3(s)G_{ss,3}(s)$ (dashed) and $K_2(s)G_{ss,2}(s)$, $K_3(s)G_{ss,3}(s)$ (dashed-dotted).

Table 4.4. Parameters of the PID controllers $K_{qs,4}(s)$, $K_{qs,5}(s)$ and $K_{qs,6}(s)$ designed for $G_{ss,4}(s)$, $G_{ss,5}(s)$ and $G_{ss,6}(s)$ assuring quadratic stability.

	K_d	K_p	K_i
$K_{qs,4}(s)$	5.92	1.329	4.904
$K_{qs,5}(s)$	3.9	1.107	4.272
$K_{qs,6}(s)$	4.583	1.443	4.466

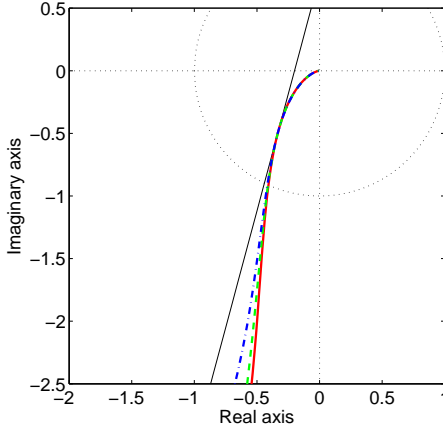


Fig. 4.13. Nyquist plots of the open-loop transfer functions $K_{qs,4}(j\omega)G_{ss,4}(j\omega)$ (solid), $K_{qs,5}(j\omega)G_{ss,5}(j\omega)$ (dashed) and $K_{qs,6}(j\omega)G_{ss,6}(j\omega)$ (dashed-dotted) guaranteeing quadratic stability.

$$P = \begin{bmatrix} 0.0236 & 0.0243 & 0.0723 & 0.0083 \\ 0.0243 & 1.2866 & 0.8864 & 1.1123 \\ 0.0723 & 0.8864 & 2.8807 & 1.1272 \\ 0.0083 & 1.1123 & 1.1272 & 3.2211 \end{bmatrix} \quad (4.54)$$

4.4.3 LPV system

In order to show the effectiveness of the method, let us consider a mass-spring-damper system where the mass changes as a function of a scheduling parameter θ . The transfer function of this system is:

$$G(s, \theta) = \frac{1}{m(\theta)s^2 + cs + k} \quad (4.55)$$

where m is the mass, c the damping coefficient and k the stiffness coefficient. The mass is an affine function of θ :

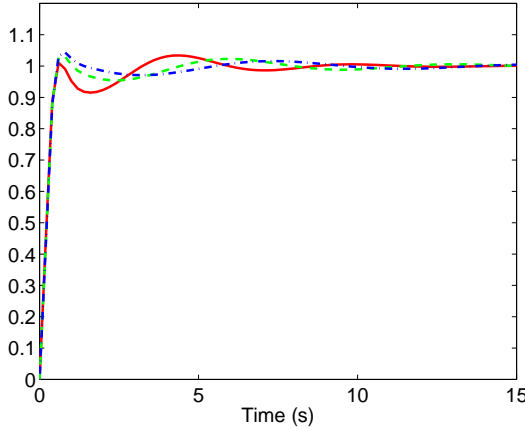


Fig. 4.14. Set point response of the closed-loop systems $K_4(s)G_{ss,4}(s)$ (solid), $K_5(s)G_{ss,5}(s)$ (dashed) and $K_6(s)G_{ss,6}(s)$ (dashed-dotted) guaranteeing quadratic stability.

$$m(\theta) = 1 + 0.5\theta \quad (4.56)$$

where

$$\theta \in [-1, 1]. \quad (4.57)$$

The damping coefficient c is equal to 0.2 and the stiffness coefficient k is equal to 1.

The objective is to design a gain-scheduled PID controller, whose parameters depend affinely on θ , maximizing the performance in terms of tracking. Thus, the controller has the following form:

$$K(s, \theta) = \frac{1}{s(1 + Ts)} [(K_{d,1}\theta + K_{d,0})s^2 + (K_{p,1}\theta + K_{p,0})s + (K_{i,1}\theta + K_{i,0})] \quad (4.58)$$

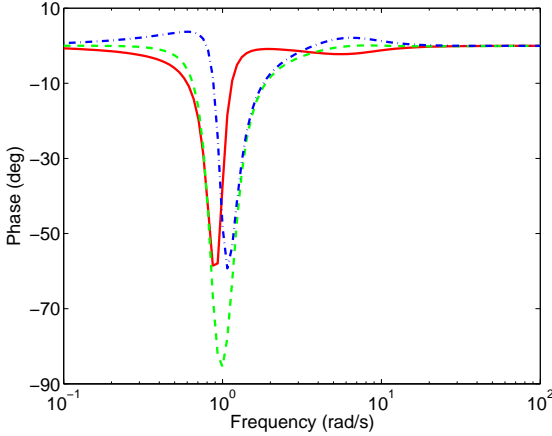


Fig. 4.15. Phase difference between the characteristic polynomials of the closed-loop systems $K_{qs,1}(s)G_{ss,1}(s)$, $K_{qs,2}(s)G_{ss,2}(s)$ (solid), $K_{qs,1}(s)G_{ss,1}(s)$, $K_{qs,3}(s)G_{ss,3}(s)$ (dashed) and $K_{qs,2}(s)G_{ss,2}(s)$, $K_{qs,3}(s)G_{ss,3}(s)$ (dashed-dotted).

Two cases are addressed: first a PID controller is designed without considering quadratic stability, then a PID controller is designed with the additional linear constraints presented in Subsection 4.2.3, thus assuring quadratic stability.

For the first case, the optimization problem (3.15) is used. To have a finite number of constraints, $G(s, \theta)$ is evaluated in 21 equally spaced discrete values of θ between -1 and 1 and in 100 logarithmically spaced discrete values of ω between 0.1 and 100 rad/s. The design variable α is set to 75° and ℓ to 0.8 to have a good robustness margin. The time constant T of the filter in the PID controller is set to 0.1. Table 4.5 shows the parameters of the gain-scheduled PID controller obtained by the design. The Nyquist plots of the open-loop transfer functions are shown in Fig. 4.16 for three particular

values of θ (-1, 0 and 1). It can be observed that the Nyquist plots respect the robustness constraint represented by the line. The set point responses of the closed-loop system are shown in Fig. 4.17.

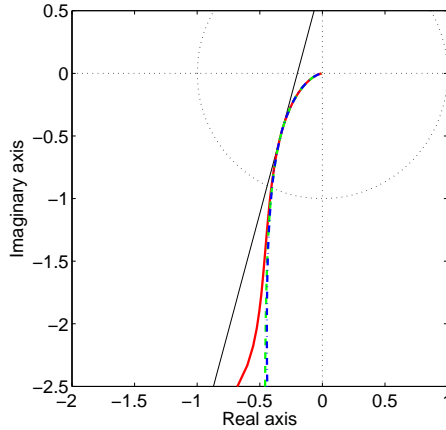


Fig. 4.16. Nyquist plots of the open-loop transfer function $K(j\omega, \theta)G(j\omega, \theta)$ for $\theta = -1$ (solid), $\theta = 0$ (dashed) and $\theta = 1$ (dashed-dotted).

Table 4.5. Parameters of the gain-scheduled PID controller.

$K_{d,1}$	$K_{d,0}$	$K_{p,1}$	$K_{p,0}$	$K_{i,1}$	$K_{i,0}$
2.4576	4.8377	-0.0936	0.9449	0	5.0111

Finally, the phase difference between the characteristic polynomial of the closed-loop system in $\theta = -1$ and in $\theta = 1$ can be observed in Fig. 4.18. As it can be seen, the absolute value of this difference is

larger than 90° for certain frequencies. According to Theorem 4.1, it means that the closed-loop system is not quadratically stable. This is confirmed by the fact that no common Lyapunov function could be found for this closed-loop LPV system. Thus, depending on the rate of variation of θ the system can become unstable. In order to assure the quadratic stability, it is necessary to use the linear constraints presented in Subsection 4.2.3.

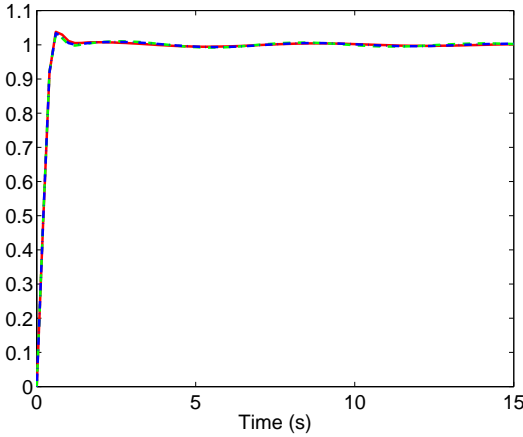


Fig. 4.17. Set point response of the closed-loop system for $\theta = -1$ (solid), $\theta = 0$ (dashed) and $\theta = 1$ (dashed-dotted).

For the second case, the optimization problem (4.35) is used. To use the additional constraints guaranteeing the quadratic stability, a desired open-loop transfer function $L_d(s)$ has to be chosen. $L_d(s)$ is chosen equal to $\omega_c/(s(1 + Ts))$ where ω_c is equal to 2.5 rad/s. This value is the largest for which the optimization problem is feasible.

Table 4.6 shows the parameters of the gain-scheduled PID controller obtained by the design assuring quadratic stability. The

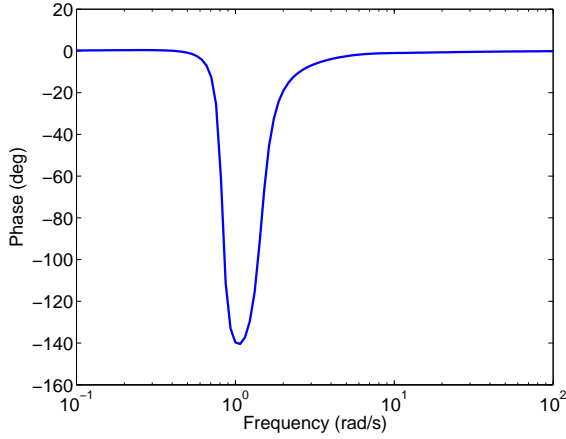


Fig. 4.18. Phase difference between the characteristic polynomial of the closed-loop system in $\theta = -1$ and in $\theta = 1$.

Nyquist plots of the open-loop transfer functions are shown in Fig. 4.19 for three particular values of θ (-1, 0 and 1). It can be observed that they respect the robustness constraint represented by the line.

Table 4.6. Parameters of the gain-scheduled PID controller assuring quadratic stability.

$K_{d,1}$	$K_{d,0}$	$K_{p,1}$	$K_{p,0}$	$K_{i,1}$	$K_{i,0}$
2.1093	4.3846	0.2988	1.4431	0.3386	3.4692

The set point responses of the closed-loop system are shown in Fig. 4.20. It can be observed that they are similar with the first case, although some additional constraints to guarantee quadratic stability are added. Finally, the phase difference between the characteristic

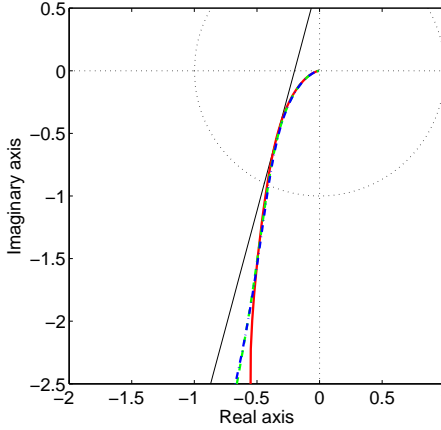


Fig. 4.19. Nyquist plots of the open-loop transfer function $K(j\omega, \theta)G(j\omega, \theta)$ for $\theta = -1$ (solid), $\theta = 0$ (dashed) and $\theta = 1$ (dashed-dotted) guaranteeing quadratic stability.

polynomial of the closed-loop system in $\theta = -1$ and in $\theta = 1$ can be observed in Fig. 4.21. Since the absolute value of this difference is smaller than 90° for all frequencies, it proves that the quadratic stability is achieved. This is confirmed by the fact that a matrix P could be found satisfying the quadratic stability conditions:

$$P = \begin{bmatrix} 0.0143 & 0.0150 & 0.0517 & 0.0129 \\ 0.0150 & 0.6800 & 0.4328 & 0.6520 \\ 0.0517 & 0.4328 & 1.8361 & 0.6717 \\ 0.0129 & 0.6520 & 0.6717 & 1.8731 \end{bmatrix} \quad (4.59)$$

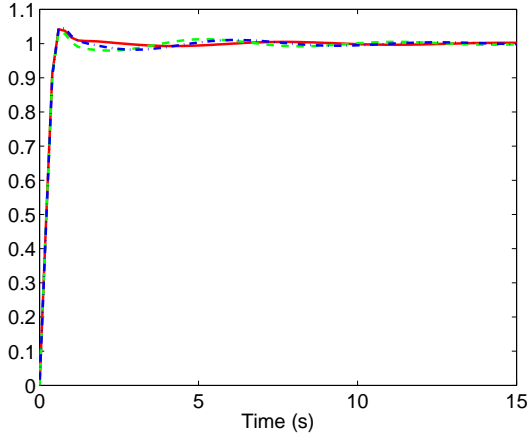


Fig. 4.20. Set point response of the closed-loop system for $\theta = -1$ (solid), $\theta = 0$ (dashed) and $\theta = 1$ (dashed-dotted) guaranteeing quadratic stability.

4.5 Conclusions

In this chapter, it is proposed to add new linear constraints to the optimization problems defined in Chapters 2 and 3. These new constraints allow the quadratic stability of switched systems composed of two or three subsystems and certain classes of LPV systems to be guaranteed within the design framework.

These constraints are derived from a theorem making the link between quadratic stability and SPRness properties and are based on the phase difference of two characteristic polynomials of the closed-loop systems. Thus, the discrete or continuous-time models of the systems are needed to guarantee the quadratic stability. Therefore, this method cannot be applied on frequency-domain data as it is the case with the methods presented in Chapters 2 and 3.

Simulation results show that the method can be easily used to guarantee quadratic stability of switched systems or LPV systems.

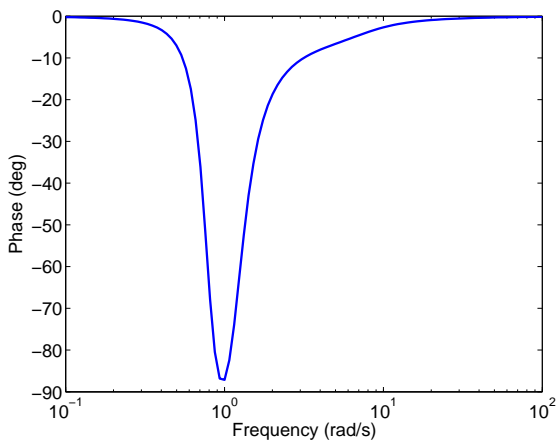


Fig. 4.21. Phase difference between the two characteristic polynomials of the closed-loop system for $\theta = -1$ and $\theta = 1$ guaranteeing quadratic stability.

Application to an Industrial Double-Axis Positioning System

5.1 Introduction

Modern mechanical systems, such as machine tools, semiconductor manufacturing equipments and automatic inspection machines, often require high-speed, high-acceleration and high-accuracy linear motion. Traditionally, these motions are realised using rotary motors connected to reduction gears and lead screws. Such mechanical transmissions, however, reduce the achievable linear motion speed, the dynamic response, introduce large frictional and inertial loads, backlash and structural flexibility. These last two points limit the accuracy of the system.

The alternative is to use linear motors. These motors are increasingly used in applications where high performances are needed. They have the following advantages:

- Higher acceleration and deceleration capabilities due to low inertia.
- No mechanical transmission chains and backlash, which gives higher accuracy and reduced friction.
- Higher mechanical stiffness so, higher natural frequencies.

However, mechanical transmission chains, which are used with rotary motors, reduce the effect of model uncertainties such as parameters variations (e.g. mass and inertia variations) and external disturbances. Such uncertainties have therefore greater effect on linear motors. Furthermore, linear motors with iron cores suffer from another disadvantage: they are subject to an important ripple force. This force has a direct effect on the motion of the load. Thus, in order to take advantage of the high-speed, high-acceleration and high-accuracy capabilities of linear motors, a control system is required to take these uncertainties, nonlinearities and disturbances into account.

The application considered in this thesis is a double-axis Linear Permanent Magnet Synchronous Motor (LPMSM) system manufactured by ETEL SA. The main objective is to improve the system's trajectory tracking performance whilst maintaining robust stability using data-driven methods.

The strategy of control is to use a two-degree of freedom controller and thereby allow tuning of the feedback loop and the precompensator individually. To design the feedback loop, the methods proposed in this thesis are used in order to take into consideration the parameter variations, unmodeled dynamics, nonlinearities and disturbances. Moreover, the use of a precompensator allows the closed-loop tracking performance to be improved without affecting the closed-loop properties.

This chapter focuses only on the design of the feedback loop. In order to design the precompensator using data-driven techniques see [6, 7] that use methods based on iterative learning control and [23] that uses a model-free precompensator tuning approach.

The outline of this chapter is the following: the system is described in Section 5.2. Section 5.3 is dedicated to the non-parametric identification of the system. In Section 5.4 robust and gain-scheduled controllers are designed and tested on the real system. A stability analysis is carried out in Section 5.5. Finally Section 5.6 gives some concluding remarks.

5.2 Description of the System

The high-precision positioning system, studied in this thesis, is composed of two LPMSMs positioned perpendicularly one above the other (see Fig. 5.1). Each motor has a stroke of 0.32 m. The

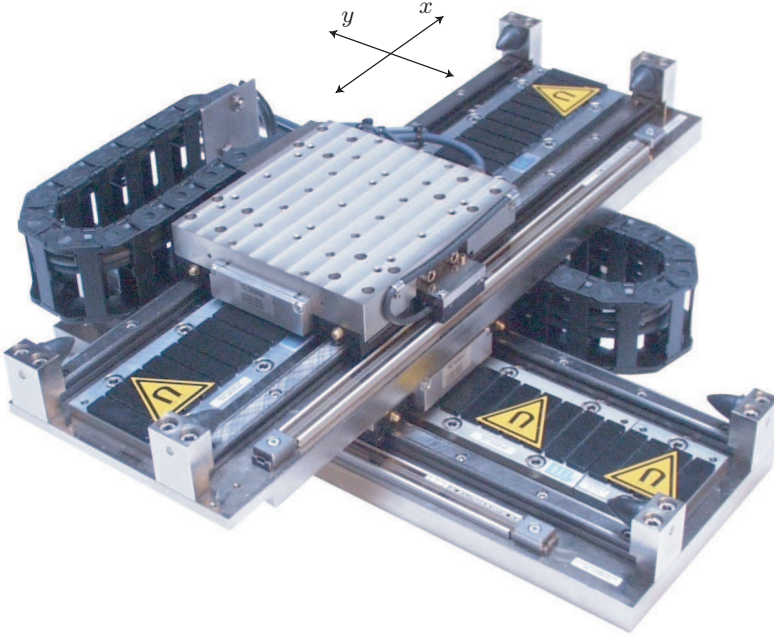


Fig. 5.1. Double-axis linear permanent magnet synchronous motor system (with courtesy of ETEL).

outputs of the system are the position of the higher axis, x , and of the lower axis, y . The positions are measured using analog position encoders whose resolution, with the help of interpolation, is 0.24 nm. The inputs consist of the desired currents. These desired

currents are transformed into desired currents for each phase of the motors. These desired phases' currents are tracked independently using current loops at a sampling frequency of 72 kHz. The positions are controlled using two-degree of freedom controllers operating at a sampling frequency of 18 kHz.

The particularity of this application is that the dynamics of each axis vary with the position of the two axes. For example, it is clear that the dynamics of the lower axis change as a function of the position of the moving part of the higher axis. If the moving part of the higher axis is at an extremity, it is connected to the lower axis with a different rigidity from the case that the moving part is at the center. Thus, this system can be considered as an LPV system whose scheduling parameters are x and y , respectively the positions of the higher and lower axes.

For the sake of succinctness, only the identification, control design and stability analysis of the higher axis is detailed.

5.3 Non-Parametric Identification

In order to measure the Frequency Response Functions (FRFs), the stroke of each axis is divided into 16 equally spaced partitions which gives a grid of 289 nodes. The higher axis is excited with a sum of sinusoidal signals from 4.4 to 9000 Hz at each position and thus 289 non-parametric models in the frequency domain are obtained. The magnitude Bode diagram of the non-parametric models of the higher axis is shown in Fig. 5.2. At low frequencies (between 10 and 100 Hz), the higher axis behaves as a single mass system, namely the amplitude plot shows a slope of -40 dB/decade. At very low frequencies, the effect of friction appears, meaning that the slope changes to -20 dB/decade. Due to the difference in the friction coefficients, the effect does not appear exactly at the same frequency. Between 100 and 140 Hz, the first decoupling of mass depending on the position can be seen (zeros, poles). At 500 and 900 Hz the same phenomenon

happens. From 1000 Hz, the magnitude Bode diagram is not plotted, since it has mainly a slope of -40 dB/decade with no important informations. In order to be convinced that the first decoupling of mass depends on the position, Fig. 5.3 and 5.4 show respectively the magnitude Bode diagram of the non-parametric models of the higher axis when $x = 0$ m and y varies from -0.16 m to 0.16 m and when x varies from -0.16 m to 0.16 m and $y = 0$ m. Both figures show clearly the above mentioned dependency.

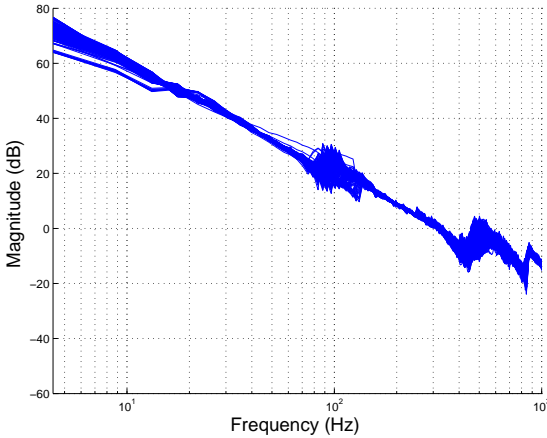


Fig. 5.2. Magnitude Bode diagram of 289 identified non-parametric models of the higher axis.

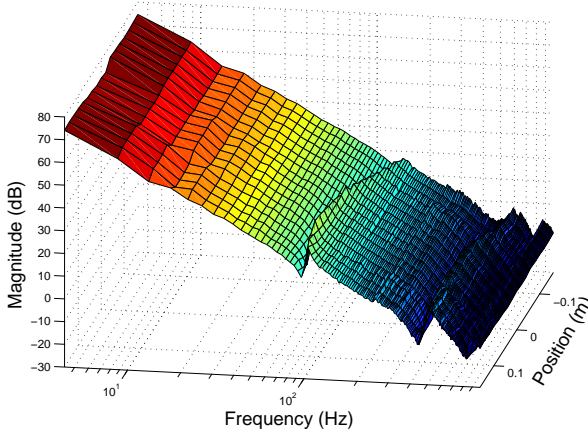


Fig. 5.3. Magnitude Bode diagram of 17 identified non-parametric models of the higher axis at $x = 0$ m and y in the interval $[-0.16, 0.16]$ m with increments of 0.02 m.

5.4 Controller Design and Experimental Results

5.4.1 Robust controller design and experimental results

First of all, the aim is to design a discrete-time controller that is robust with respect to the parameter variations and high frequency uncertainties and that maximizes the load disturbance rejection at the plant input. Therefore, the controller should contain an integrator. Let the following structure be considered for the feedback part of the controller:

$$K(z^{-1}) = \frac{S(z^{-1})}{R(z^{-1})} \quad (5.1)$$

where:

$$S(z^{-1}) = s_0 + s_1 z^{-1} + \dots + s_{n_c} z^{-n_c} \quad (5.2)$$

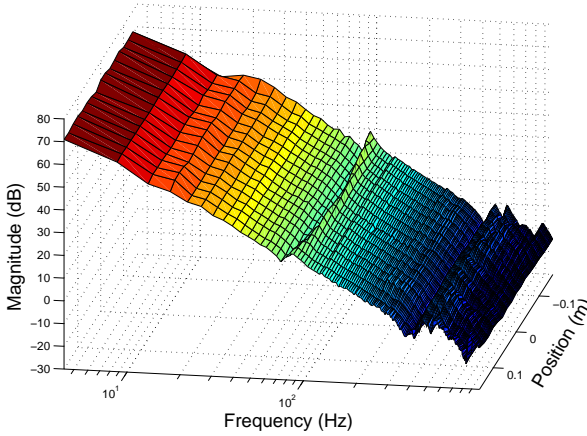


Fig. 5.4. Magnitude Bode diagram of 17 identified non-parametric models of the higher axis at x in the interval $[-0.16, 0.16]$ m with increments of 0.02 m and $y = 0$ m.

and the polynomial $R(z^{-1})$ is fixed to:

$$R(z^{-1}) = 1 - z^{-1} \quad (5.3)$$

In general, to maximize the load disturbance rejection, the low frequency gain is maximized. For a rational discrete-time controller with fixed denominator, it corresponds to maximizing the sum of the controller parameters $\sum_j s_j$. When the denominator contains only one integrator, maximizing the sum of the controller parameters corresponds to minimizing IE.

The optimization problems defined in Chapter 2 to maximize the load disturbance rejection have to be adapted to design discrete-time controller and to the case of open-loop transfer functions containing three integrators (the system contains approximately two integrators and the controller one). Thus, the optimization problem (2.23) is

adapted as follows. At very low frequencies the Nyquist diagram will be located in region II (see Fig. 2.2) but very far from the critical point. Let us suppose that the Nyquist diagram intersects d_2 in ω_l . Thus, for frequencies lower than ω_l the open-loop transfer function is not subject to any constraint. At different frequencies, the constraints used in the optimization problem (2.23) are conserved. Thus, at middle frequencies (frequencies between ω_l and ω_x), the Nyquist diagram is below d_2 (in regions III and IV) and at high frequencies in region I. Hence, the following optimization problem is considered:

$$\max_{\rho} \sum_{j=0}^{n_c} \rho_j$$

Subject to:

$$\begin{aligned} \rho^T (\cot \alpha \mathcal{I}_i(\omega_k) - \mathcal{R}_i(\omega_k)) + \ell &\leq 1 && \text{for } \omega_k > \omega_x, \\ & && i = 1, \dots, 81 \\ \rho^T (\cos \beta \mathcal{I}_i(\omega_k) + \sin \beta \mathcal{R}_i(\omega_k)) &\leq -1 && \text{for } \omega_l < \omega_k \leq \omega_x, \\ & && i = 1, \dots, 81 \end{aligned} \quad (5.4)$$

where:

$$\rho^T = [s_0 \ s_1 \ \dots \ s_{n_c}] \quad (5.5)$$

$$\mathcal{R}_i(\omega_k) = \text{Re}[\phi(e^{-j\omega_k h})G_i(e^{-j\omega_k h})] \quad (5.6)$$

$$\mathcal{I}_i(\omega_k) = \text{Im}[\phi(e^{-j\omega_k h})G_i(e^{-j\omega_k h})] \quad (5.7)$$

$$\phi^T(e^{-j\omega_k h}) = \frac{1}{1 - e^{-j\omega_k h}} [1 \ e^{-j\omega_k h} \ \dots \ e^{-jn_c \omega_k h}] \quad (5.8)$$

G_i represents the non-parametric identification of the higher axis at one position and h the sampling period (1/18000 s).

First of all, a second-order controller (equivalent to a discrete-time PID controller) is designed. The specifications regarding the linear robustness margin are set to: $\ell = 0.4$ and $\alpha = 30^\circ$. These

values lead to a minimal modulus margin of 0.2, a minimal phase margin of 12.54° and a minimal gain margin of 1.67. The lower bound of the crossover frequency ω_x is set to 170 Hz and ω_l to 80 Hz. Finally β is set to 30° in order to respect the inequalities (2.19) and (2.20). The optimization problem (5.4) is then solved using 81 non-parametric models. It should be noted that for the identification procedure 289 non-parametric models have been identified. Given that these models do not differ significantly, it is sufficient to use only 81 models for the controller design procedure (the stroke of each axis is divided into 8 equally spaced partitions which gives a grid of 81 nodes). The Nyquist plots of the open-loop transfer function for the 81 models obtained with this method are shown in Fig. 5.5. It can be noticed that the constraints are respected, thus a minimal robustness margin and a minimal bandwidth are assured for all the models. The load disturbance response of the second-order controller at the middle of the grid is shown in Fig. 5.6 (dashed-dotted line). The load disturbance response is generated by the addition of a step disturbance at the input of the system, simulating an external force disturbance of 5.87 N. This disturbance, while not being realistic, is the only way to test the designed controller. The set point response is not included, since a two-degree of freedom controller is used for this application. Thus, the feedforward part still needs to be designed.

In order to improve the result in terms of load disturbance rejection, a higher-order controller (fourth-order) is designed. The same specifications as for the second-order controller are used. The result is shown in Fig. 5.6 (dashed line). The load disturbance rejection is really improved, since the overshoot due to the disturbance is divided by more than 2.

Now, suppose that the load disturbance rejection and the crossover frequency of the second-order controller are satisfactory, but that it is required to increase the linear robustness margin. In order to fulfil this requirement, a higher order controller (fourth-order) is designed using the optimization problem (2.21) with some minor modifications. In this optimization problem, the limit represented by ω_x between the low and high frequencies is extremely

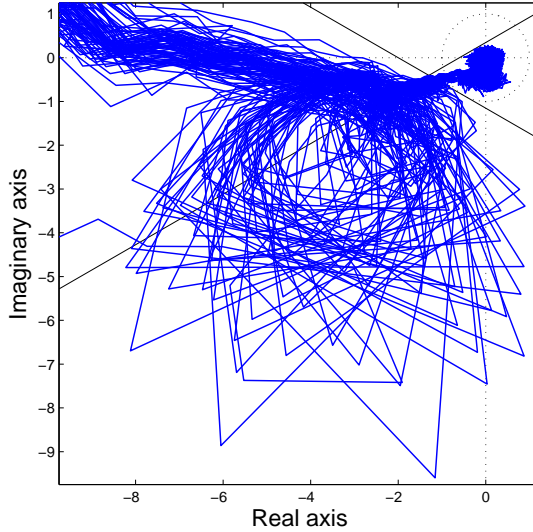


Fig. 5.5. Nyquist plots of the open-loop transfer function for the 81 models obtained with the second-order controller ($\max \sum_j \rho_j$).

hard to respect. Frequencies larger than ω_x have to be in region I, whereas frequencies lower than ω_x have to be in region III or IV (see Fig. 2.2). Since in this optimization problem 81 models are used, the limit between low and high frequencies cannot be respected for all the models, thus it can be softened by adding a margin for ω_x . Frequencies over $\omega_x + m$ have to be in region I, whereas frequencies under $\omega_x - m$ have to be in region III or IV. The second modification is due to the open-loop transfer function containing three integrators: the Nyquist diagram at very low frequencies will be located in region II (see Fig. 2.2). Thus, as for the previous optimization problem, no constraints are considered for frequencies lower than ω_l . Finally

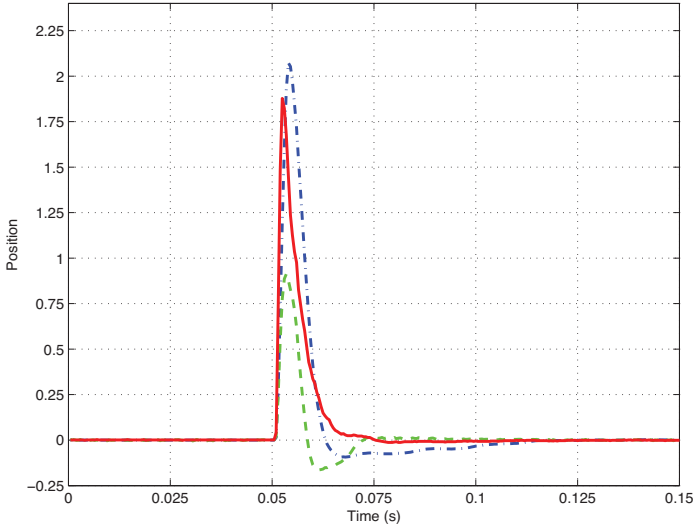


Fig. 5.6. Load disturbance responses: second-order controller ($\max \sum_j \rho_j$) (dashed-dotted), 4th-order controller ($\max \sum_j \rho_j$) (dashed), 4th-order controller ($\max \ell$ with $\sum_j \rho_j > K_{\min}$) (solid).

an additional constraint on the sum of the parameters is also added in order to preserve the load disturbance rejection achieved with the second-order controller. Hence, the following optimization problem is considered:

$$\max_{\rho} \ell$$

Subject to:

$$\rho^T (\cot \alpha \mathcal{I}_i(\omega_k) - \mathcal{R}_i(\omega_k)) + \ell \leq 1 \quad \text{for } \omega_k > \omega_x + m, \\ i = 1, \dots, 81$$

$$\rho^T (\cos \beta \mathcal{I}_i(\omega_k) + \sin \beta \mathcal{R}_i(\omega_k)) > -1 \quad \text{for } \omega_k > \omega_x + m, \\ i = 1, \dots, 81$$

$$\rho^T (\cos \beta \mathcal{I}_i(\omega_k) + \sin \beta \mathcal{R}_i(\omega_k)) \leq -1 \quad \text{for } \omega_l < \omega_k \leq \omega_x - m, \\ i = 1, \dots, 81$$

$$\sum_{j=0}^{n_c} \rho_j \geq K_{\min} \quad (5.9)$$

Given that the crossover frequency obtained with the second-order controller is equal to about 200 Hz, the lower approximation of the crossover frequency ω_x is set to 180 Hz. Then, ω_l is set to 80 Hz, α to 30° and β to 30° (in order to satisfy the inequalities (2.19) and (2.20)). Finally, K_{\min} is equal to the sum of the parameters achieved by the second-order controller. The load disturbance rejection of the designed controller is shown in Fig. 5.6 (solid line). In order to facilitate the comparison, the details of the designs are shown in Table 5.1, where ω_c stands for the crossover frequency (in [Hz]), $M_{m,\min}$ for the minimum modulus margin of the 81 models, o_d for the overshoot of the load disturbance response (in $[\mu m]$) and t_d for the settling time to 1 % of the biggest overshoot (in [s]). It can be seen that the controller designed to optimize the robustness margin has about the same load disturbance rejection capability as the second-order controller. This is normal, since they have the same sum of parameters. It should also be noted that the controller designed to maximize the linear robustness margin has a smaller modulus margin. Thus, maximizing the linear robustness margin does not lead automatically to a bigger modulus margin.

Table 5.1. Properties of the robust controllers obtained for the higher axis.

Method	Max $\sum_j \rho_j$ (order 2)	Max $\sum_j \rho_j$ (order 4)	Max ℓ with $\sum_j \rho_j > K_{\min}$ (order 4)
ω_c	198.89	215.87	200.20
$M_{m,\min}$	0.37	0.44	0.36
ℓ	0.4	0.4	0.61
$\sum_j \rho_j$	0.0019	0.0054	0.0019
o_d	2.07	0.91	1.88
t_d	0.056	0.020	0.017
IAE_d	0.0146	0.0061	0.0103
IE_d	0.0093	0.0031	0.0097

5.4.2 Gain-scheduled controller design

As explained in Section 5.3, the dynamics of the system depend on the position of the lower (y) and higher (x) axis. Thus, designing a gain-scheduled controller certainly improves the robustness and performance of the closed-loop system. As an illustration, a gain-scheduled controller is designed for the higher axis when x is around 0 m and y varies between -0.16 m to 0.16 m. The 17 non-parametric models shown in Fig. 5.3 are thus used to design this controller. The aim is to design a low-order controller that maximizes the robustness with a closed-loop bandwidth of 180 Hz. Thus, a gain-scheduled controller with the following form

$$K(z^{-1}, y) = \frac{S(z^{-1}, y)}{R(z^{-1})} \quad (5.10)$$

with

$$\begin{aligned} S(z^{-1}, y) &= s_0(y) + s_1(y)z^{-1} + s_2(y)z^{-2}, \\ R(z^{-1}) &= (1 - z^{-1}) \end{aligned}$$

is designed, where y is the scheduling parameter. The order p_c of the polynomial in y describing the parameters of the controller is

set to 2. A modified version of the optimization problem (3.13) is used. The modifications are due to the three integrators of the open-loop transfer functions (as before, for frequencies lower than ω_l no constraints are applied) and to design a discrete-time controller. Moreover, when the robustness is maximized, this may lead to a vanishing integral action of the controller. To be sure to keep the integral action (which is needed to reject the load disturbances), the following constraints are added:

$$s_0(y) + s_1(y) + s_2(y) \geq K_{\min} \quad (5.11)$$

for y in the interval $[-0.16, 0.16]$ m with increments of 0.02 m. The design variables are ω_x , ω_l , α , β and K_{\min} . The lower bound of the crossover frequency ω_x is set to 180 Hz and ω_l to 80 Hz. The value of 30° is used for α and β . By practical expertise, K_{\min} is set to 0.004. It should also be noted that, a tolerance of 5 % on ω_x is used to soften the constraints, meaning that the frequencies near ω_x (up to 5 %) can be anywhere and not necessarily in region I, III or IV.

The Nyquist plots of the open-loop transfer functions obtained by the design are shown in Fig. 5.7 for three particular values of y (-0.16 m, 0 m and 0.16 m). It can be observed that the Nyquist plots respect the constraints represented by the two lines and lead to a linear margin ℓ of 0.520. If a robust controller is designed with the same specifications, the linear robustness margin ℓ obtained is equal to 0.498. Thus, the gain-scheduled controller allows an improvement of the linear robustness margin of 4.6 %.

Unfortunately, this gain-scheduled controller could not be tested on the real application, since the firmware used does not support gain-scheduled controllers.

5.5 Stability Analysis

The idea is to analyze the stability of the higher axis in closed-loop with the designed gain-scheduled controller. To be able to do it, an

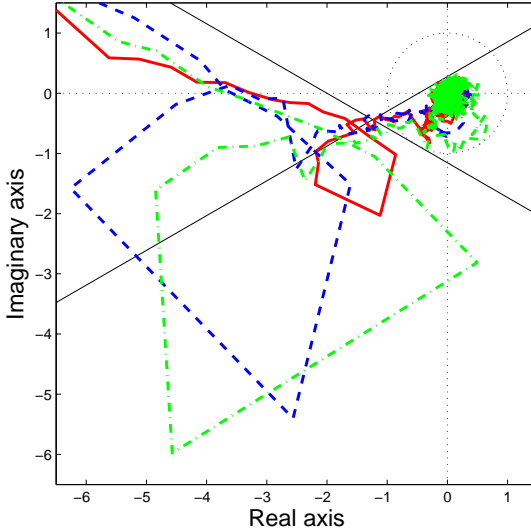


Fig. 5.7. Nyquist plots of the open-loop transfer functions of the gain-scheduled controller and the system for $y = -0.16$ m (solid), $y = 0$ m (dashed) and $y = 0.16$ m (dashed-dotted).

LPV parametric model of the higher axis is needed. Since the gain-scheduled controller is designed for x around 0 m and y between -0.16 m and 0.16 m, the LPV parametric model is also computed for x around 0 m and y between -0.16 m and 0.16 m.

5.5.1 LPV Parametric identification

In order to compute the LPV parametric model, the procedure proposed by Steinbuch et al. [38] is used, that is: (i) measuring the FRF at different positions giving non-parametric models, (ii) fitting

a discrete parametric model on each non-parametric model, (iii) combining these models by linking parameters via a polynomial fit as a function of the position. The first step of the procedure is presented in Section 5.3. 17 non-parametric models are available at the positions: $x = 0$ m and y in the interval $[-0.16, 0.16]$ m with increments of 0.02 m.

To find parametric models from frequency domain data, the method of Levy is used in continuous-time (see [33] for more details). From Fig. 5.3 it can be seen that the higher axis has a double integrator behavior as well as three resonances. Only the first one is important for control. Hence, a fourth order continuous-time model is used to fit these curves. Moreover, two poles are set to 0 to represent the double integrator effect. These models are then discretized using a sampling frequency of 2000 Hz (the Nyquist frequency is thus about 10 times greater than the resonance). Fig. 5.8 shows the Bode diagram of the discrete parametric model at $x = 0$ m and $y = 0.14$ m compared to the non-parametric model. It can be observed that the first resonance is well identified. Such a parametric model is computed for the 17 non-parametric models. Thus, the parametric models obtained have the following form:

$$G(z^{-1}) = \frac{b_4 + b_3 z^{-1} + b_2 z^{-2} + b_1 z^{-3} + b_0 z^{-4}}{1 + a_3 z^{-1} + a_2 z^{-2} + a_1 z^{-3} + a_0 z^{-4}} \quad (5.12)$$

The last step for the obtention of an LPV model is to combine these models by linking parameters via a polynomial fit as a function of the position. Fig. 5.9 shows one parameter of the numerator (b_0) and one parameter of the denominator (a_1) of the parametric models in function of y and the polynomials obtained by interpolation. It can be seen that a_1 is well fitted by a second-order polynomial. Additionally b_0 is fitted by a linear function. All the parameters of the denominator as well as the parameters of the numerator b_1 , b_2 and b_3 are also fitted by a second-order polynomial, whereas b_4 is fitted by a linear function. It should be noted that the parametric model obtained for $y = -0.10$ m does not fit adequately the corresponding

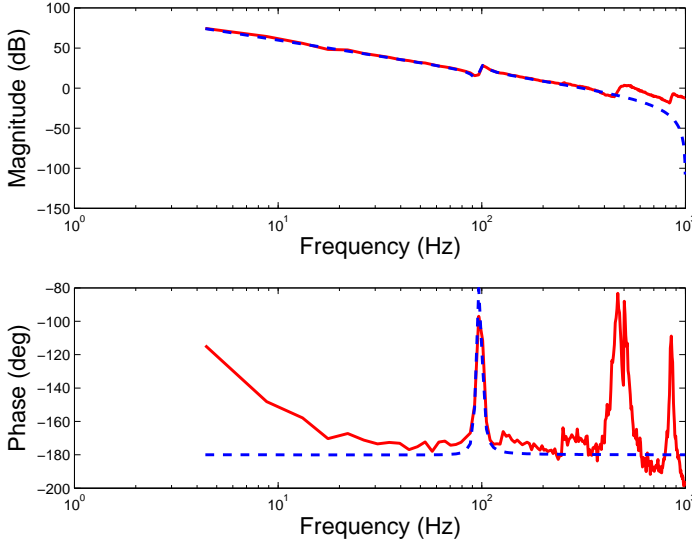


Fig. 5.8. Bode diagram of the non-parametric (solid) and discrete parametric (dashed) models for the higher axis at $x = 0$ m and $y = 0.14$ m.

non-parametric model, thus it is not taken into account to compute the polynomial fit. Fig. 5.10 shows the magnitude Bode diagram of the LPV model obtained for the higher axis at $x = 0$ m and $y \in [-0.16, 0.16]$ m. It can be observed that this model looks similar to the non-parametric models of Fig. 5.3, especially the first resonance.

It should be noted that some parameters of the LPV model depend on y and y^2 . Thus, this LPV system does not belong to the class of LPV systems described in Chapter 4 for which the quadratic stability can be assured directly within the design. For this LPV system, the stability can only be verified after the design.

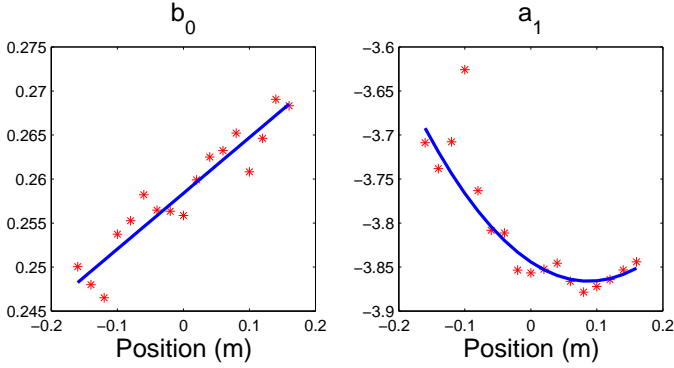


Fig. 5.9. Parameters of the numerator and denominator of the parametric models for the higher axis in function of y ($x = 0$ m and y is in the interval $[-0.16, 0.16]$ m with increments of 0.02 m) (star) and polynomials obtained by interpolation (solid line).

5.5.2 Stability analysis using Lyapunov theory

Once the LPV model is identified, the stability can be analysed. With this objective, Lyapunov stability theory is used. A closed-loop LPV system is globally stable if:

$$\begin{aligned} \exists P > 0 \quad \text{such that:} \\ A(\theta)^T P A(\theta) - P < 0 \quad \forall \theta \end{aligned} \quad (5.13)$$

Since the number of Linear Matrix Inequalities (LMIs) is infinite, the problem is not directly solvable. If the LPV model can be written in

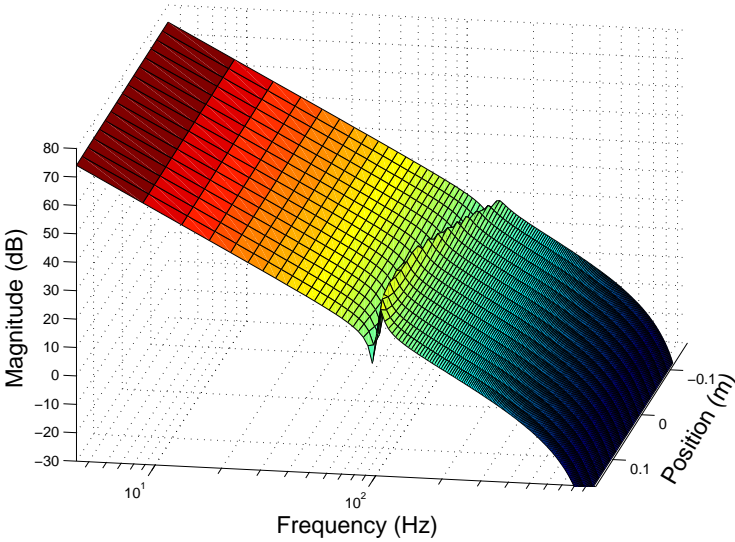


Fig. 5.10. Magnitude Bode diagram of the LPV model for the higher axis at $x = 0$ m and $y \in [-0.16, 0.16]$ m.

an affine or polytopic form, the number of LMIs is finite. Another solution to solve approximately the problem consists of gridding the scheduling parameter θ . Thus, the problem (5.13) becomes:

$$\begin{aligned} &\exists P > 0 \quad \text{such that:} \\ &A(\theta_l)^T P A(\theta_l) - P < 0 \quad \text{for } l = 1, \dots, m \end{aligned} \quad (5.14)$$

If such constraints are satisfied, the LPV system is stable whatever the speed of the scheduling parameter is. For some applications, the maximal speed of the scheduling parameter is known. Thus, this information can be taken into account to reduce the conservatism of the result by using a parameter dependent Lyapunov matrix. Thus,

the stability problem becomes:

$$\begin{aligned} \exists P_0 + \theta_l P_1 > 0 \quad \text{for } l = 1, \dots, m \quad \text{such that:} \\ A(\theta_l)^T (P_0 + \theta_{l+n} P_1) A(\theta_l) - (P_0 + \theta_{l+n} P_1) < 0 \quad \text{for } l = 1, \dots, m \end{aligned} \quad (5.15)$$

n is related to the maximal speed of the scheduling parameter: it is the maximal number of discrete scheduling values that can be reached at the next sampling time. In our case, the scheduling parameter is y , the position of the lower axis. Thus, the closed-loop LPV model is evaluated in 21 equally spaced discrete values of y between -0.16 m and 0.16 m. Then, the problem (5.15) is solved recurrently to find the maximal speed for which the system is stable. The stability could be proven for a motion of 0.08 m with a maximal speed of 9 m/s. For this application, a typical motion has an amplitude of 0.025 m and a maximal speed of 0.5 m/s. Thus, the stability obtained is sufficient.

5.6 Conclusions

In this chapter, the methodologies presented in this thesis are applied successfully to a high-precision double-axis positioning systems. Through this application, the advantages of the methodologies can be highlighted. The major advantage is that the method works directly with frequency-domain data. This is particularly useful for an industrial application, since parametric identification can be complex and time consuming. On the other hand frequency-domain data are easily obtained. The second major advantage is that the method is really simple and can be easily implemented. This is especially important for methods used on real applications.

The above mentioned advantages have convinced ETEL SA to incorporate this methodology in their products to design controllers. Previous to this work, a trial and error procedure was employed by ETEL SA for the design of controllers. Thus, this method provides

an enormous improvement in terms of time needed to design the controllers.

Conclusions and Perspectives

6.1 Contributions

In this thesis a new framework for the design of fixed-order linearly parameterized controllers is proposed. It consists of shaping the open-loop transfer functions in the Nyquist diagram by optimization under robustness and performance constraints. In order to solve this optimization problem by linear programming, the classical robustness margins are replaced by a line and the crossover frequency by another line representing a lower approximation. Subsequently, either the closed-loop performance in terms of load disturbance rejection, output disturbance rejection and tracking or the robustness margin are maximized. This new design framework provides tools to design controllers for systems using either parametric models or directly frequency-domain data. Moreover, it can also treat directly multi-model systems and systems with frequency-domain uncertainties.

An extension of this framework is proposed to design gain-scheduled controllers for LPV systems. This method uses either frequency-domain data obtained in different operating points or LPV models of the systems and needs no interpolation to get the LPV controllers.

Finally, the addition of new frequency-domain constraints to the design framework is proposed in order to guarantee the quadratic stability when designing controllers for switched systems composed of two or three subsystems or when designing controllers for certain classes of LPV systems.

This methodology is tested on numerous simulations and applied to an industrial plant that of a double-axis high-precision positioning system. The simulations and the application illustrate the efficiency of the method.

6.2 Perspectives

The extension of the new design methodology is the subject of present research undertaken by the Laboratoire d'Automatique of the Ecole Polytechnique Fédérale de Lausanne. The subject of this research is:

- Extension of the method to design controllers for multiple-input multiple-output systems.
- Extension of the method to design controllers for unstable systems.
- Extension of the method to satisfy \mathcal{H}_∞ robust performance conditions.

These extensions are the subject of different papers [14, 15, 24].

Nevertheless, there are still a number of interesting extensions that could be considered in future research. These are briefly presented below:

- The optimization problems defined in this thesis have a finite number of frequency-domain constraints for a finite number of frequency points. Thus, between two frequency points, there is no guarantee that the open-loop transfer functions satisfy the robustness and performance constraints. From a practical point of view, a sufficiently large number of frequency points should simply be considered. Nevertheless, from a theoretical point of view, it would be interesting to study this issue.

- In Chapter 4, frequency-domain conditions are presented to guarantee the quadratic stability of switched systems composed of two or three subsystems. The methodology used to define these constraints can be enlarged to guarantee quadratic stability of switched systems composed of more than three subsystems. Nevertheless, the results become very conservative. Thus, it would be interesting to search for less conservative new frequency-domain conditions to guarantee quadratic stability of switched systems composed of more than three subsystems.
- The different methods propose the design of linearly parameterized controllers, meaning that the denominators of the controllers are chosen a priori to the optimization procedure. From a theoretical point of view this is not a problem, since every transfer function can be approximated by a finite impulse response of sufficiently large order. However, from a practical point of view, it is preferred to use low-order controllers. Thus, the extension of the method to design also the denominators of the controllers would be interesting to design directly low-order controllers.
- Systems with parametric uncertainties cannot be treated by the proposed methods. Since a lot of systems have parametric uncertainties, it would be interesting to extend the methods to this kind of uncertainties.

A

Quadratic Stability and Positive Realness in Discrete Time

A.1 Quadratic Stability of Two Systems in Discrete Time

The theorem detailed in this section is the discretized version of Theorem 4.1.

Let a stable monic polynomial of order n be defined as:

$$c(z) = z^n + c_1 z^{n-1} + \dots + c_n. \quad (\text{A.1})$$

We can assign to this polynomial a vector C :

$$C = [c_1 \ c_2 \ \dots \ c_n] \quad (\text{A.2})$$

and a matrix A :

$$A = \begin{bmatrix} -c_1 & -c_2 & \dots & -c_{n-1} & -c_n \\ 1 & 0 & & 0 & 0 \\ 0 & 1 & \dots & 0 & 0 \\ \vdots & \vdots & & \vdots & \vdots \\ 0 & 0 & \dots & 1 & 0 \end{bmatrix}. \quad (\text{A.3})$$

Then the relation between SPRness and the quadratic stability in discrete time can be stated in the following theorem, which is

directly related to the equivalence between bounded real lemma and positive real lemma [1]. This result may be known by the experts in the domain. However, to the best of the author's knowledge, the way that it is formulated is new.

Theorem A.1 *Consider $c_1(z)$ and $c_2(z)$, two stable polynomials of order n , then the following statements are equivalent:*

- $\frac{c_1(z)}{c_2(z)}$ and $\frac{c_2(z)}{c_1(z)}$ are SPR.
- $|\arg(c_1(e^{j\omega h})) - \arg(c_2(e^{j\omega h}))| < \frac{\pi}{2} \quad \forall \omega$
- A_1 and A_2 are quadratically stable meaning that:
 $\exists P = P^T > 0 \in \mathbb{R}^{n \times n}$ such that
 $A_1^T P A_1 - P < 0,$
 $A_2^T P A_2 - P < 0.$

Proof: (1) \Leftrightarrow (2): This equivalence is immediate. It comes from the definition of SPR transfer function: $\frac{c_1(e^{j\omega h})}{c_2(e^{j\omega h})}$ is in the RHP, so $-\frac{\pi}{2} < \arg(c_1(e^{j\omega h})) - \arg(c_2(e^{j\omega h})) < \frac{\pi}{2} \quad \forall \omega$. For more details see [27].

(1) \Rightarrow (3): Consider the transfer function $\frac{c_1(z)}{c_2(z)}$:

$$\frac{c_1(z)}{c_2(z)} = 1 + \frac{c_1(z) - c_2(z)}{c_2(z)}. \quad (\text{A.4})$$

Using a controllable canonical form, (A.4) leads to the following state space realization:

$$\left[\begin{array}{c|c} A_2 & B \\ \hline C_1 - C_2 & 1 \end{array} \right] \quad (\text{A.5})$$

with $B = [1 \ 0 \ \dots \ 0]^T$. Using the KYP lemma for discrete-time systems, (A.5) is SPR iff [28]:

$$\exists P = P^T > 0 \text{ s.t.}$$

$$\begin{bmatrix} A_2^T P A_2 - P & A_2^T P B - (C_1 - C_2)^T \\ B^T P A_2 - (C_1 - C_2) & -2 + B^T P B \end{bmatrix} < 0. \quad (\text{A.6})$$

Using the Schur lemma, we have:

$$\begin{aligned} & A_2^T P A_2 - P - \\ & [A_2^T P B - (C_1 - C_2)^T] [-2 + B^T P B]^{-1} [B^T P A_2 - (C_1 - C_2)] < 0. \end{aligned} \quad (\text{A.7})$$

With simple matrix manipulations, we can have:

$$\begin{aligned} & [A_2 - B(C_1 - C_2)]^T P [A_2 - B(C_1 - C_2)] - P - \\ & [(A_2 - B(C_1 - C_2))^T P B - (C_2 - C_1)^T] [-2 + B^T P B]^{-1} \\ & [B^T P (A_2 - B(C_1 - C_2)) - (C_2 - C_1)] < 0 \end{aligned} \quad (\text{A.8})$$

Knowing that $A_1 = A_2 - B(C_1 - C_2)$ gives:

$$\begin{aligned} & A_1^T P A_1 - P - \\ & [A_1^T P B - (C_2 - C_1)^T] [-2 + B^T P B]^{-1} [B^T P A_1 - (C_2 - C_1)] < 0. \end{aligned} \quad (\text{A.9})$$

Since the third terms in (A.7) and (A.9) are negative semi-definite, we obtain $A_1^T P A_1 - P < 0$ and $A_2^T P A_2 - P < 0$. This proves that A_1 and A_2 are quadratically stable.

(3) \Rightarrow (1): This equivalence is proved using the bounded real lemma. If A_1 and A_2 are quadratically stable, it means that the following matrix is stable:

$$\frac{A_1 + A_2}{2} + \gamma B \frac{C_2 - C_1}{2} \quad (\text{A.10})$$

for all values of γ between -1 and 1. According to the discrete-time bounded real lemma we have [10]:

$$\begin{aligned}
& \left(\frac{A_1 + A_2}{2} \right)^T P \left(\frac{A_1 + A_2}{2} \right) - P + \\
& \left(\frac{A_1 + A_2}{2} \right)^T PB(I - B^T PB)^{-1} B^T P \left(\frac{A_1 + A_2}{2} \right) + \\
& \left(\frac{C_2 - C_1}{2} \right)^T \left(\frac{C_2 - C_1}{2} \right) < 0 \quad (\text{A.11})
\end{aligned}$$

It is well known that the bounded real lemma is equivalent to the positive real lemma with [1]:

$$\bar{A} = A - BC = \frac{A_1 + A_2}{2} - B \frac{C_2 - C_1}{2} = A_2, \quad (\text{A.12})$$

$$\bar{B} = B, \quad (\text{A.13})$$

$$\bar{C} = -2C = C_1 - C_2, \quad (\text{A.14})$$

$$\bar{D} = 1, \quad (\text{A.15})$$

and

$$\bar{P} = 2P. \quad (\text{A.16})$$

Thus, we get:

$$\begin{aligned}
\exists \bar{P} = \bar{P}^T > 0 \text{ s.t. } & \begin{bmatrix} \bar{A}^T \bar{P} \bar{A} - \bar{P} & \bar{A}^T \bar{P} \bar{B} - \bar{C}^T \\ \bar{B}^T \bar{P} \bar{A} - \bar{C} & \bar{B}^T \bar{P} \bar{B} - \bar{D} \end{bmatrix} = \\
& \begin{bmatrix} A_2^T P A_2 - P & A_2^T P B - (C_1 - C_2)^T \\ B^T P A_2 - (C_1 - C_2) & -2 + B^T P B \end{bmatrix} < 0. \quad (\text{A.17})
\end{aligned}$$

This inequality is the same as (A.6). Thus, we can conclude that $\frac{c_1(z)}{c_2(z)}$ is SPR. Using the properties of SPR systems, the inverse, $\frac{c_2(z)}{c_1(z)}$, is also SPR. \blacksquare

A.2 Quadratic Stability of Three Systems in Discrete Time

The theorem detailed in this section is the discretized version of Theorem 4.2

Theorem A.2 Consider $c_1(z)$, $c_2(z)$ and $c_3(z)$, three stable polynomials of order n and A_1 , A_2 and A_3 , their associated matrix. If the ratio of each pair of polynomials, $\frac{c_1(z)}{c_2(z)}$, $\frac{c_1(z)}{c_3(z)}$ and $\frac{c_3(z)}{c_2(z)}$, is SPR, then the three matrices A_4 , A_5 and A_6 associated with the stable polynomials $c_4(z)$, $c_5(z)$ and $c_6(z)$ are quadratically stable, where $c_4(z) = \frac{c_1(z)+c_2(z)}{2}$, $c_5(z) = \frac{c_2(z)+c_3(z)}{2}$ and $c_6(z) = \frac{c_3(z)+c_1(z)}{2}$.

Proof: Define P_1 as the common Lyapunov matrix for A_1 and A_2 , P_2 as the common Lyapunov matrix for A_2 and A_3 and P_3 as the common Lyapunov matrix for A_3 and A_1 . Consider the transfer function $\frac{c_2(z)}{c_1(z)}$. Using the KYP lemma, $\frac{c_2(z)}{c_1(z)}$ is SPR iff [28]:

$$\exists P_1 = P_1^T > 0 \text{ s.t.} \\ \begin{bmatrix} A_1^T P_1 A_1 - P_1 & A_1^T P_1 B - (C_2 - C_1)^T \\ B^T P_1 A_1 - (C_2 - C_1) & -2 + B^T P_1 B \end{bmatrix} < 0. \quad (\text{A.18})$$

For the same reason, $\frac{c_3(z)}{c_1(z)}$ is SPR iff;

$$\exists P_3 = P_3^T > 0 \text{ s.t.} \\ \begin{bmatrix} A_1^T P_3 A_1 - P_3 & A_1^T P_3 B - (C_3 - C_1)^T \\ B^T P_3 A_1 - (C_3 - C_1) & -2 + B^T P_3 B \end{bmatrix} < 0. \quad (\text{A.19})$$

By adding (A.18) and (A.19), we get:

$$\begin{bmatrix} A_1^T (P_1 + P_3) A_1 - (P_1 + P_3) \\ B^T (P_1 + P_3) A_1 - (C_2 + C_3 - 2C_1) \\ A_1^T (P_1 + P_3) B - (C_2 + C_3 - 2C_1)^T \\ -4 + B^T (P_1 + P_3) B \end{bmatrix} < 0. \quad (\text{A.20})$$

If we divide (A.20) by 2, we get the condition for $\frac{(c_2(z)+c_3(z))/2}{c_1(z)}$ to be SPR. According to the results of Theorem A.1, it means that $P_1 + P_3$ is a Lyapunov matrix for $(A_2 + A_3)/2$. On the other hand, P_2 is also a Lyapunov matrix for $(A_2 + A_3)/2$, thus $P_1 + P_2 + P_3$ is a Lyapunov matrix for $(A_2 + A_3)/2$. Similarly, we can show that $P_1 + P_2 + P_3$ is a Lyapunov matrix for $(A_1 + A_2)/2$ and $(A_1 + A_3)/2$. Since $(A_2 + A_3)/2$ is A_5 , $(A_1 + A_2)/2$ is A_4 and $(A_1 + A_3)/2$ is A_6 , the three matrices A_4 , A_5 and A_6 are quadratically stable. ■

References

- [1] B. D. O. Anderson. The small-gain theorem, the passivity theorem and their equivalence. *Journal of the Franklin Institute*, 293(2):105–115, February 1972.
- [2] P. Apkarian and P. Gahinet. A convex characterization of gain-scheduled H_∞ controllers. *IEEE Transactions on Automatic Control*, 40(5):853–864, May 1995.
- [3] G. Becker and A. Packard. Robust performance of linear parametrically varying systems using parametrically-dependent linear feedback. *Systems & Control Letters*, 23(3):205–215, 1994.
- [4] A. Besançon-Voda and H. Roux-Buisson. Another version of the relay feedback experiment. *Journal of Process Control*, 7(4):303–308, August 1997.
- [5] H. W. Bode. *Network Analysis and Feedback Amplifier Design*. D. Van Nostrand, Princeton, N. J., 1945.
- [6] M. Butcher, A. Karimi, and R. Longchamp. Iterative learning control based on stochastic approximation. *submitted to Automatica*, 2008.
- [7] M. Butcher, A. Karimi, and R. Longchamp. A statistical analysis of certain iterative learning control algorithms. *International Journal of Control*, 81(1):156–166, January 2008.

- [8] G. C. Calafiore and M. C. Campi. The scenario approach to robust control design. *IEEE Transactions on Automatic Control*, 51(5):742–753, May 2006.
- [9] Y. Chait, Q. Chen, and C. V. Hollot. Automatic loop-shaping of QFT controllers via linear programming. *Journal of Dynamic Systems, Measurement and Control*, 121(3):351–357, September 1999.
- [10] C. E. de Souza and L. Xie. On the discrete-time bounded real lemma with application in the characterization of static state feedback \mathcal{H}_∞ controllers. *Systems & Control Letters*, 18(1):61–71, January 1992.
- [11] A. J. den Hamer, S. Weiland, M. Steinbuch, and G. Z. Angelis. Stability and causality constraints on frequency response coefficients applied for non-parametric \mathcal{H}_2 and \mathcal{H}_∞ control synthesis. In *Proceedings of the 47th IEEE Conference on Decision and Control*, pages 3670–3675, Cancun, Mexico, December 2008.
- [12] J. C. Doyle, B. A. Francis, and A. R. Tannenbaum. *Feedback Control Theory*. Macmillan, New York, 1992.
- [13] Y. Fujisaki, F. Dabbene, and R. Tempo. Probabilistic design of LPV control systems. *Automatica*, 39(8):1323–1337, August 2003.
- [14] G. Galdos, A. Karimi, and R. Longchamp. Robust loop shaping controller design for spectral models by quadratic programming. In *Proceedings of the 46th IEEE Conference on Decision and Control*, pages 171–176, New Orleans, USA, December 2007.
- [15] G. Galdos, A. Karimi, and R. Longchamp. \mathcal{H}_∞ controller design for spectral MIMO models by convex optimization. In *Proceedings of the 10th European Control Conference (submitted)*, Budapest, Hungary, August 2009.
- [16] D. Garcia, A. Karimi, and R. Longchamp. Data-driven controller tuning using frequency domain specifications. *Industrial & Engineering Chemistry Research*, 45(12):4032–4042, June 2006.

- [17] C. C. Hang, K. J. Åström, and W. K. Ho. Refinements of the Ziegler-Nichols tuning formula. *IEE Proceedings D Control Theory & Applications*, 138(2):111–118, March 1991.
- [18] S. Hara, T. Iwasaki, and D. Shiokata. Robust PID control using generalized KYP synthesis: Direct open-loop shaping in multiple frequency ranges. *IEEE Control Systems Magazine*, 26(1):80–91, February 2006.
- [19] I. M. Horowitz. *Quantitative Feedback Design Theory (QFT)*, volume 1. QFT Publications, Boulder, Colorado, 1993.
- [20] P. Ioannou and G. Tao. Frequency domain conditions for strictly positive real functions. *IEEE Transactions on Automatic Control*, 32(1):53–54, January 1987.
- [21] K. J. Åström, H. Panagopoulos, and T. Häggglund. Design of PI controllers based on non-convex optimization. *Automatica*, 34(5):585–601, May 1998.
- [22] K. J. Åström and T. Häggglund. Automatic tuning of simple regulators with specifications on phase and amplitude margins. *Automatica*, 20(5):645–651, September 1984.
- [23] A. Karimi, M. Butcher, and R. Longchamp. Model-free precompensator tuning based on the correlation approach. *IEEE Transactions on Control Systems Technology*, 16(5):1013–1020, September 2008.
- [24] A. Karimi, G. Galdos, and R. Longchamp. Robust fixed-order H_∞ controller design for spectral models by convex optimization. In *Proceedings of the 47th IEEE Conference on Decision and Control*, Cancun, Mexico, December 2008.
- [25] L. H. Kell and S. P. Bhattacharyya. Data driven synthesis of three term digital controllers. In *Proceedings of the 2006 American Control Conference*, pages 262–267, Minneapolis, Minnesota, USA, June 2006.
- [26] H. K. Khalil. *Nonlinear Systems*. Prentice-Hall, Upper Saddle River, New Jersey, third edition, 1996.
- [27] I. D. Landau, R. Lozano, and M. M’Saad. *Adaptive Control*. Springer, London, 1998.

- [28] L. Lee and J. L. Chen. Strictly positive real lemma for discrete-time descriptor systems. In *Proceedings of the 39th IEEE Conference on Decision and Control*, Sydney, Australia, December 2000.
- [29] D. J. Leith and W. E. Leithead. Survey of gain-scheduling analysis and design. *International Journal of Control*, 73(11):1001–1025, July 2000.
- [30] D. Liberzon, J. P. Hespanha, and A. S. Morse. Stability of switched systems: a lie-algebraic condition. *Systems & Control Letters*, 37(3):117–122, July 1999.
- [31] D. Liberzon and A. S. Morse. Basic problems in stability and design of switched systems. *IEEE Control Systems Magazine*, 19(5):59–70, October 1999.
- [32] H. Lin and P. J. Antsaklis. Stability and stabilizability of switched linear systems: A short survey of recent results. In *Proceedings of the 2005 IEEE International Symposium on Intelligent Control*, pages 24–29, Limassol, Cyprus, June 2005.
- [33] R. Longchamp. *Commande numérique de systèmes dynamiques: cours d'automatique*. Presses Polytechniques et Universitaires Romandes, Lausanne, second edition, 2006.
- [34] B. Paijmans, W. Symens, H. Van Brussel, and J. Swevers. A gain-scheduling-control technique for mechatronic systems with position-dependent dynamics. In *Proceedings of the 2006 American Control Conference*, pages 2933–2938, Minneapolis, Minnesota, USA, June 2006.
- [35] H. Panagopoulos, K. J. Åström, and T. Hägglund. Design of PID controllers based on constrained optimisation. *IEE Proceedings Control Theory & Applications*, 149(1):32–40, 2002.
- [36] W. J. Rugh and J. S. Shamma. Research on gain scheduling. *Automatica*, 36(10):1401–1425, October 2000.
- [37] R. N. Shorten and K. S. Narendra. Necessary and sufficient conditions for the existence of a common quadratic lyapunov function for a finite number of stable second order linear time-invariant systems. *International Journal of Adaptive Control and Signal Processing*, 16(10):709–728, December 2002.

- [38] M. Steinbuch, R. van de Molengraft, and A. van der Voort. Experimental modelling and LPV control of a motion system. In *Proceedings of the American Control Conference*, pages 1374–1379, Denver, Colorado, USA, June 2003.
- [39] K. J. Åström and T. Hägglund. *PID Controllers: Theory, Design, and Tuning*. International Society of Automation, 2nd edition, 1995.
- [40] J. G. VanAntwerp and R. D. Braatz. A tutorial on linear and bilinear matrix inequalities. *Journal of Process Control*, 10(4):363–385, August 2000.
- [41] Q. G. Wang, C. C. Hang, and Q. Bi. Process frequency response estimation from relay feedback. *Control Engineering Practice*, 5(9):1293–1302, September 1997.
- [42] M. G. Wassink, M. van de Wal, C. Scherer, and O. Bosgra. LPV control for a wafer stage: beyond the theoretical solution. *Control Engineering Practice*, 13(2):231–245, February 2005.
- [43] O. Yaniv and M. Nagurka. Automatic loop shaping of structured controllers satisfying QFT performance. *Journal of Dynamic Systems, Measurement, and Control*, 127(3):472–477, September 2005.
- [44] K. Zhou and J. C. Doyle. *Essentials of Robust Control*. Prentice Hall, Upper Saddle River, New Jersey, 1998.
- [45] J. G. Ziegler and N. B. Nichols. Optimum settings for automatic controllers. *Transactions of the ASME*, 64:759–768, November 1942.
- [46] A. C. Zolotas and G. D. Halikias. Optimal design of PID controllers using the QFT method. *IEE Proceedings Control Theory & Applications*, 146(6):585–589, November 1999.

Curriculum Vitæ

Kunze Marc

Chemin de Pierrefleur 4
1373 Chavornay (VD), Switzerland
phone: +41 24 441 71 30
e-mail: kunze.marc@gmail.com

Born the 30th January 1980
Nationality: Swiss and German
Single

Education

- 2004 - 2009: **Doctoral studies and research** at the Automatic Control Laboratory, Swiss Federal Institute of Technology Lausanne (EPFL).
- 1999 - 2004: **Master of Science in Microengineering**, EPFL.

Publications

Published:

- M. Kunze, A. Karimi and R. Longchamp. Frequency domain controller design by linear programming guaranteeing quadratic stability. In *Proceedings of the 47th IEEE Conference on Decision and Control*, pages 345-350, Cancun, Mexico, December 2008.
- M. Kunze, A. Karimi and R. Longchamp. Gain-scheduled controller design by linear programming. In *Proceedings of the European Control Conference 2007*, pages 5432-5438, Kos, Greece, July 2007.
- A. Karimi, M. Kunze and R. Longchamp. Robust controller design by linear programming with application to a double-axis po-

sitioning system. *Control Engineering Practice*, 15(2):197-208, February 2007

- A. Karimi, M. Kunze and R. Longchamp. Robust PID controller design by linear programming. In *Proceedings of the 2006 American Control Conference*, pages 3831-3836, Minneapolis, Minnesota, USA, June 2006.
- S. Thiery, M. Kunze, A. Karimi, A. Curnier and R. Longchamp. Friction modeling of a high-precision positioning system. In *Proceedings of the 2006 American Control Conference*, pages 1863-1867, Minneapolis, Minnesota, USA, June 2006.

Accepted:

- V. Reymond, M. Kunze, A. Karimi and R. Longchamp. Modeling and control of a magnetically levitated planar motor. *Accepted to the European Control Conference 2009*, Budapest, Hungary, August 2009.

Submitted:

- M. Kunze, A. Karimi and R. Longchamp. Frequency-domain controller design by linear programming guaranteeing quadratic stability. *Submitted to Automatica*.
- M. Kunze, A. Karimi and R. Longchamp. Gain-scheduled controller design by linear programming with application to a double-axis positioning system. *Submitted to IEEE Transactions on Control Systems Technology*.